NERVE GUIDANCE CONDUIT APPLICATION OF MAGNESIUM ALLOYS

MAGNEZYUM ALAŞIMLARININ SİNİR KILAVUZ KANALI İÇİN UYGULANMASI

OZAN ÖZKAN

PROF. DR. ERHAN BİŞKİN

Supervisor

ASSOC. PROF. DR. HİLAL TÜRKOĞLU ŞAŞMAZEL

Co-Supervisor

Submitted to

Graduate School of Science and Engineering of Hacettepe University

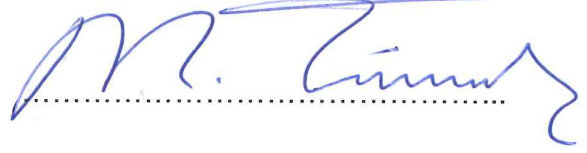as a Partial Fulfillment to the Requirements

for the Award of the Degree of Doctor of Philosophy

in Bioengineering

2019

This work titled "**Nerve Guidance Conduit Application of Magnesium Alloys**" by **OZAN ÖZKAN** has been approved as a thesis for the Degree of **Doctor of Philosophy** in **Bioengineering** by the Examining Committee Members mentioned below.
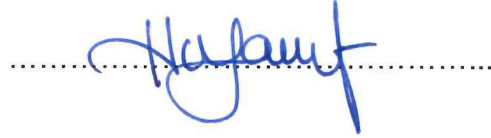
Prof. Dr. Mustafa TÜRK
Head
....
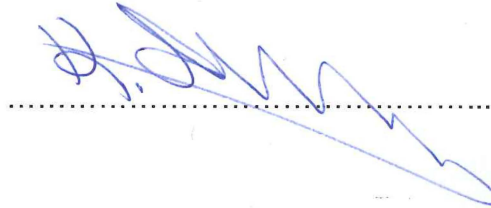
Prof. Dr. Erhan BİŞKİN
Supervisor
....

Prof. Dr. Handan YAVUZ ALAGÖZ
Member
....

Assoc. Prof. Dr. Sinan EĞRİ
Member
....

Assist. Prof. Dr. Kemal DAVUT
Member
....

This thesis has been approved as a thesis for the Degree of **Doctor of Philosophy** in **Bioengineering** by Board of Directors of the Institute of Graduate School of Science and Engineering on ...../...../...........

Prof. Dr. Menemşe GÜMÜŞDERELİOĞLU
Director of the Institute of
Graduate School of Science and Engineering

To my family...

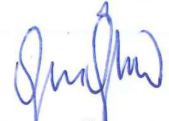*...my biggest treasure and my greatest achievement.*

ETHICS

In this thesis study, prepared in accordance with the spelling rules of Institute of Graduate School of Science and Engineering of Hacettepe University,

I declare that;

- all the information and documents have been obtained in the base of the academic rules,
- all audio-visual and written information and results have been presented according to the rules of scientific ethics,
- in case of using others works, related studies have been cited in accordance with the scientific standards,
- all cited studies have been fully referenced,
- I did not do any distortion in the data set,
- and any part of this thesis has not been presented as another thesis study at this or any other university.

06.02.2019

Ozan ÖZKAN

YAYIMLAMA VE FİKRİ MÜLKİYET HAKLARI BEYANI

Enstitü tarafından onaylanan lisansüstü tezimin/raporumun tamamını veya herhangi bir kısmını, basılı (kağıt) ve elektronik formatta arşivleme ve aşağıda verilen koşullarla kullanıma açma iznini Hacettepe Üniversitesine verdiğimi bildiririm. Bu izinle Üniversiteye verilen kullanım hakları dışındaki tüm fikri mülkiyet haklarım bende kalacak, tezimin tamamının ya da bir bölümünün gelecekteki çalışmalarda (makale, kitap, lisans ve patent vb.) kullanım hakları bana ait olacaktır.

Tezin kendi orijinal çalışmam olduğunu, başkalarının haklarını ihlal etmediğimi ve tezimin tek yetkili sahibi olduğumu beyan ve taahhüt ederim. Tezimde yer alan telif hakkı bulunan ve sahiplerinden yazılı izin alınarak kullanması zorunlu metinlerin yazılı izin alarak kullandığımı ve istenildiğinde suretlerini Üniversiteye teslim etmeyi taahhüt ederim.

Yükseköğretim Kurulu tarafından yayınlanan *"Lisansüstü Tezlerin Elektronik Ortamda Toplanması, Düzenlenmesi ve Erişime Açılmasına İlişkin Yönerge"* kapsamında tezim aşağıda belirtilen koşullar haricinde YÖK Ulusal Tez Merkezi / H. Ü. Kütüphaneleri Açık Erişim Sisteminde erişime açılır.

☐ Enstitü / Fakülte yönetim kurulu kararı ile tezimin erişime açılması Mezuniyet tarihimden itibaren 2 yıl ertelenmiştir.

☐ Enstitü / Fakülte yönetim kurulu gerekçeli kararı ile tezimin erişime açılması mezuniyet tarihimden itibaren ..... ay ertelenmiştir.

☐ Tezim ile ilgili gizlilik kararı verilmiştir.

06,02,2019

Ozan ÖZKAN

ÖZET

MAGNEZYUM ALAŞIMLARININ SİNİR KILAVUZ KANALI İÇİN UYGULANMASI

Ozan ÖZKAN

Doktora, Biyomühendislik ABD
Tez Danışmanı: Prof. Dr. Erhan BİŞKİN
Eş Danışman: Doç. Dr. Hilal TÜRKOĞLU ŞAŞMAZEL
Ocak 2019, 113 sayfa

Periferik sinir yaralanmalarında, 5 mm'den büyük hasarlarda cerrahi müdahale ile tedavi yetersiz kaldığı ve sinir dokusunun iyileşme hızı göreceli olarak yavaş olduğu için oluşan boşluk inflamasyon hücrelerinden oluşan yara dokusuyla kapanarak sinir hattında fonksiyon kaybına sebep olmaktadır. Dolayısıyla büyük hasarların tedavisi için bölgenin çevre dokudan izole edilmesi gerekmektedir. Bu amaçla, literatürde yaygın olarak çalışılan ve klinik uygulamalarda da tercih edilmeye başlanılan sinir kılavuz kanalı kullanımı öne çıkmaktadır. Biyouyumlu ve biyobozunum hızı düşük olması gereken sinir kılavuz kanalları, oksijen/besin/atık alışverişine olanak sağlayacak ancak inflamasyon hücreleri girişine izin vermeyecek ölçüde yarıgeçirgen gözenekli yapıda olmalıdır. Dolayısıyla, seçilen malzemenin biyodegradasyon hızı ve degradasyon ürünlerinin toksisitesi ile üretim için tercih edilen yöntemin gözeneklilik kontrolü sağlaması oldukça önemlidir. Literatürde, polimerler kullanılarak düşük maliyetli ve kolay üretilebilen sinir kılavuz kanalları üzerine yoğun çalışmalar yapılmaktadır. Metaller ise yüksek mekanik dayanım ve iletkenlik sağlayabilmelerine rağmen geleneksel yöntemlerle mikron seviyesinde gözeneklilikte üretilemediklerinden, tercih edilememektedir. Bu tezde, literatürde

yaygın olarak stent uygulamaları için çalışılmakta olup, ticari seviyede kullanılmak üzere FDA onayı almış ve dolayısıyla biyolojik yeterliliği stent uygulaması için kanıtlanmış bir magnezyum alaşımına benzer kompozisyonda bir magnezyum bileşiğinin sinir kılavuz kanalı uygulamaları için kullanılmak üzere geliştirilmesi çalışılmıştır. Magnezyum düşük yoğunluğa, yüksek özgül dayanıma, elektrik iletkenliğine ve düşük toksisiteye sahip, vücutta bolca bulunan ve insan metabolizmasını besleyici bir elementtir. Böylece geliştirilen sinir kılavuz kanalının, magnezyum temelli bir alaşım-benzeri bileşikten oluşması sayesinde, fiziksel, kimyasal ve biyolojik olarak üstün performans göstermesi öngörülmüştür. Söz konusu metalik alaşım-benzeri bileşiğin üretiminde, geleneksel yaklaşımlardan farklı olarak, proses kolaylığı ve üstün gözeneklilik kontrolü sağlayan elektroeğirme yöntemi seçilmiş ve söz konusu alaşımın bileşenlerinin nitratlı bileşikleri ile polivinilpirolidon veya polivinilalkol çözelti ham maddesi olarak kullanılarak elektroeğirme gerçekleştirilmiştir. Bu süreçte, ham madde/çözücü konsantrasyonları, sıcaklık, vizkozite gibi çözelti parametreleri ile voltaj, uzaklık, besleme hızı gibi elektroeğirme parametreleri gözle muayene ve SEM görüntülemeleriyle optimize edilmiştir. Optimum parametreler ile elektroeğirilen numuneler daha sonra, asal gaz (argon) atmosferi altında gaz akışı-sıcaklık-süre kontrollü kalsinasyona tabi tutularak bileşenlerinin istenilen alaşım kompozisyonunda kristalleşmesi ve alaşım harici bileşenlerin uzaklaştırılması sağlanmaya çalışılmıştır. Kalsinasyon sürecinde uygulanan, birden fazla sıcaklık ve süre kademesinden oluşan ısıl işlem profili, elektroeğirilmiş numunelere yapılan termal analizler sonucunda başta camsı geçiş sıcaklığı, erime sıcaklığı, kristalizasyon sıcaklığı gibi olası faz dönüşümlerinden kaynaklanan endotermik ve ekzotermik piklerin belirlenmesi ve bu piklere matematiksel reaksiyon kinetiği yaklaşımı ile uygulanmasıyla tasarlanmıştır. Kalsinasyon süreci sonrası elde edilen nihai numunelerin kristalografik yapısı, elemental kompozisyonu, morfolojik özellikleri ve alaşım harici bileşenlerin uzaklaştırıldığı/uzaklaştırılamadığı sırasıyla XRD, EDX, SEM ve XPS ile tayin edilmiştir. Ayrıca elde edilen numunelerin absorplama/şişme kapasitesi, ıslatılabilirliği, geçirgenliği ve degredasyon hızı gibi fiziksel ve kimyasal özellikleri de gerçekleştirilen tezdeki karakterizasyon çalışmaları kapsamında gerçekleştirilmiştir. Tez çalışmalarının son basamağında, geliştirilen sinir kılavuz kanalı materyali adayının hücre-materyal etkileşimi, fare

fibroblast hücre hattı ile MTT analizi, hemositometrik sayım ve çeşitli boyama/görüntüleme teknikleri kullanılarak hücre canlılığı, yapışma, yayılma ve üreme kabiliyetleri bakımından incelenmiştir. Tamamlanan tez çalışmasından elde edilen fiziksel, kimyasal ve biyouyumluluk performans verileri, elektroeğirme yöntemiyle magnezyum temelli alaşım benzeri bileşikten oluşan fibröz gözenekli yapıların sinir kılavuz kanalı uygulamalarında kullanılabilme potansiyeli olabileceğini göstermiştir.

Anahtar Kelimeler: Magnezyum Alaşımı, WE43, Elektroeğirme, Kalsinasyon, Sinir Kılavuz Kanalı, Biyouyumluluk.

ABSTRACT

NERVE GUIDANCE CONDUIT APPLICATION OF MAGNESIUM ALLOYS

Ozan ÖZKAN

Doctor of Philosophy, Department of Bioengineering
Supervisor: Prof. Dr. Erhan BİŞKİN
Co-Supervisor: Assoc. Prof. Dr. Hilal TÜRKOĞLU ŞAŞMAZEL
January 2019, 113 pages

Surgery is insufficient for peripheral nerve injuries larger than 5 mm. Function loss and scar formation occur as a result of slow healing rate and inflammation cells filling the damaged gap. Therefore, isolation of damaged area from surrounding tissue is crucial for treatment. For this purpose, NGCs have increasingly gained interest both in literature and clinic. Biocompatibility, slow biodegradation and semi-permeable structure that allow oxygen/nutrition/waste transfer and prohibits inflammation cells are the main requirements for NGCs. Therefore, biodegradation rate and degradation product toxicity of the material and a fabrication method that provides porosity control are crucial. In the literature, fabrication of NGCs with low cost and easy to use methods by using polymers is widely studied. On the other hand, even though metals can provide higher mechanical strength and electrical conductivity, they are not preferred for NGCs since it is not possible to obtain micro-scale porosity by conventional methods. In this thesis, development of a magnesium alloy-like compound with a similar composition of a magnesium alloy widely studied in the literature for stent applications and obtained FDA approval, for the use of NGC applications was studied. Magnesium is an abundant element found in human body, with

high nutritional value, low density, high specific strength, high electrical conductivity and low toxicity. Therefore, it was planned to achieve enhanced physical, chemical and biological performance by using magnesium based alloy-like compound for NGC. For the fabrication of the compound, instead of conventional approaches, electrospinning were selected due to its ease of use and porosity control capability, and the spinning was conducted with the nitrates of alloy components and polyvinylpyrrolidone or polyvinylalcohol used as raw materials of the solution. Solution parameters such as concentration, temperature and viscosity, and electrospinning parameters such as voltage, distance and feeding rate were optimized with naked-eye observations and SEM. Electrospun samples were then underwent a gas flow-temperature-time controlled calcination under argon atmosphere in order to crystallize the components into alloy-like compound and remove non-alloy components. The calcination profile containing multiple temperature and duration steps was designed according to the thermal analyses applied to electrospun samples where all possible endothermic and exothermic phase transformations such as glass transition temperature, melting temperature and crystallization temperature were measured and analyzed with mathematical reaction kinetics. The crystallographic structure, elemental composition and morphological properties of the calcinated samples as well as removal of non-alloy components were determined with XRD, EDX, SEM and XPS. Additionally, physical and chemical properties such as absorption/swelling capacity, wettability, permeability and degradation rate were obtained as a part of characterization studies. In the final stage of the thesis, the cell-material interaction of the developed NGC candidate material was examined with MTT assay, haemocytometric counting and several staining/imaging techniques in terms of cell viability, attachment, proliferation and growth using fibroblast cell line. The physical, chemical and biocompatibility data obtained in this thesis showed that the fibrous magnesium based alloy-like compound fabricated with electrospinning could be a potential candidate for NGC applications.

Keywords: Magnesium Alloy, WE43, Electrospinning, Calcination, Nerve Guidance Conduit, Biocompatibility.

ACKNOWLEDGEMENTS

Ozan ÖZKAN
January 2019, Ankara

TABLE OF CONTENTS

LIST OF TABLES

LIST OF FIGURES

NOMENCLATURE AND ABBREVIATIONS

Nomenclature

v/v	Volume per Volume percent
wt.%	Weight percent
θ	Diffraction Angle
Ω	Ohm

Abbreviations

2D	Two Dimensional
3D	Three Dimensional
AF-488	Alexa Fluor 488 Phalloidin
AMS	Absorbable Metallic Stents
ASTM	American Society for Testing and Materials
ATCC	American Type Culture Collection
bFGF	Basic Fibroblast Growth Factor
BMP-2	Bone Morphogenetic Protein-2
BSA	Bovine Serum Albumin
BSI	Bothersomeness Index
CLSM	Confocal Laser Scanning Microscope
CPT	Camptothecin
DC	Direct Current
DLDM	Double-Nozzle Low-Temperature Deposition Manufacturing
DMEM/F12	Dulbecco's Modified Eagle Medium/Ham's F-12 medium
DMSO	Dimethyl Sulfoxide
DNA	Deoxyribonucleic Acid

DOX	Doxorubicin
DRAQ5	Deep Red Anthraquinone 5
DTA	Differential Thermal Analysis
ECM	Extracellular Matrix
EDX	Energy-Dispersive X-Ray Spectroscopy
FBS	Fetal Bovine Serum
FDA	Food and Drug Administration
FDM	Fused Deposition Modeling
FOG	Feruloyl-Oleyl-Glycerol
HA	Hyaluronic Acid
KET	Ketoprofen
LDH	Lactate Dehydrogenase
MET	Metronidazole Benzoate
$Mg(NO_3)_2.6H_2O$	Magnesium Nitrate Hexahydrate
MRC	Medical Research Council
MTT	Methyl Thiazolyl Tetrazolium
MW	Molecular Weight
NaCl	Sodium Chloride
$Nd(NO_3)_3.6H_2O$	Neodymium Nitrate Hexahydrate
NGC	Nerve Guidance Conduit
NGF	Nerve Growth Factor
NRS	Numeric Rating Scale
OD	Optical Density
PBS	Phosphate Buffer Saline
PCL	Poly(ε-caprolactone)
PCU	Poly(carbonate urethane)
PDGF	Platelet-Derived Growth Factor

PELCL	Poly(ethylene glycol)-b-poly(l-lactide-co-ε-caprolactone)
PGA	Poly(glycolic acid)
pH	Power of Hydrogen
PHB	Poly(hydroxybutyrate)
PLA	Poly(lactic acid)
PLGA	Poly(lactic-co-glycolic acid)
PLLA	Poly(l-lactide)
PLLA-CL	Poly(l-lactic acid co-ε-caprolactone)
POSS	Polyhedral oligomeric silsesquioxane
PTX	Paclitaxel
PU	Polyurethane
PVA	Poly(vinyl alcohol)
PVP	Poly(vinyl pyrrolidone)
RE	Rare Earth
RP	Rapid Prototyping
SA	Salicylic Acid
SEM	Scanning Electron Microscopy
TCPS	Tissue Culture Polystyrene
TG	Thermogravimetry
USA	United States of America
UV	Ultraviolet
VEGF	Vascular Endothelial Growth Factor
WVTR	Water Vapor Transmission Rate
XPS	X-Ray Photoelectron Spectroscopy
XRD	X-Ray Diffraction
$Y(NO_3)_3.6H_2O$	Yttrium Nitrate Hexahydrate
$ZrO(NO_3)_2.xH_2O$	Zirconium Oxynitrate Hydrate

1. INTRODUCTION

Full recovery and regaining of the functions after peripheral nerve injuries caused by accidents still remain as an important clinical problem to this day [1]. Every year, millions of people became partially disabled or bedridden because of peripheral nerve damages and only a small fraction of these injuries can be treated with surgical intervention [2]. Neurorrhaphy is one of the most used surgical interventions for these injuries and is simply a method of suturing the ruptured nerve endings together as long as the nerve gap is less than 5 mm. For the larger gaps, this method usually fails because of the strain on the sutures [3]. Therefore, several studies are being conducted every year for larger nerve gaps by enclosing the gap with a biocompatible conduit [4].

The main reason of enclosing the gap between the ruptured nerves is that the nerve healing is slower than the surrounding tissue growth. Since the nerve regeneration process depends on the communication between both nerve endings, a scar tissue formation or a surrounding tissue migration in the gap will prevent nerve cells to connect with each other and therefore cause nerve degeneration quickly. Therefore, in the recent years, nerve conduits are becoming more and more a "Golden Standard" for the treatment of peripheral nerve injuries [5].

There are certain aspects that required from a nerve conduit compiled according to the recent studies. The first important aspect is that the conduit should have a certain level of biocompatibility so that there is no inflammatory reaction harming the damaged nerve endings. Another most important requirement for a nerve conduit is semi-permeability. Several studies shows that the permeability of a nerve conduit should be so that it allows oxygen, nutrients and waste transfer while preventing inflammation cells entering to or healing components escaping from the wounded site [6, 7].

There are several types of materials and methods studied to meet these two important requirements for nerve conduits in the literature. However, a

significant portion of these studies utilized synthetic polymers with different porosity levels, obtained by using some complex fabrication methods [1]. Therefore, true biocompatibility obtained with feasible manufacturing are still remain challenging in the literature.

In this thesis, it is aimed to propose an alternative biocompatible material to polymers and to investigate the suitability of this material to a wide known, feasible fabrication technique. The material considered to be the alternative is a magnesium based alloy called WE43. Magnesium is a lightweight, high strength, elastic, conductive, non-toxic element with density close to bone tissue and found as the 4th abundant element in the human body [8]. A lot of magnesium based alloys were studied extensively for biomedical applications and there are FDA approved and patented stents fabricated with magnesium based alloys [9, 10]. In this thesis, it is believed that a highly biocompatible and commercially approved alloy like this can be a suitable high performance candidate for a conduit application. However, a stent is usually fabricated from an extruded metal tube by using laser cutting and therefore not only require expensive high temperature and deformation processes but also not properly suitable in terms of porosity/pore size. As a result, in this thesis, an alternative but more easy and feasible fabrication technique is also investigated for applicability to the selected magnesium alloy. The investigated fabrication technique, electrospinning, is a widely utilized and studied fibrous network fabrication method that is usually only applicable to polymeric materials, since the method requires solution based precursors for fabrication. Fabrication of metallic alloy/alloy-like compounds by using electrospinning technique attract the attention of the researchers in the recent years. The approach is based on simply using the highly water soluble nitrates of the elemental components of the alloys for preparing the precursor solution required for electrospinning technique. Also, since the nitrate solutions have very low viscosity, the studies also utilized polymer addition to these precursor solutions in order to adjust the viscosity of the solution to a more spinnable level. The final step in preparing the alloy/alloy-like compound by using electrospinning is the calcination/heat treatment applied after electrospinning in which the polymer used to adjust viscosity is pyrolized away and the remaining nitrates are calcinated into the

alloy-like compound in form of a fibrous network. In the literature, binary compounds such as alumina borate [11], titanium dioxide [12], silicate [13], cobalt oxide [14], nickel oxide [15], copper oxide [16], niobium oxide [17], vanadium pentoxide [18] and zinc oxide [19] fibers were successfully prepared with electrospinning technique. However, in this thesis, an alloy-like compound mimicking highly biocompatible and commercially approved WE43 magnesium alloy which contains four components were investigated in terms of suitability for prepared by electrospinning technique as well as biocompatibility. Therefore, it is aimed to create an alternative material with desired fibrous network using a low cost, easy to use fabrication method that provides extensive porosity/pore size control. This thesis study report the optimization of the precursor solution as well as electrospinning parameters, calculation and optimization of the calcination process applied following the electrospinning fibrous mat production and finally investigation of physical and chemical properties as well as biocompatibility performance, in the following sections. Detailed methods, calculations, results and extensive discussions are provided.

2. LITERATURE SURVEY

2.1. Peripheral Nerve Injuries

Peripheral nervous system is the bridge between the central nervous system and the limbs/organs of the mammals. It consists of nerves and ganglia that provide neural communication. This neural communication is essential for the bodily functions [20]. Physical injuries due to the accidents sometimes severe these connections of nerves, leaving a gap between proximal and distal stumps. The nerves have the capability to regenerate from the proximal stump however it is a very slow process in order of several months [5]. Peripheral nerve regeneration mechanism consists of four main stage; namely, a protein-rich fluid phase containing neurotrophic factors, formation of fibrin-rich matrix phase, cellular phase in which perineural, endothelial and Schwann cells migrate, and axonal phase in which the axonal cables elongate (Figure 2.1) [21].
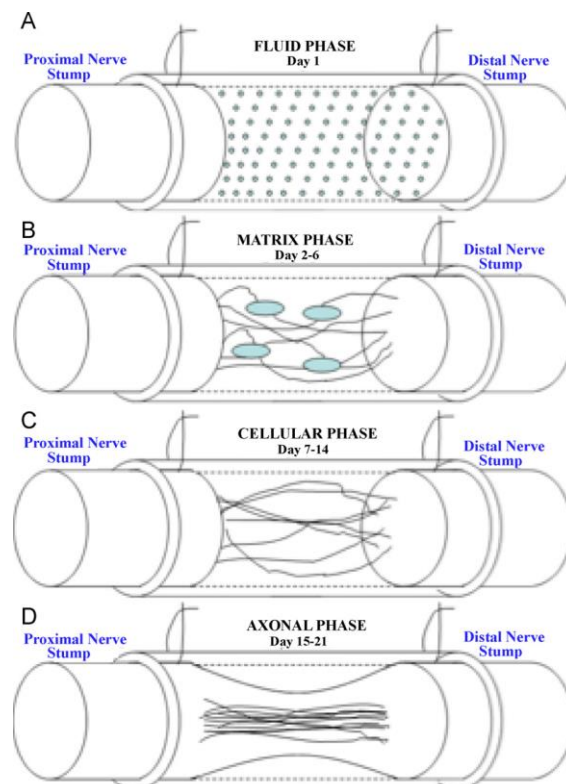
Figure 2.1.   Peripheral nerve regeneration mechanism [22]

Depending on the degree of injury and the nature of these regeneration steps, the rate of axon growth can range from 1-5 mm/day up to 2 mm/month [23].

However, the surrounding tissue in the injury site can form a scar tissue faster than the rate of nerve regeneration which fills the gap between proximal and distal stumps with inflammation cells, severing the connection permanently and leaving the distal nerve line nonfunctional [24]. Additionally, Wallerian degeneration starts in the distal stump of the injured nerve within hours, preventing the regeneration of axon and/or myelin sheath. In order to minimize the Wallerian degeneration, four critical factors must be present in the injury site; the Schwann cells, the neurotrophic factors, the basal lamina which is the ECM of nerve cells, and the distal stump which found to provide neurotrophic factors for axon regeneration [25]. Therefore, if this scar formation between nerve endings and the resulting Wallerian degeneration can be prevented, the peripheral nerves can regenerate and neurofunctions can be restored by the help of physiotherapy.

2.1.1. Current Medical Approach

Treatment of peripheral nerve injuries are still a clinical problem in terms of full healing and functional recovery. Every year, millions of people become partially handicapped and/or bedridden because of the peripheral nerve injuries, and only a minority of them can be treated with surgical approaches such as neurolysis, neurorrhaphy or nerve graft [26, 27]. Neurolysis is the removal of scar tissue from the injury site which blocks the nerve tissue that is otherwise regenerates itself. However, this type of surgery only works on the nerve injuries small enough to heal on their own. Neurorrhaphy is a type of surgical intervention in which both of the nerve stumps of the injured nerve are sutured by the myelin sheath. The critical size for this surgical operation is around less than 5 mm nerve gaps, therefore it cannot be used for the repair of larger injuries, as it causes tension on the suture line, resulting poor healing of the injury [28]. Relatively larger nerve gaps can be repaired surgically with nerve grafts. Nerve grafts can be autograft, allograft or xenograft [29–31]. Autografts are donations of tissue from another part of patient's own body. There are several commonly used donation sites in the body for nerve grafting such as sural nerve in the back of the legs or medial antebrachial cutaneous nerve in inner upper arms, depending on the size of graft needed. However autografting approach causes a secondary surgery site on the patient's body, resulting a

scar, numbness/tingling sensation and/or loss of motor functionality [32–34]. In allograft tissue donations, nerve graft is taken from the body of another healthy person and implanted to the injury site. However, in this approach, in addition to the problems encountered in autografting, issues such as operation on a healthy person, scar formation, loss of functionality and/or sensation, tissue rejection via immune response due to the lack of tissue compatibility between the donor and the recipient as well as a life-time treatment with immunosuppressive drugs for the patient are also serious concerns [35, 36]. Xenograft tissue donations, on the other hand, solve donor site problems, since the donation is taken from a genetically compatible animal, bred commercially for this sole purpose. However this time, the disease transmission is a serious concern in this type of grafting along with the possibility of tissue rejection even though the animal is genetically compatible and immunosuppressive treatment is applied to prevent rejection. At last but not least, xenografting also raises international ethical debates on utilizing animals for human treatment without their consent [1].

All of these surgical interventions, whether direct procedural repair or a type of grafting, have a variable recovery rate and follow-up pain level, and none of them provides complete solution to the injury every time. For instance, a two year study conducted with eight neurolysis patients based on Likert scale resulted in only 25% complete recovery (Likert 1) and 12.5% almost complete recovery (Likert 2), both of which were deemed successful, and an average of mild to moderate pain were found according to NRS and BSI [37]. Another study conducted for seven years with 37 patients showed an average effective motor recovery rate between 43-54% according to MRC grading [38]. Another clinical study with ten patients showed no evidence of motor recovery after neurorrhaphy, leading the surgeons to abandon the technique in the hospital which the study conducted [39]. Grafting was also found to be ineffective in most cases, as indicated in several studies such as a 6 year study with 6 autograft patients showing only 33% full recovery [40], a study conducted between 1975-1994 with 242 autograft repairs showing 30% good, 28% fair and 42% failed results [41] or a 17 patient allograft repair study with 39% success rate according to Taras outcome criteria [42]. Therefore, even though new

surgical techniques or advanced surgery equipment are still being developed constantly, surgeons and medical scientist all around the world are looking for alternative solutions that yield better efficiency with less or no post-op complications.

2.2. Nerve Guidance Conduits

In order to overcome the issues encountered in surgical interventions, a novel approach called nerve guidance conduits (or channels), in which the injured nerve stumps and the gap between them are enclosed in an artificial conduit (or channel) to prevent scar tissue blockage resulting a Wallerian degeneration [43].

NGCs are artificially fabricated tubular structures that cover the injured nerve gap in order to protect the healing process from the surrounding as well as contain the inner mechanisms at injury site. Several physical, chemical and biological properties have been proposed for NGCs requirements which can be summarized as follows [29, 41, 44–51]:

(1)   The material used for fabrication of NGC must be biocompatible, show no cytotoxicity and trigger no inflammatory reaction at implant and surrounding sites.

(2)   The NGC must have mechanical properties such that it must be flexible enough to prevent compression of regenerating nerves, but rigid enough to resist mechanical forces from the surrounding.

(3)   The NGC must be durable enough for surgical handling so that it must retain sutures and prevent tearing.

(4)   The NGC structure must be semi-permeable, allowing oxygen and nutrients into the healing site while preventing inflammatory cell or scar tissue ingrowth as well as growth and/or neurotrophic factor exudation.

Biocompatibility, as with all artificially fabricated biomedical materials and

devices, is important in developing NGCs. Biocompatibility is a general term for the ability of a material or a device to perform without any adverse biological reaction from the implanted location [52]. It depends on the physical, chemical and biological properties of the material, in which topographical structure as well as the functionality of the contact points play the main role [53]. The cells can attach to a surface from multiple points through biological functionality of their cell walls; therefore, any surface with high area and multiple functional reactive species can perform adequately in terms of biocompatibility [54]. However, topography and functionality are not the only properties affecting the biocompatibility, since the toxicity of the material used is also important which triggers immune response of the body, resulting the breakdown or isolation of the material and disconnecting the material from the cells [55]. Since the mammalian cells are anchorage dependent, they require a substrate, or more commonly known as scaffold, to attach before they can grow, multiply or show cellular activity [56]. NGCs act as a scaffold for the regenerating nerve cells; therefore, biocompatibility is the first requirement for developing such materials. Materials used in nerve tissue scaffolds, or in this case, nerve guidance conduits should meet the biocompatibility criteria before they even be considered a usable candidate.

Apart from the physical and/or functional support, NGCs should also have adequate mechanical support in order to sustain regeneration process. Peripheral nervous system is different from other tissues such as muscle or skin, in terms of the forces affecting. Since nerve cells are highly sensitive to strain forces [57], peripheral nerve system is positioned biologically to avoid such forces. However, nerves are still surrounded by several different types of tissues; therefore, compressive forces are an important issue [58]. The main purpose of a NGC is to protect the healing site from external factors, one of which is the compressive forces caused by the surrounding tissues. Since the NGCs are fabricated in tubular form, these compressive forces exerted can be counteracted with radial support. Therefore, NGCs should have adequate radial rigidity to prevent the regenerating nerve cells from being crushed [59]. On the other hand, this rigidity is restricted by the need of a certain level of flexibility in order to endure the suturing process during the surgical implantation of the

NGC. The NGCs are fixated to the injured nerve gaps from the endpoints by suturing myelin sheath to the NGC. Therefore, a certain flexibility of the material is required for both during and after the suturing [60].

The most important property for an NGC, however, is the requirement of a semi-permeable porous structure. One of the most significant reasons for nerve regeneration failure is the blockage of the nerve gap by the infiltrated inflammatory cells. This blockage severs the connection between proximal and distal stumps, bringing the regeneration potential to a halt, due to lack of signal communication [24]. Therefore, it is crucial to prevent this blockage as soon as possible after the injury. It is also important to keep valuable growth and/or neurotrophic factors secreted to the injury site inside the healing zone, once the regeneration starts to take effect. As a result, NGCs should act as a two-way barrier to prevent inflammatory cells and healing factors from passing to the opposite side. However, no matter how effective it will be to stop inflammation cells entering the injury site or healing factors escaping, a complete impermeable channel will be impractical as it is also required to sustain oxygenation and nourishing of the nerves during regeneration [44]. Therefore NGCs should have a certain level of porosity to be able to act as a semi-permeable barrier. Several studies reported that pores smaller than 5 μm inhibit cell proliferation where pores larger than 30 μm fail to prevent migration of inflammation cells. Therefore, the suggested pore size for an optimum barrier capability, is between 5 and 30 μm, in which 10 to 20 μm pore size distribution is generally preferred [29].

Last but not least, the following aspects are also important for NGCs, and have been proposed by many studies for enhancing the nerve regenerative performance of the candidate material developed and the resulting quality of life [3, 29, 41, 45, 46, 49–51]:

(1)   The material used in NGC can be biodegradable for a better post-healing physiology. Even though, the biodegradability may not be crucial as long as the material is biocompatible with the surrounding tissue [61], if present, the structure must maintain its mechanical support, especially the

radial support, during the regeneration to prevent premature failure of barrier properties. Additionally, the degradation products must also be biocompatible, and show no local and/or systemic toxicity.

(2)   The alignment of the inner structure of NGCs may also be build such that it can direct axonal growth along the tube. It has been proposed by many researchers that preventing misdirection and guiding the nerve growth with physically aligned structures within the tubular channel could increase the healing efficiency as well as the resulting functionality gain [62].

(3)   The NGC should also withstand further handling such as sterilization, transportation, storage or other surgical processes [63].

2.2.1. NGC Materials

Materials used in biomedical applications are generally classified by the origin of commercial derivation. Mostly utilized type of materials for nerve tissue engineering can be divided as natural or synthetic according to which source they are obtained.

2.2.1.1. Natural Materials

Natural materials have the advantage of containing adhesion sites and naturally occurring cell binding molecules, since they are directly derived commercially from animals, plants or microorganisms. Therefore, they provide enhanced biocompatibility properties in terms of topography and biofunctionality. However, they have also several disadvantages that needed to be addressed such as poor mechanical properties, possibility of impurities or diseases and lack of consistency in raw product quality/properties due to different in vivo sources [64].

Collagen is one of the most commonly used natural materials for not only nerve tissue engineering but also all kinds of tissue engineering applications. Because, it is the most abundant protein present in mammals and can also be found in peripheral nerve system [65]. There are at least 28 different types of

collagen identified in the literature, of which Type I is the majority of collagen found in human body. The key advantage of collagen is the several binding domains occurred naturally on the surface which provides multiple anchorage points for cells to attach and proliferate. Therefore, it offers topographical guiding to nerve cells in axonal regeneration process [65, 66]. There are several FDA approved nerve conduits commercially available, such as NeuraGen®, Neuroflex™, NeuroMatrix™, NeuroWrap™ and NeuroMend™ that is based on Type I collagen [22, 67]. Several clinical as well as research studies reported that collagen can be used for NGC material, however high cost and poor mechanical properties such as high stiffness and low flexibility are still a concern [68].

Fibrin is another biodegradable protein found in mammals and plays a crucial role in blood clotting mechanism [69, 70]. It has been suggested for the use in nerve damage repair, and several studies showed that it is possible to promote nerve regeneration and motor functional recovery for injuries less than 20 mm [71–73].

Other natural materials such as chitosan, gelatin, fibronectin, silk fibroin, keratin and hyaluronic acid are also widely studied for NGCs [74–79]. As with the most natural materials, they provide controllable biodegradability and enhanced biocompatibility, making them possible candidates for neural regeneration applications. However, difficulties in processability and lack of sufficient mechanical support as well as fast enzymatic degradation are primary concerns and need further tuning in order to obtain viable NGCs for commercial usage [80, 81].

2.2.1.2. Synthetic Materials
Synthetic materials have a completely different set of advantages over natural materials. They have high consistency in quality and reproducibility at industrial scale as well as abundancy in adjustability of the properties. However, they lack the biofunctionality that comes with natural materials, but especially good mechanical properties and resistance to enzymatic degradation make them attractive for tissue engineering applications nevertheless [82, 83].

PGA is one of the widely used synthetic polymers for NGCs with excellent mechanical properties such as high Young's modulus, and is the first synthetic NGC approved by FDA in 1999 under the commercial name, Neurotube® [22, 84]. It also became the gold standard amongst the surgeons when it comes to using synthetic NGCs up to 20 mm nerve gaps due to its length, low cost and widely available clinical studies, and is proven to be a viable candidate for neural regeneration, despite its synthetic nature [24]. However, its low solubility in organic solvents, high degradation rate and acidic degradation products that may cause tissue necrosis limit its application in nerve repair [85].

PCL is also one of the few synthetic materials approved by FDA for the use in NGCs. It is a cheap, easy to fabricate, highly soluble and biodegradable polyester that has good mechanical properties and non-toxic, non-inflammatory degradation products. Poly-D,L-lactide-co-ε-carprolactone NGC with a commercial name Neurolac® obtained FDA approval in 2005, and is the first and only transparent NGC commercially available that provides visual aid to surgeons during implantation [22]. It was proved to have a regeneration capability comparable to autografts as well as efficiency comparable to be the gold standard for nerve gaps up to 20 mm [86]. However, high rigidity and low flexibility remain as the major setback for handling of Neurolac® NGC during and after surgery, resulting in poor statistical performance for nerve injury repairs [87–89].

PVA is the only non-degradable synthetic polymer that achieved FDA approval under commercial names, SaluTunnel™ and Salubridge™. They are both hydrophilic hydrogels with same composition and structure with the only difference being the longitudinal opening present in SaluTunnel™ that provides easier surgical implantation. Both have sufficient flexibility due to the combination of water with similar ratio of human tissue and PVA. However, its non-degradable nature was found to cause issues such as tension and compression of the regenerated nerves at suture lines [22, 90].

There are other synthetic materials demonstrated to be promising for NGC applications and waiting for FDA approval for clinical practice such as PHB [91],

a long-term biodegradable polyester with good biocompatibility, widely used in sutures and wound dressings, or POSS, an organosilicon compound, found to be non-immunogenic when combined with polymers such as PCU or PCL [68, 92]. Synthetic polymers such as PLA, PLLA, PLGA and PU are still being in research phase with promising results, however further extensive in vitro and in vivo pre-clinical studies are necessary in order to pursuit clinical approval [93, 94].

2.2.2. NGC Fabrication

There are several different techniques that can be utilized for fabrication of NGCs; however, all of them have one crucial aspect in common which is to obtain the porosity level desired for ideal NGC. Therefore, any technique that is considered to be suitable for NGC fabrication should be based on fabrication of a porous structure, in general. Porogen leaching, freeze drying, phase separation, rapid prototyping and electrospinning are some of the pore-generating fabrication techniques that are commonly utilized for fabrication of NGCs [5].

Porogen leaching technique basically consists of combining a polymer solution with a secondary porogen component such as inorganic NaCl salt or another polymer with a solvent different from the main polymer. By this way, when the blended solution is cured, the porogen component can be removed from the bulk by dipping the structure in a selective solvent capable of dissolving the porogen but not the main polymer. The resulting structure will be the main polymer with porous structure where the pore size depends on the size of the secondary porogen component blended [95]. This technique has been widely used for fabrication of NGCs with the possibility of pore size range of 10 to 300 μm [96]. However, pore interconnectivity was found to be problematic in this technique, but it is possible to overcome this issue by increasing the porosity level more than 80% with tunable pore morphology where studies showed that pore morphology and porosity level depend on the morphology and weight fraction of salt crystals used, respectively. Additionally, preventing fibroblast infiltration can be achieved by increasing the thickness of NGC wall for structures with pore sizes larger than the suggested range [44]. On the other

hand, using low-cost polymers as porogen provides tailored pore size depending on the blend composition and process parameters, but interconnectivity became the main challenge at the expense of enhanced mechanical properties [97]. Therefore, further efforts have to be made to optimize the balance between the enhanced mechanical properties and the tailored porosity [98].

Freeze drying is another porous bulk preparation technique in which a secondary porogen is not needed as opposed to leaching technique. Instead, the aqueous content of the polymer solution prepared act as a porogen when the structure is dried under vacuum at temperatures lower than the triple point of water. As a result, the water content of the polymer solution will freeze like a porogen particle and then sublimate, leaving interconnected pores behind [99]. Natural polymers are the most suitable polymer type for freeze-dried porous NGCs, since they have good water solubility [100]. One of the most interesting achievements of this technique is that, it is possible to obtain oriented pores with an approach called "unidirectional freezing" by using liquid nitrogen [101] or specialized freezing setup [102]. Briefly, before the freeze drying is applied to remove the water, the scaffold is subjected to a pre-freezing step in which cooling applied starting from one end, instead of applying to the whole sample. Therefore by this way, the water content forms dendritic ice instead of spherical, and the resulting pores after freeze drying will be in spindle-like shape with an orientation depending on the pre-freezing direction [103].

Phase separation technique is a relatively new technique that is being explored for NGC fabrication in recent years. The technique is based on the separation of a homogeneous solution into the polymer and the solvent where the solvent is later removed and left pores behind [5]. The separation can be induced thermally or by another solvent that the polymer is insoluble. In thermal route, the polymer solution is prepared at temperatures higher than the critical temperature and then cooled below it at high speeds. This triggers the separation of the polymer and the solvent. On the other hand, the polymer prepared with a specific solvent can also precipitate when it is cast into another solvent that it is insoluble in, and therefore is separated from its solvent. The

14

residual solvent is then removed from the phase separated biphasic polymer structure by immersing in a washing solution which dissolves the solvent but not the polymer [104]. Phase separation technique is particularly utilized for NGC fabrication to develop multi-sized porosity along the cross-section of the conduit wall to obtain asymmetrical permeability [93]. The technique can also be combined with other techniques such as wet spinning [105] or injection molding [106] to obtain hollow or multi-channeled conduits that can guide the orientation of regenerating axons, therefore improve the success of healing process.

Rapid prototyping is a set of emerging fabrication techniques that can be used to fabricate complex shaped scaffolds with precision in a controllable fashion that is otherwise not possible with conventional methods. It is possible to fabricate a computer-generated 3D model of a scaffold that is designed to meet any structural requirement needed with top-down or bottom-up approaches. In these techniques, the data of the 3D model to be fabricated is separated into cross-sectional slices which are then constructed layer by layer on top of each other with specialized equipment to build the bulk structure [107]. Several biocompatible and biodegradable polymers are suitable already to be used in rapid prototyping, and new polymers are added to the list as the techniques advance [108]. Since the techniques utilize layer by layer fabrication approach, complex shapes with any desired pore size and shape, interconnectivity, porosity degree up to 90%, alignment and homogeneous/heterogeneous pore distribution, are theoretically not an issue, as long as the resolution of the rapid prototyping instrument allows [109]. Natural and synthetic polymers such as PLA, PCL, PGA, PLGA, PU, collagen or even live cells such as genetically modified human embryonic kidney cells that produce nerve growth factor (hNGF-EcR-293) were already adapted for fabrication NGCs with rapid prototyping techniques [110–112]. Additive manufacturing (bottom-up) techniques that use polymer solution or melt such as ink-jet micro-dispersing, FDM and DLDM were recently studied and found to be applicable rapid prototyping techniques for NGC fabrication [110, 112]. Rapid prototyping techniques and used materials are still in early research phase for fabrication of viable NGCs; and therefore, more biological assessments are needed, however given the remarkable versatility in achieving so many different options, the

techniques will expected to become one of the most preferred NGC fabrication technique in the future [5].

Electrospinning is probably the most studied NGC fabrication technique that allows development of scaffolds or conduits consisting aligned or non-woven fibers with controllable fiber diameter and pore size [113]. The technique briefly utilizes electrical field to eject a solution from a nozzle onto a grounded collector. Depending on the design of the nozzle and the collector as well as the voltage of applied electric field, the rate of solution feeder and the distance between the nozzle and the collector, it is possible to obtain a vast number of diversity in fiber size, shape, structure and/or orientation [64]. However in general, NGCs fabricated via electrospinning utilize either stationary collectors in which the fabricated scaffold is wrapped into a conduit and sutured/glued longitudinally or rotating collectors in order to obtain channeled shape directly [34, 114–116]. Since in this study, electrospinning was chosen as the primary fabrication approach, a more detailed introductory survey was given in the following section with state of the art studies.

2.3. Electrospinning

The origins of electrospinning technique went back to 16th century where William Gilbert was first observed an electrostatically charged amber that ejected small droplets which was the first known electrospraying in the history [117]. By the end of 18th century, it was found that with suitable experimental setup and enough voltage, fibers could be obtained from viscous liquids, and eventually the technique was patented in early 19th century [118]. In 1960s, Geoffrey Ingram Taylor described the behavior of liquids under the influence of electrostatic forces which form a cone shaped droplet, later called Taylor cone, that the liquid is ejected in form of fiber [119]. The term electrospinning became popular in 1990s when the number of research conducted on the technique was significantly increased [120]. Today, electrospinning is one of the most widely utilized fiber fabrication techniques, especially of polymers, for applications such as filtration, wound dressing, drug delivery and tissue engineering [64].

2.3.1. Instrumental Setups

Electrospinning technique is based on the electrostatic forces applied by a high voltage generator overcoming the surface tension of a liquid. The instrumental setup basically consists of three main parts; a conductive nozzle or spinneret, a grounded collector and a DC high voltage electrical field generator between two. When a liquid solution fed through the nozzle tip is subjected to high voltage electric field, it becomes charged and a stretched droplet called Taylor cone is formed. At a critical point, the electrostatic forces affecting the solution overpower the surface tension of the droplet and a stream of liquid is ejected. As the jet travels through the gap between the nozzle and the collector, unstable whipping occurs because of the charges migrating to surface of the fiber jet, and causes evaporation of the solvent before solid fibers are deposited on collector [64]. As long as suitable conditions are met, aligned or non-woven continuous bead-free fibers with diameters ranging from nanometer (1-500 nm) to micrometer (1-200 µm) can easily be achieved with electrospinning [121].

The instrumental setup can be classified according to several different criteria; however, the most basic classification can be made based on the layout of the nozzle and the collector which can be either horizontal or vertical (Figure 2.2.a,b) [64].

More sophisticated instrumental layouts can be set with multiple solution feeding nozzles and oscillating/rotating collectors. For instance, an oscillating collector with dual solution nozzle can lead multilayered or mixed collection of different types of fibers on single pass (Figure 2.2.c). This type of setup can be useful for combining multiple types of materials with different properties in one structure to obtain advanced hybrid/composite materials [122]. Electrospinning on stationary or oscillating collectors generally yields non-woven or non-aligned fibers. On the other hand, some applications such as nerve tissue engineering require fiber alignment to guide cells to a specific direction [123]. Therefore, a rotating mandrel is usually utilized as a collector to guide fiber jet to a certain direction (Figure 2.2.d). This rotating mandrel can also oscillate under a dual spinneret system, in order to obtain not only multilayered/mixed but also aligned fibers (Figure 2.2.e) for applications require more complex structures [124].
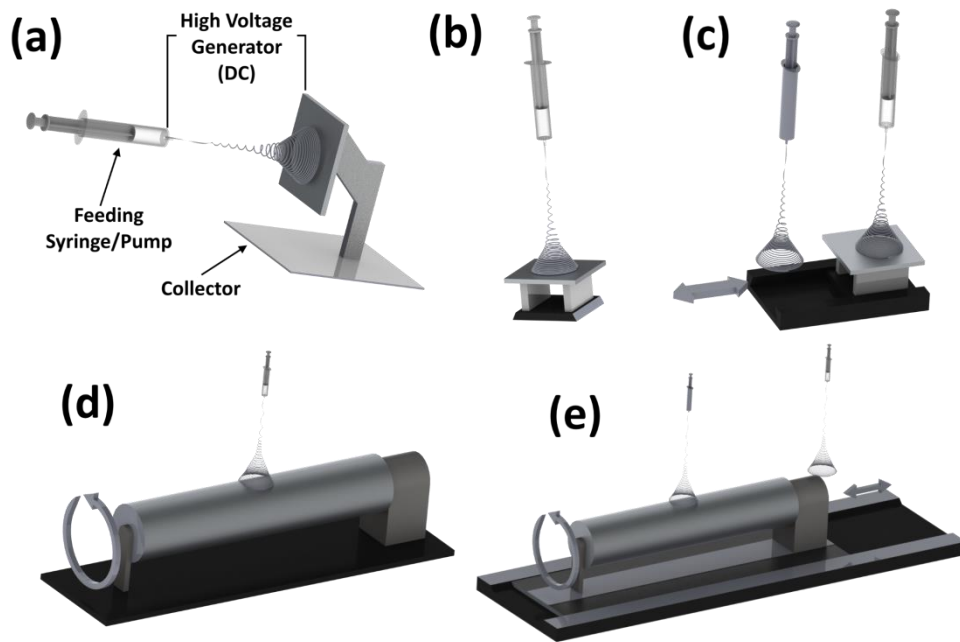
Figure 2.2.   Electrospinning with different layouts; (a) horizontal, (b) vertical, (c) dual spinning system with oscillating collector, (d) single electrospinning on rotating mandrel, (e) dual spinning system with oscillating and rotating mandrel.
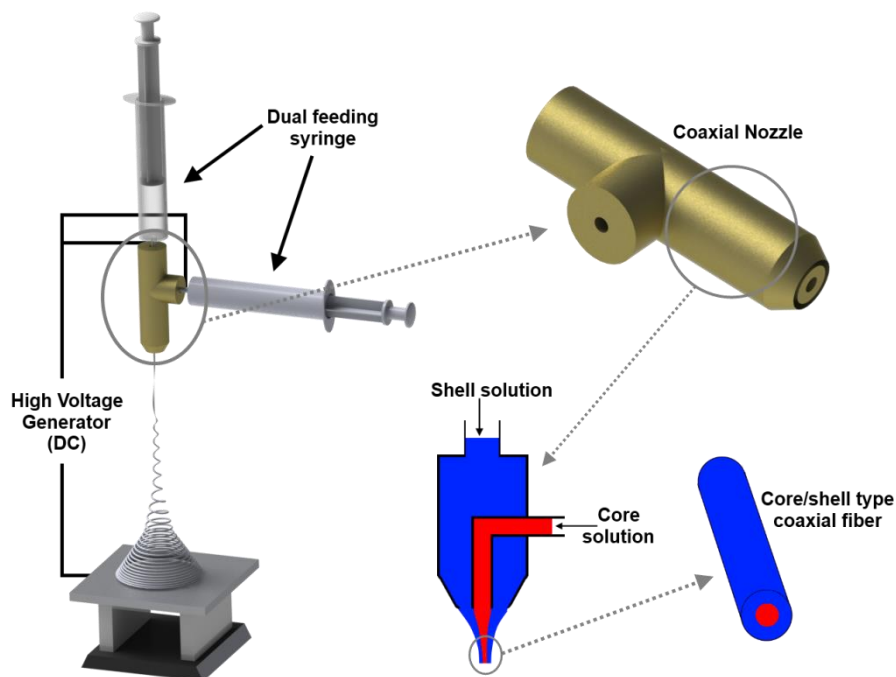
Figure 2.3   Coaxial electrospinning setup and the resulting core-shell fiber.

The nozzle from where the liquid solution is fed can be a syringe or a pipette tip or a specially manufactured spinneret as long as it allows conductivity needed

to create high voltage electric field between the nozzle and the collector. Single orifice nozzles usually lead to continuous fibers of a single material to be fabricated; however, it is also possible to obtain coaxially aligned or core-shell fibers with multiple materials using a specially designed coaxial nozzle (Figure 2.3). In this type of instrumental setup, two different immiscible solutions are fed through the coaxial nozzle at the same time, and the applied voltage stretches both solutions coaxially, resulting a distinctive core-shell separation. Depending on the solution properties of two solutions such as viscosity and conductivity, different core and shell thicknesses can be obtained [125].

2.3.2. Process Parameters

Instrumental setup is an important aspect in obtaining different fiber structures; however, the properties of the fibers collected with different setups depend on the parameters affecting the electrospinning process. These parameters are divided into two main categories of which the solution parameters are divided further into viscosity and conductivity, and the spinning parameters are divided further into magnitude of the electric field applied, nozzle-collector distance and solution feeding rate. Each affects the resulting fiber size, shape as well as continuity [64].

2.3.2.1. Solution Parameters

Viscosity of a solution depends on several factors such as concentration or molecular weight, and is a crucial solution parameter for not only obtaining fibers, but also obtaining continuity in fibers. For instance, concentration of a polymer in a solution must be optimal so that the solution has a viscosity level just enough to be able to be stretched under electrostatic forces applied. Because if the concentration is lower than the minimum value required, the electric field will be too powerful and the solution viscosity will not be high enough to resist stretching, and therefore, electrospraying will occur instead. On the contrary, if the concentration is higher than the optimum range, the stretching resistance of the solution, or in other words viscosity of the solution, will be too high for the electric field to stretch the liquid, and as a result, no fiber formation will be obtained. However, as long as the viscosity is in the optimum

range for spinnability, the fiber diameter depends on the concentration proportionally [126]. Multiple studies in the literature showed that the low solvent content in solutions with high concentration dry faster, leading to thicker fibers, and solutions with higher solvent content remain viscoelastic longer before complete drying and therefore, subjected to thinning of fibers more [127–129]. Molecular weight of a polymer also behaves similar to the concentration when it comes to affecting the rheological properties of a solution. Because, molecular weight affects entanglements and Van der Waals interactions of monomer chains, the repeated subunits of the polymer. Therefore, as the molecular weight increases, the level of entanglement and/or the interaction forces between the chains increases [130, 131]. This result in reduction of chain mobility which in turn, increases the viscosity of the polymer solution. Therefore, molecular weight of the polymer used in electrospinning solution should also be at an optimal range in order to obtain favorable viscosity for a successful electrospinning. However, it should be noted that the optimum molecular weight range highly depends on the polymer type since different polymers have different intra-chain interactions [132, 133]. For instance, synthetic polymers such as PVA or PVP can be electrospun even at molecular weights as high as ~1.3×10^6 [134, 135], whereas natural polymers such as chitosan require very low molecular weights for even being considered as spinnable [136].

Conductivity of the solution is another important solution parameter which depends on the polymer and the solvent used as well as the resulting ion content. As the conductivity increases, the charge carrying capacity of the solution increases and as a result, it becomes more influenced by the electrical field applied and subjected to more stretching. This leads to thinner fiber diameter since conductivity increases jet instability and solvent evaporation [64]. Baumgarten suggested a relation between fiber diameter and conductivity where the fiber diameter is inversely proportional to cube root of solution conductivity [137]. Conductivity, similar to other solution parameters, should be at an optimum range since low conductivity will result in insufficient elongation and bead formation whereas high conductivity causes severe jet instability and varied fiber diameter distribution [138, 139]. Apart from the type of polymer and solvent used as well as their concentrations in the solution, addition of salts

such as NaCl can increase charge carrying ion concentration and provide adjustable conductivity for a solution that has low or no conductivity as Beachley and Wen showed [128].

2.3.2.2. Spinning Parameters

Spinning parameters are mostly related to the capacity of the electrospinning instrument. The magnitude of the electric field applied, the distance between the nozzle and the collector, and solution feeding rate are three major spinning parameters that affect the final fiber size and morphology.

The electric field voltage applied is generally in the range of kV and should be strong enough to overcome the surface tension of the spinning solution. However, the effect of voltage on the fiber diameter is debated amongst the researchers since there are studies that showed the level of electric field has no significant effect on fiber diameter [132] whereas there are authors reported that as the voltage increases, the fiber diameter increases due to the increase in the amount of solution ejected [140] or decreases due to the increase in stretching, jet instability and solvent evaporation [141]. The effect of voltage on bead formation is also disputed, and contrary studies exist, some of which argue that high voltage causes beads because more solution is ejected while others support the opposite because low voltage fails to stretch the solution enough to form fine fibers [130, 142].

On the other hand, the gap between the nozzle and the collector affects the fiber diameter in inverse proportion. As the distance increases, the polymer jet is subjected to longer stretching, evaporation time and jet instability all of which result in deposition of finer and thinner fiber on the collector [141]. However, an optimal distance range is required since short distances can cause bead formation due to lack of evaporation, and unfavorably long distances can weaken the electrostatic forces that fail to eject the solution from nozzle tip [143]. Nevertheless, the optimal distance range depends on the polymer type and solution properties [144, 145].

Solution feeding in electrospinning process is not a mandatory feature but may

be favorable in some cases, depending on the instrumental setup. For instance, in vertical electrospinning layouts, it is possible to have feeding from a nozzle on top to a bottom collector or from a nozzle at the bottom to a collector on top. Therefore depending on this layout, the solution is fed against or in direction to the gravitational force. As a result, an additional feeder component such as a syringe pump may be required to assist the feeding [64]. Also, highly viscous solutions or solutions with short span of curing may require additional feeding to maintain liquid Taylor cone. However, if the solution is already viscous and conductive enough to be electrospun, high feeding rate can cause bead formation due to lack of solvent evaporation [143, 146]. Therefore, feeding rate slow enough to allow sufficient evaporation is desired for finer and thinner fibers [147].

2.3.3. Materials Used

Electrospinning gained wide attention in the past few decades, because it is the most versatile, low-cost, easy to use fiber fabrication technique in which a vast number of materials, mostly polymers, can be utilized in different structures and properties [64]. More than 200 electrospun synthetic and natural polymers as well as their combinations have been reported in the literature [148]. It is also possible to utilize other types of materials such as ceramics or metals, as long as a spinnable solution can be obtained or the raw materials are soluble in polymer solutions. Last but not least, therapeutic agents such as drugs, growth factors or even live cells can also be electrospun by incorporating with polymer solutions that act as carrier [64].

A significant number of studies that focused on electrospinning contain polymers, since it is easy to obtain them in solution form. Various synthetic and natural polymers can be utilized to obtain several different structures, by using different electrospinning setups, for applications such as filtration, wound dressing, drug delivery and tissue engineering. Various state of art examples include synthetic polymers such as PGA [149], PLGA [150], PCL [151], PLLA [152], PU [153], PVA [154], P(LLA-CL) [155] and PELCL [156], and natural polymers such as cellulose acetate [157], silk fibroin [158], chitosan [154], gelatin [159], hyaluronic acid [160] and collagen [161]. Polysaccharides such as

22

alginates, starch and dextran can also be electrospun with the help of other spinnable natural or synthetic polymers [162–167].

Since electrospun fibrous structures provide high surface area, and it is possible to utilize a vast number of degradable polymers with this technique, the incorporation of therapeutic agents into the electrospun structures is one of the recent approaches that gained interest amongst the researchers in biomedical field [64]. The most common strategies for therapeutic incorporation are direct blending of agents with polymer solutions, encapsulation of agents in polymer structure or core-shell electrospinning where shell polymer act as a reservoir and contains the agents in the core. Several anti-biotic, anti-tumorigenic, anti-coagulant, anti-viral, immunomodulatory and anti-inflammatory agents as well as vitamins, growth factors and plasmids such as fenbufen [168], ketoprofen [169], salicylic acid [170], ferulic acid [171], feruloyl-oleyl-glycerol [172], ibuprofen [173], acyclovir [174], captopril [175], acetazolamide [176], timolol maleate [176], lactobacillus [177], Vitamin B12 [178], camptothecin [179], shikonin [180], metronidazole benzoate [181], paclitaxel [182], doxorubicin [183], nifedipine [184], fusidic acid [185], FNIII$_1$-derived P12 (hydrophilic peptide) [186], basic fibroblast growth factor [187], nerve growth factor [154], vascular endothelial growth factor [188], platelet-derived growth factor [189], adenovirus (type V) [190], pDNA [191], bone morphogenetic protein-2 [192] and lactate dehydrogenase [193] have been reported as a part of electrospun structures, in recent years.

2.3.4. Applications

The electrospinning technique has gained a wide interest among the researchers since its development in 60s, especially in the last few decades. Because, the technique enables researchers to create fibrous structures with different fiber sizes and orientation as well as pore sizes and shapes. The gained attention of the technique comes from the usefulness of the fibrous structures for different types of applications. There are several applications that can benefit from a fibrous network. Since different applications require different types of fibrous networks, a technique such as the electrospinning which can easily alter the state of the fibers in the network is very beneficial in creating

different products for different applications. This ability combined with the possibility of using a wide variety of materials during the processing is the reason the electrospinning has a great interest in research still to this day [64, 120, 126, 194].

There are several aspects of an electrospun structure that can be beneficial to different types of applications. For instance, porosity is highly desired for particle filtration of liquids. The fibrous networks can be selectively permeable to solid particles based on the pore size distribution of the network. Since it is very easy to adjust the pore size of a fibrous network fabricated by electrospinning by adjusting several solution and/or process parameters, it is possible to easily create a filtration membrane based on the particle size [195]. However, the filtration ability of a fibrous network does not rely only on the physical structure of the fibers. It is also possible to create a fibrous network with functionalized fibers in which the fiber surfaces contain chemical/biological substances that act as catalyst or inhibitor to different types of contents of a liquid medium [196, 197]. Since the electrospinning technique benefits from the ability to utilize a wide range of not only base materials such as polymers, but also other types of highly reactive chemical and biological molecules, it is also possible to create a filtration system based on the chemical/biological content. Another widely studied application that can benefit highly from a fibrous network is tissue engineering [64]. In tissue engineering, the goal is to create a supporting material called scaffold for live cells during a healing process of a damaged tissue. Because animal cells are anchorage dependent which means they require solid attachment points or areas in order to divide, proliferate, grow and/or function. Therefore, they require a 3D network of supporting material around them at all times. Normally, this supporting material is synthesized by the surrounding cells in the natural tissue and called ECM [198]. The structure of the ECM highly resembles the non-woven fibrous structures obtained with the electrospinning technique. Therefore, by utilizing different types of base materials, it is possible to create an artificial tissue engineering scaffold that mimics the natural supporting material of biological tissues. The obtained fibrous structures can contain either aligned or non-woven fibers where it is also possible to adjust the fiber and pore size so that the structure become suitable

for different types of cells in human body that have different sizes and shapes [199–202]. Drug delivery/release systems are also another application area that can utilize electrospun fibrous mats. Drug delivery or release is basically the expression of therapeutic agents to a targeted location in the body with a controlled behavior so that the therapeutic component remains effective without showing any kind of toxicity to the healthy tissues and cells. Since these therapeutic components are usually foreign to the body, a biocompatible carrier is generally used to contain these components and prevent the immune system from metabolizing them before they affect the required location [174, 203, 204]. Because electrospun fibrous structures have high surface area to volume ratio, mats prepared with this technique have more surfaces to interact with the tissue implanted, therefore, it is possible to adjust the drug release behavior by adjusting the surface area which can easily be possible with fiber diameter and pore size [205, 206]. Also, since the electrospinning utilizes a solution to fabricate the fibrous structures, a wide variety of biocompatible materials as carrier and chemical/biological components as therapeutic agents can be used to create a drug delivery/release mats [64]. Another application type that benefits from the electrospun fibrous structures is wound dressing in which a fibrous mat is basically used as an ex vivo tissue engineering scaffold. In wound dressing, the main goal is to protect an external injury site from pathogens and to prevent loss of humidity as well as sustenance, both of which required for a proper healing [207]. The electrospun fibrous mats can act as a selective barrier for maintaining the humidity as well as transferring the sustenance, gases and waste while preventing exogenous pathogens from entering the wound site [208, 209]. Because of the ability to adjust the porosity/pore size in between the fibers by using the electrospinning parameters is relatively easy, this technique can widely be utilized to create dressing structures for different types of wounds/tissues. It is also possible to incorporate anti-pathogenic substances into the designed dressing material with this technique so that the fibrous mats not only act as a barrier but also actively kill the pathogens, increasing the protection effectiveness of the dressing material [210, 211]. Besides from the widely studied application areas, the mats fabricated with electrospinning technique can also be used as reinforcement in composites, especially in polymer composites. Once the electrospun fibers are properly dried, it is

possible to use those dried fibrous network inside of a bulk polymer, in which the mechanical support provided by the fibers can enhance the mechanical behavior of the bulk polymer as long as the dried fibers are not affected by the solution of the bulk polymer [99].

2.4. Magnesium and Magnesium Alloys

Magnesium is an alkaline earth metal, abundantly found in the universe (9th most found) as well as in the Earth (3rd most found in seawater, 8th most found in the crust, 4th most found overall). More than 50 naturally occurring minerals are documented for magnesium, of which the most commercially important ones are carnallite, brucite, magnesite and dolomite. Magnesium is also the 4th most abundant metallic element found in the human body with an approximate concentration of 0.5 g per kg of body weight. It is one of the essential nutritional elements in a healthy adult that involves in functioning of brain, heart and skeletal muscles. It is also the 2nd most positively charged ion found in intracellular fluids. Magnesium is also crucial in activation for more than 500 enzymatic processes that use phosphorus for energy metabolism such as ATPase, glycolysis or protein synthesis, and known to be a useful supplement for treating medical conditions such as cardiovascular diseases, arrhythmias, dyspepsia, headaches, dysmenorrhea, eclampsia and asthma [212]. Abnormal levels or lack of magnesium, called hypomagnesemia which can also be hereditary, can affect almost any organ in the body, creating mild to life-threatening complications. The recommended daily intake dosage is 240–420 mg.day^{-1} [213]. It is a very lightweight and elastic material which has a density (1.74 g/cm^3) and Young's modulus (41–45 GPa) close to human bone (1.75 g/cm^3 and 40–57 GPa) [214]. It has a systemic toxicity level of 0.7-1 milimol per L (serum) (or 1.7–2.4 mg/dL) and therefore, is not toxic except local conditions [8]. It is also electrically and thermally conductive which is known to enhance cell biocompatibility of several tissues such as cardiovascular and orthopedic tissues [215]. Therefore, magnesium based alloys have gained a wide interest in biomedical field in the last few decades. The only downside of the Mg-based alloys is that the degradation rate is very high, especially in dynamic conditions such as blood vessels, which causes local toxicity, loss of mechanical integrity and failure in catching up the healing rate. Several solutions have been

proposed to overcome these issues, from coatings to micro-arc oxidation, which showed promising results in several recent studies [216–219]. For instance, micro-arc oxidation is a technique that resembles anodizing in which localized plasma created by high voltage potential generate a thick protective oxide layer on the surface. In aqueous or humid environments, magnesium and its alloys are highly prone to galvanic or pitting corrosion. Similar to aluminum, which naturally forms a thin protective oxide layer on its surface (passivation), magnesium and its alloys also have this capability at some extent, but still require additional processes for protection purposes. Since micro-arc oxidation technique can create a durable, wear-resistant and thick oxide layer efficiently with low cost, it is one of the most studied methods for improving the corrosion resistance of magnesium. This technique can also be used for other alloys such as aluminum or titanium in order to improve weak corrosion and wear resistances [220, 221].

Magnesium alloys are designated with an international code adopted by ASTM International. This code generally presented as two letters followed by two numbers. The letters represent the two main alloying elements (Table 2.1). The alloying element with higher composition in the alloy is written first. However, if both of the main alloying elements are equally present in the alloy in terms of composition, the letters presenting the elements are written alphabetically. The numbers in the code, on the other hand, represent the nominal compositions of these two elements. These numbers are written as single digit integers by rounding off the composition values in terms of weight per cent. For instance, AZ91 is a magnesium alloy containing primarily aluminum and zinc. However, even though the numbers corresponding to the compositions are given as 9 and 1, the accurate values are between 8.3-9.7 wt.% for aluminum and 0.4-1.0 wt.% for zinc. This coding system and similar designations are used commonly not only for magnesium alloys but also for other types of alloys and it is very convenient for recognizing the alloys quickly in documentation and labeling. However, this type of coding generally limits the information regarding the other alloying elements present in the alloy. Standard alphabetic letters are also used as suffix to these codes to indicate composition variations or purity. The coding system for heat treated or work hardened magnesium alloys are similar to those

used for aluminum alloys [222].

Table 2.1. Some of the main lettering used for identification of magnesium alloys.

Letter(s)	Corresponding information	Letter(s)	Corresponding information
A	Aluminum	Q	Silver
B	Bismuth	R	Chromium
C	Copper	S	Silicon
D	Cadmium	T	Tin
E	Rare Earths	W	Yttrium
F	Iron	Y	Antimony
H	Thorium	Z	Zinc
K	Zirconium	A, B, C, etc.*	Composition variation or purity
L	Lithium	X*	Experimental
M	Manganese	T5*	Artificially aged after casting
N	Nickel	T6*	Solution treated, quenched, artificially aged
P	Lead	T7*	Solution treated, stabilized

* Used as suffix to the main designation code.

2.4.1. Traditional Fabrication Methods

Magnesium alloys are generally classified as cast alloys and wrought alloys. However, more than 90% of magnesium alloys are fabricated conventionally with casting, especially by various die-casting methods. Cast alloys are the

majority of the European magnesium products covering 85-90% of the market. The earliest commercial magnesium alloy was produced with aluminum and zinc which is still the most used cast alloy. On the other hand, magnesium alloyed with 1.5 wt.% manganese was the first wrought alloy developed. It was widely used as sheet metal and suitable for extrusion or forging but eventually succeeded with more advance wrought alloys [222].

Magnesium cast alloys are mainly fabricated with die-casting methods. Especially high pressure die-casting allows the usage of cold chambers for larger parts. Because of the possibility to obtain pressures higher than 100 MPa, molten alloy weighing more than tens of kilograms can be fed into the die cavity less than a second. On the other hand, majority of the magnesium applications require small parts and therefore, short die-casting cycles in order to lower the cost. As a result hot chamber die-casting are utilized instead [223]. The fabrication of magnesium alloys via die-casting methods is especially advantageous because of the nature of magnesium as well as its alloys. For instance, most of the magnesium alloys are usually easy to cast at high pressures for complex and/or thin shapes because of the fluid nature of molten alloy and low density of magnesium. Magnesium alloys also cool rapidly because of the low specific heat of magnesium element. This ability particularly contributes to shorter casting cycles which in turn reduce the cost significantly in terms of fabrication rate and die maintenance. Another important aspect that significantly contributes to shorter die-casting cycles is the usage of iron-based casting dies. Iron is usually not soluble in molten magnesium alloys. Therefore, cast magnesium alloy parts tend to not adhere to the die surface which increases the efficiency of the die-casting cycle.

Apart from die-casting, sand casting or gravity casting are two other methods that are used for fabrication of magnesium parts [224]. However, magnesium is a highly reactive material. Therefore, oxidation and/or slag formation can occur because of the turbulent flow caused by conventional pouring techniques used in these casting methods. In order to counteract this problem, a bottom filling technique has been developed and widely used for automotive wheel fabrication, even to this day. In this technique, the mold is filled unidirectionally

from the bottom with a controlled pressure to prevent turbulence [225].

There are other techniques used for fabrication of high quality products such as squeeze casting or thixotropic casting. Squeeze casting is generally used for alloys and shapes that are not possible to fabricate with conventional casting methods. For instance the magnesium alloy containing 12% Zn, 1% Cu and 1% Si which has very good mechanical properties (yield stress: 200 MPa) up to 200°C, can easily be cast with this method [226]. Thixotropic casting, on the other hand, is an alternative to high pressure die-casting. The technique basically utilizes the semi-solid form of the alloy, generally just below the melting temperature. Then, this pasty semi-solid is injected into the die with high torque using a screw mechanism similar to the injection systems used for plastics. It is possible to obtain magnesium alloys with fine grains at a relatively reduced cost which can provide significant improvement of the alloy toughness [227].

Magnesium has hexagonal crystal structure. Therefore, the deformation capacity is limited, especially at low temperatures. The deformation mechanism at these temperatures is mostly slip and twinning on <1120> direction family and {1012} plane family. However, the deformation is only possible as compression or tension depending on whether the stress is parallel or perpendicular. On the other hand, at elevated temperatures, the deformation also occurs as slip on {1011} plane family. Therefore, the deformation becomes easier, making hot working a more preferred fabrication method for wrought magnesium alloys [228]. As a result, hot working techniques such as extrusion, rolling or forging are the major production techniques used for wrought magnesium alloys [229, 230]. There is various magnesium alloys that can be classified as wrought. For instance, aluminum, zinc and manganese containing AZ31 has good strength, ductility and corrosion resistance, and therefore is one of the widely used wrought magnesium alloys. HM21 is another wrought magnesium alloy that contains thorium and has good creep resistance at elevated temperatures [231, 232]. Magnesium alloys such as aluminum, zinc and manganese containing AZ81, zinc and zirconium containing ZK61, and zinc, copper and manganese containing ZCM711 are amongst the high strength

wrought alloys that are equivalent to aluminum wrought alloys with similar strength-to-weight ratio [233–235]. Zinc and manganese containing ZM21 is the cheapest wrought magnesium alloy that can be fabricated with high speed extrusion [236]. Similar to HM21, HM31 which is another wrought magnesium alloy that contains thorium, has the most optimum mechanical properties at high temperatures [237]. Even though extrusion and rolling are much more common, it is also possible to forge magnesium wrought alloys, and the compositions of forgeable alloys are similar to the magnesium alloys mentioned previously. But it is often a common practice to subject the alloy to a certain level of extrusion beforehand in order to obtain refined microstructures, and press forming is the most common forging method applied [238].

2.4.2. Applications

Magnesium alloys has gained increasing attention over the past decade because of its mechanical properties, electrical and thermal conductivity, dimensional stability, damping capacity, lightness and recyclability [239]. Especially in industries such as aerospace, automotive, electronic consumer products and biomedical applications, where low weight is crucial along with high mechanical resistance at high temperatures [240]. Conventionally, the most used alloy in order to meet high mechanical requirements is steel. However, as much as several steels provide superior mechanical properties, they have a disadvantage of being quite heavy for many types of applications. Novel alloys such as magnesium alloys provide lighter solutions at a cost of reduced mechanical properties compared to steels. However, since higher does not always mean better for some applications, such as biomedical devices, the most important point is to create a balance between the weight and the durability without compromising the minimum mechanical requirements. As a result, magnesium alloys have gained a widespread attention, especially in biomedical field, for the last decade [241].

The magnesium alloys are significantly used in automotive industry such as cast engine and transmission housings as well as other automobile components such as clutch housings, oil pans, steering columns, cylinder blocks, case housings, oil sumps, valve covers, air cleaners, camshaft covers, induction

covers, clutch/brake pedals, steering column brackets, drive brackets, seat frames, wheels, cylinder head covers, steering wheels, front cover assemblies with the majority of these parts are fabricated from AZ91 alloy [242]. Appliances and sporting goods are the other main applications in which magnesium alloys are trending. Die-cast magnesium alloys has also seen an increasing attention in applications such as computer and mobile phone cases/housings which require low weight, low wall thickness and electromagnetic shielding [243–245].

Another important application area of magnesium is aerospace industry. The aerospace industry has always been known to seek the reduction of weight in order to lower the cost of operation and increase the efficiency of the aircraft without sacrificing the safety. Magnesium is one of the lightest materials that can be utilized as a structural material. It has low specific gravity (~1.74) compared to other possible metals used in aerospace industry such as aluminum (~2.5-2.8) or steel (~7.8-7.9). Magnesium is also on a similar level with other structural materials in terms of strength, stiffness, thermal and dampening properties [246]. In the second half of the 19th century, magnesium has been widely used for various types of both military and civilian aircrafts. The majority of the usage during that period was used to be mainly as a structural component. However, similar to the automotive industry, it has also been widely used as housings, cases, component covers, transmission and gears. Alloys such as ZE41, QE22 or WE43 are few of the most utilized low-weight Mg-based component materials in aerospace industry [247]. The main disadvantages that limit the usage of magnesium alloys are its corrosion behavior and its potential flammability/ignition. Typical ignition temperature of magnesium was determined around 400°C, as reported by multiple studies and can be improved up to ~800°C with proper alloying [248]. Same alloying approach was also beneficial in providing corrosion resistance behavior to magnesium alloys. Aluminum, zirconium and manganese are major alloy elements used to fabricate magnesium alloys with finer grains and better corrosion performance [249].

Majority of the biomedical applications that utilized Mg-based alloys comprised of cardiovascular applications such as stents and shunts, and orthopedic

applications such as implants and screws [250]. For instance, Heublein et al. was first to show the possibility of AE21 Mg-alloy used as a coronary stent. The radial support was found to be good and no thromboembolic occurrences observed initially with pig models [251]. However, also the first major setback of Mg-alloys as a biomedical application mentioned above, the high degradation rate, was also observed. Biotronik, one of the major companies that specialized in stent applications of Mg-alloys, fabricated a WE43 stent that reached clinical trials after successful in vitro animal testing in following years [9]. Di Mario et.al. also successfully implanted Biotronik Mg-based absorbable metallic stents into below-knee lesions of 20 patients which degraded completely in 6 weeks without any toxic reaction [252]. Zartner et.al. successfully carried out the first implantation of magnesium alloy stents into pulmonary artery in 2005, in which the level of magnesium in serum was found to be slightly higher (1.7 milimol/L) than the normal range on the first day but returned to within the normal range on the second day [253]. The results showed continuous reperfusion over 4 months and the stent was completely degraded in 5 months. In 2007, an extensive clinical trial was conducted in 8 centers with 63 patients, in which no infarction, thrombosis or patient loss observed [254]. Further advancements were obtained with drug eluding Mg-alloy stents loaded with antiproliferative drug, and Haude et al. conducted clinical trials for 12 months in 5 centers with 46 patients without any cardiac death or scaffold thrombosis [255].

Magnesium were first attempted to use as orthopedic implant in the beginning of 1900s. Lambotte used pure magnesium plates and gold-coated steel nails for fixation of a leg bone fracture in 1907. However in vivo corrosion of pure magnesium was found to be too rapid, and the plates degraded in less than two weeks generating high amount of gas under the skin, failing the magnesium as an implant [214]. Various magnesium alloys were researched in vitro/in vivo ever since to improve the corrosion resistance and mechanical strength of potential magnesium implants [8, 215, 241, 256]. In 1944, a magnesium-cadmium alloy was tried as plate and screw for fracture fixation on 34 patients. Any hydrogen accumulation as a result of corrosion was removed with subcutaneous needles. The authors, Troitskii and Tsitrin, reported that nine attempts were failed due to infection and lack of gas removal as a result of

orthopedic cast fixation. However, improvement in fracture healing was observed without any significant inflammation or any increase of magnesium in serum, and the implants kept their structural integrity up to 2 months. On the other hand, it was found that some of the implants could not survive more than a month because of the acidic accumulation on fracture site, but in general the material was degraded completely in one year. Similarly, a magnesium-aluminum alloy was utilized in 2 patients for fractures caused by gunshot in 1945. Znamenski reported that the fracture healing was completed in 6 weeks where plates and pins used were completely resorbed after a month [257]. Mg-Al-Mn screws, pegs and plates were also utilized as fracture/bone grafting for twenty patients by McBride. The results showed no improvement in cancellous bones but distinctive improvement in periosteum and callus ossification/deposits without any systemic reaction and/or inflammation at the implantation site. It is also concluded that even though trauma could increase the degradation rate, the alloy would definitely degrade no more than four months [258]. These initial attempts and studies showed that magnesium alloys are not significantly toxic and could be a potential candidate for stimulating the healing process in bone tissue engineering. However, it has been widely agreed in the literature that at least 3 months are required for an implant to retain its integrity for a sufficient healing process. Therefore, the fast corrosion rate of these early magnesium-based implants should be improved with further alloying. It has been found that complex alloys, especially alloyed with rare-earth elements even at amounts less than 4%, could significantly improve the resistance. The studies showed that a magnesium alloy containing rare-earth elements (<4 wt.%), cadmium (<1 wt.%), calcium/aluminum (<1 wt.%) and manganese, silver, zirconium or silicon (trace amounts). Stroganov et al. found that orthopedic pins fabricated with this type of alloy had significantly improved corrosion resistance, and showed in vivo degradation times depending on the size of the pin, between 20 weeks and 44 weeks for 3.0 mm and 8.0 mm pins, respectively. However, it should be noted that the study did not consider the potential toxicity of the elements or the duration of structural integrity [257]. In orthopedic field of medicine, fixtures such as plates, screws, pins, nails, wires and/or needles were used to treat a significant number of broken bones every year in vivo. Magnesium alloys such as ZEK 100 [259], LAE442 [260], MgCa0.8 [261] and MgYREZr [262] have

been tested with animal models as well as clinical trials for 12 months and found to have osteogenetic ability. One of the major findings in these studies was that MgCa0.8 has stronger bone-implant interface than LAE442, which was also comparable with clinically accepted S316L screws [261]. In a 6 month clinical trial, another magnesium alloy with trademark name MAGNEZIX®, which is an MgYREZr alloy, showed no foreign-body response, osteolysis or systemic inflammation; and therefore, was found to be equivalent to clinically accepted titanium screws widely used in the market [263].

2.4.3. WE43 Alloy

WE43 is rare earth magnesium alloy having a composition around 92-94 wt.% magnesium, 4-4.2 wt.% yttrium, 2.25-2.3 wt.% neodymium and 0.15-0.6 wt.% zirconium with a density of ~1.8 g/cm^3 and a melting point between 550-650°C [264]. It has a particular attention amongst the researchers because of its good castability, mechanical properties and lightness which makes this alloy a good candidate for applications require feasible and mass fabrication as well as specific strength and specific stiffness, such as aerospace, automotive and biomedical industry [265–267]. These properties are the result of densely packed fine precipitations in the microstructure which also provides good creep and corrosion resistance up to elevated temperatures [268]. According to the multiple studies in the literature, WE43 has yield strength (nominal) between 150-270 MPa, Young's modulus around ~45 GPa, ultimate tensile strength (nominal) between 220-320 MPa, ductility (nominal) between 1.0-15.0% and hardness (Vickers) between 90-120, based on the manufacturing method as well as consequent treatments and the resulting grain size, structure and texture [266, 268–274]. The alloy also has a coefficient of linear thermal expansion around ~26 μm/m°C, a thermal conductivity of ~51 W/mK, an electrical conductivity around 6.8x10^6 S/m. As it can be seen, WE43 has moderate thermal and electrical conductivity as well as thermal expansion capacity which, when combined with its lightweight structure and good mechanical properties, provide unusual benefits for complex parts and components in a wide variety of applications.

Another important aspect that is needed to be mentioned is the toxicity of the

alloying elements in WE43. As a rare earth magnesium alloy, WE43 contains two rare earth elements, yttrium and neodymium, with a combined composition of more than 6%. There is no definitive toxicity research indicating significant toxic behavior of both of these elements, however, rare earth elements have been known to cause low to moderate toxicity if not handled properly and/or exposed long terms. On the other hand, there is also no report of cytotoxicity associated to these elements when used for alloying as a part of WE43 alloy, and therefore generally considered safe [275]. However, the 4th alloying element of WE43, zirconium, has been extensively investigated for toxicity in the literature. It is known to be present in human body up to 250 mg and recommended as a part of dietary daily intake as well as widely used for dental/skeletal implants, prosthetics and dialysis. Therefore, zirconium is widely accepted as a biocompatible, non-toxic element.

3. MATERIALS AND METHODS

3.1. Materials

PVP (MW $\approx$ 1.3 x 10^6 g/mol), PVA (MW $\approx$ 8.5-12.4 x 10^5 g/mol), $Mg(NO_3)_2.6H_2O$, $Y(NO_3)_3.6H_2O$, $Nd(NO_3)_3.6H_2O$, $ZrO(NO_3)_2.xH_2O$, PBS, lysozyme (from egg white), BSA, DMEM/F12, penicillin, streptomycin, FBS, MTT, ethanol (99.99%, v/v), paraformaldehyde, DMSO, hexamethyldisilazane, Triton X-100 and L-glutamine were purchased from Merck (Germany). AF-488 and DRAQ5 was obtained from Thermo Fisher Scientific (USA). All of these chemicals and biochemicals were purchased as either research grade and/or cell culture grade. Therefore, no further sterilization or purification was carried out.

3.2. Fibrous WE43 Magnesium Alloy-Like Compounds

In the initial step of this study, the fabrication of WE43 magnesium alloy-like compound was carried out. In order to obtain suitable porosity level (5-30 µm, preferably 10-20 µm) that meets the nerve guidance conduit requirements, electrospinning, a low cost fabrication technique that provides porosity control easily was chosen, and the solution as well as the process parameters were optimized in order to obtain the desired porosity. After the electrospinning step, the samples fabricated with optimized parameters were calcinated in order to remove residual solvents and organic/polymeric components while crystallizing the metallic components into an alloy-like compound.

3.2.1. Preparation of Electrospinning Solutions

The targeted WE43 alloy has a composition of 93.6% Mg, 4% Y, 2.25% Nd and 0.15% Zr. The solution for electrospinning of the alloy-like compound was prepared by solving nitrate salts of each alloy component with distilled water. Therefore, to achieve the same composition with WE43 alloy, $Mg(NO_3)_2.6H_2O$, $Y(NO_3)_3.6H_2O$, $Nd(NO_3)_3.6H_2O$ and $ZrO(NO_3)_2.xH_2O$ were weighed according to the corresponding stoichiometric ratio of Mg, Y, Nd and Zr, respectively, and dissolved with distilled water. Additionally, since the aqueous solutions of nitrate salts have extremely low viscosity therefore not suitable for electrospinning, a

polymer, generally PVA or PVP is dissolved with nitrate salts using water/ethanol solvent in order to adjust the viscosity of the solution for continuous spinnability. In this study, the solution parameter, viscosity, was adjusted with different concentrations of PVA or PVP as well as different solvent concentrations of water/ethanol mixture. Since the nitrate salt concentrations were calculated according to the stoichiometric ratio of the target alloy, the only solution parameter to be optimized was the viscosity depending on the polymer concentration and solvent concentration. Therefore, the optimization of these parameters were carried out by naked-eye observations of solution preparation in this section as well as the observations of the electrospinning and SEM images obtained from electrospun samples which were both carried out in the following sections.

3.2.2. Electrospinning of WE43 Magnesium Alloy-Like Compounds

The electrospinning of the prepared solutions were carried out with a vertical single nozzle electrospinner (Inovenso NE200, Turkey) at an ambient temperature of 24°C and 35% relative humidity using a copper nozzle with 0.9 mm inner diameter. Different applied voltages, nozzle-collector distances and solution feeding rates were used for electrospinning of the solutions with different viscosity. Since these three process parameters as well as the viscosity of the spinning solution affect the fiber thickness, the interfiber distances, which can be interpreted as pore size, will also be affected depending on the optimizations. For instance lower viscosity and/or higher voltages, further distances and lower feeding rates cause thinner fiber deposition because of higher stretching of jet, more evaporation of solvent and low amount of solution fed, respectively. As a result of thinner fiber deposition, higher pore sizes can be achieved. Therefore, the optimizations of these parameters are crucial for obtaining a desired porosity level. In this study, the optimizations were carried out; first with the naked eye observations based on continuous spinnability, and then with SEM images obtained from the electrospun samples based on fiber thickness and the resulting interfiber pore sizes, until samples with continuous, bead-free fibers and desired porosity level were achieved.

3.2.3. Calcination of Electrospun Alloy-Like Compound

In this part of the study, in order to remove residual solvents, other organic components and the polymer used to control viscosity of the electrospinning solution as well as to crystallize the alloy-like compounds, the electrospun samples were calcinated. Since the water affinity of the nitrate compounds of metals is high, when dissolved in aqueous solvents they decompose into oxide compound, oxygen and nitrogen oxide instead of dehydration as in the following reaction; $M(NO_3)_X \rightarrow MO + NO_2 + O_2$ (Non-stoichiometric representation, M: metallic element). Therefore, a WE43 magnesium alloy-like compound with a formula $Mg_aY_bNd_cZr_dO_x$ was expected after this calcination process.

In the literature, studies conducted for similar alloy-like compounds utilized calcination temperatures between 500-1100°C. The alloy-like compound targeted in this study, has composition similar to commercial WE43 alloy which contains mainly magnesium element (>93%). Magnesium is an element with high oxygen affinity and therefore, a protective oxide layer is formed on the surface of WE43 alloy. This protective layer retains its stability and protection up to the eutectic temperature of the alloy, according to the literature. Since the eutectic temperature and the melting temperature of WE43 alloy are ~540°C and ~650°C, respectively, and based on the studies in the literature related to the thermal analysis of WE43 alloy, the calcination temperature used in this study was planned to be between 300-500°C. However, the exact calcination profile, in terms of temperatures as well as durations, were determined according to the DTA/TG analysis conducted with the samples successfully electrospun with the optimized parameters for desired porosity.

Additionally, since a polymer was used in order to control the viscosity of the electrospinning solution, the resulting continuous fibers were expected to be structurally smooth. However, after the calcination process, as a result of the removal of the polymer from the structure, the structure was expected to have rough surfaced crystalline fibers, which were also expected to affect the final fiber diameter and pore size.

On the other hand, the duration of calcination process was determined

according to the approach proposed by Zivkovic and Dobovisek [276]. Briefly, it is possible to calculate reaction kinetics from thermal analyses by using first-order reaction rate and Arrhenius equation. The first-order reaction is represented with the following equation;

$$\ln\left(\frac{a}{a-x}\right) = k.t \qquad \text{Eq. (1)}$$

where a is the initial concentration of the reactants and x is the amount of materials reacted after a time t, both in terms of moles, and k represents the rate of reaction. The k in this equation can also be expressed with Arrhenius equation;

$$k = Ae^{-E/RT} \qquad \text{Eq. (2)}$$

where E, A, R and T are activation energy, pre-exponential factor (or frequency factor), gas constant and temperature in K, respectively. If two equations are combined and rearranged, the following equation can be written:

$$\log\left[\frac{\ln(a/a-x)}{t}\right] = \log A - \frac{E}{2.303RT} \qquad \text{Eq. (3)}$$

The initial concentration, a, and the amount reacted after a certain time, x, can also be expressed as the area under the DTA peak of the reaction in concern where a is the area under the peak up to maximum peak point (designated as S) and x is the area under the peak after a certain reaction time (designated as S_t). Therefore the equation becomes;

$$\log\left[\frac{\ln(S/S-S_t)}{t}\right] = \log A - \frac{E}{2.303RT} \qquad \text{Eq. (4)}$$

As a result, the slope of a straight plot line obtained with log [ln (S / S-S_t) / t] vs 1/T graph can give theoretical estimation about activation energy and pre-exponential factor for the reaction. Finally, it is possible to estimate the reaction time necessary to complete a reaction up to 99.99% using these data, or in case of this study, the time required to calcinate the components at a certain temperature. Therefore, this mathematical approach was applied to the significant peaks obtained from DTA/TG analyses of the samples in order to predict the duration of the calcination steps. The area under the corresponding peaks was determined by using Riemann sum approach which is a mathematical approximation of an integral (area under the curve) by dividing the

area under into calculable shapes such as rectangular and adding the area of these shapes to find the final area in which by decreasing the size of the shapes, it is possible to have a good approximation of an area under a curve. Therefore, in order to obtain the target pore size, both electrospinning parameters as well as calcination parameters were optimized according to the final structure after calcination step.

3.2.3.1. Differential Thermal Analysis and Thermogravimetry

The calcination process applied in this study was a crucial and one of the most important steps for developing the WE43 alloy-like compound nerve guidance conduit with the desired properties. Because, the process affects not only the removal of the polymeric component and the reduction of the fiber/pore size, but also the formation of crystallographic components from the metallic elements present in the structure. In the literature, studies with similar metallic scaffolds utilized calcination processes with different temperatures and durations. The thermal behavior of the magnesium as well as those literature studies suggested the calcination process to be conducted between 300-500°C and 1-48 h. However, since an alloy or an alloy-like compound containing 4 different elements have never been studied in the literature before, the WE43 alloy-like compound scaffolds were examined with DTA/TG (Setaram Labsys DTA/TGA, USA) after the electrospinning, in order to obtain all the possible exothermic and endothermic peaks representing the thermal properties such as glass transition, melting, crystallization, etc. Additionally, both the polymer, used for controlling the viscosity of the electrospinning solution, individually electrospun without the metallic salts and the metallic salts dissolved without the polymer in the same solvent used for the electrospinning solution were also subjected to thermal analyses. As a result, the calcination profile, in terms of temperature and duration, was determined by comparing the thermal behavior of the polymer, the metallic salts and the polymer-metallic salt compound.

3.3. Characterizations

3.3.1. Scanning Electron Microscopy and Energy-Dispersive X-Ray Spectroscopy

In this study, the main goal in developing a nerve guidance conduit is to obtain

a fibrous scaffold with a certain level of interconnected porosity and an elemental composition similar to WE43 magnesium alloy. Since the electrospinning solution and process parameters as well as the calcination parameters affect the fiber size and the resulting pore size, all of these parameters were optimized based on the SEM images and the corresponding fiber/pore sizes. Therefore, the samples after electrospinning with different parameters as well as the samples electrospun with optimized parameters after calcination with different parameters were morphologically inspected with SEM (Quanta 400F FE-SEM, FEI, USA).

Additionally, the EDX analysis was conducted with the samples electrospun and calcinated with the optimized parameters, in order to confirm elemental composition of the developed scaffolds.

3.3.2. X-Ray Photoelectron Spectroscopy

In addition to SEM images, the complete removal of the polymer used after the calcination process was confirmed with XPS spectrometer (PHI 5000 VersaProbe, USA). The binding energy peaks for both the samples before and after the calcination step were obtained in order to confirm the presence of the characteristic peaks of the polymer and therefore, confirming the successful electrospinning as well as to compare the absence of those peaks after the calcination and therefore, confirming the successful removal.

3.3.3. X-Ray Diffraction

One of the main reasons for applying a calcination process to the electrospun samples is to crystallize the metallic components into an alloy-like compound. Therefore, the crystallographic structure of the calcinated alloy-like compound scaffolds was determined with X-Ray Diffractometer (Rigaku Ultima-IV, Japan).

3.3.4. Wettability

The wettability of the electrospun WE43 alloy-like compounds developed was measured by using static contact angle measurement technique, in terms of water contact angle values using an optical goniometer (Phoenix 300, Surface

Electro Optics, South Korea). Ultra-pure water (18 MΩ.cm) was utilized as measurement medium and the measurements were repeated at least three times. The values were presented as average values with standard deviation.

3.3.5. In Vitro Degradation

The in vitro degradation rate of the developed alloy-like compound was obtained by a series of experiments described in international ASTM F1635-04 standard [277]. Briefly, the initial weights of the samples were measured first. Then, the samples were placed in test tubes containing 0.1 M PBS and lysozyme (≥40000 units/mg) at pH 7.3. The test tubes were then stored in an incubator for 180 days. At 30-day intervals, the samples corresponding to the interval to be measured were taken out of the test tubes and gently rinsed to remove residual test medium. Then, the samples were placed in a vacuum oven for 24 h to further clean the residuals. Finally, the weights of the samples were measured again after the drying process. The amounts of degradation at that specific interval were then estimated in terms of percent weight remaining with the following equation;

$$\text{Weight remaining (\%)} = 100 - \left(\frac{W_i - W_f}{W_i} \times 100 \right) \qquad \text{Eq. (5)}$$

where W_i is the initial weight of the sample at the beginning of the test and W_f is the weight of the sample at the specific interval that the degradation amount calculated.

3.3.6. Permeability Assays

One of the desired properties expected from a nerve guidance conduit is a certain level of permeability. The conduit should behave like a semi-permeable membrane in order to allow nutrition and waste transfer while preventing the healing factors to escape and the scar tissue cells to enter. The FDA guidelines and the literature studies suggest optimum porosity level between 5-30 μm (preferably 10-20 μm) to meet this criterion, however little information can be found about the transfer rate at this ideal porosity level. Therefore, in this study permeation rate of the scaffolds fabricated with desired porosity level was defined in terms of WVTR according to method described in ASTM E96

standard [278] as well as in terms of lysozyme and bovine serum albumin. For water vapor transmission rate, briefly, the opening of a cylindrical test tube (50 mm diameter) containing 10 ml distilled water was tightly sealed with square shaped samples with 60mm x 60 mm dimension and 2 mm thickness. The prepared test tubes was then weighed and placed in an incubator at 37°C. The tubes were weighed at 3 h intervals for one day and the WVTR were calculated in terms of g/m.day by using the following equation;

$$\text{WVTR} \left(g/m^2.day \right) = \frac{W_i - W_f}{A \times 10^6} \qquad \text{Eq. (6)}$$

where A (mm^2) is the cross-section area of the tube opening, and W_i and W_f were the initial weight and the weight of the test tube at the certain interval, respectively.

On the other hand, lysozyme and bovine serum albumin permeation rate was obtained similarly in which a 2 ml test tube containing 1 ml of lysozyme or BSA, both prepared in PBS, was sealed with the prepared samples and immersed in a larger container filled with PBS only. After 24 h and 48 h in an incubator at 37°C, the optical densities of solutions retrieved from the larger container were obtained with a UV spectrometer (600 nm, PG Instruments T80+, UK), in compared to the optical density of PBS only solution.

3.3.7. Absorption and Swelling

Regardless of the target application, all tissue supporting scaffolds should resist volume and shape changes in surrounding fluidic environment as much as possible because high amount of such changes can cause pressure on the healing cells and deteriorate the healing process. This is especially more important for cells as sensitive to pressure as nerve cells. Therefore, absorption and swelling properties of the alloy-like compounds were determined according to the methods similar to those described in ASTM D570 standard [279], and at least three measurements were obtained for average values and corresponding standard deviations. In absorption test, briefly, 10 mm x 10 mm square shaped samples were weighed and placed in test tubes containing PBS at neutral pH (~7.3-7.5). The tubes then stored in an incubator for one day at 37°C. After the incubation period, the specimens were removed from the tubes and dried gently

with a clean and uncontaminated fabric to remove all excessive water. Finally, the weights of the samples were measured again immediately, and the absorption capacities were estimated with the following equation;

$$\text{Absorption (\%)}=\left(\frac{W_f - W_i}{W_i}\right) \times 100 \qquad \text{Eq. (7)}$$

where W_i and W_f were the weights of the samples at the beginning and at the end of incubation, respectively.

The samples obtained at the end of the incubation were also placed in a drying oven for swelling test. The swelling ratio was then estimated after 12 h with the following equation;

$$\text{Swelling (\%)}=\left(\frac{A_f - A_i}{A_i}\right) \times 100 \qquad \text{Eq. (8)}$$

where A_i and A_f were measured at the beginning of the incubation and after the drying of the samples obtained at the end of the incubation, respectively.

3.4. In Vitro Cell Culture Studies

In the final part of this study, the alloy-like compound scaffolds with desired porosity and elemental composition similar to WE43 magnesium, fabricated with optimized electrospinning and calcination processes, and characterized physically and chemically, were examined for biocompatibility performance by using purchased fibroblast cells lines (L-929, ATCC CCL-1). Fibroblast cells are one of the mostly recommended cell types by ASTM for cell cytotoxicity studies. This cell type can also be utilized for the evaluation of materials for neural tissue engineering. The aim of this thesis was to create a metallic alloy-like compound scaffold for nerve tissue engineering by using novel approaches. Cell lines that can be cultured fast and easily with low cost, such as L-929 fibroblast cell lines, are widely preferred for the in vitro biocompatibility evaluation of this kind of novel scaffolds. Because, the fibroblast cells are one of the most common connective tissue cells, found in almost every part of the body of mammals, and any material aiming for biocompatibility should perform sufficiently against fibroblast cells. Therefore, if the developed material fails against fibroblast cells, in terms of cytotoxicity and/or cell-material interactions, it is not expected to

perform sufficient against more specific cell types, such as nerve cells.

In this study, in vitro cell culture assays were conducted using circular samples with 1 mm diameter, placed in parafilm coated TCPS and UV-sterilized for 15 min. Fibroblast cells were seeded on the samples (1 ml for each sample) at a concentration of 1×10^5 cells/ml. The incubation was carried out for 7 days under standard cell culture environment (5% CO_2, 37°C). The culture medium used was DMEM/F12 supplied with FBS and L-glutamine (10% v/v and 1 ml/100ml, respectively). Additionally, a combination of penicillin (100 units/ml) and streptomycin (100 µg/ml) was added to all media (1% v/v in total) as a contamination protection. The culture media were replaced completely every 48 h of the 7 day culture period.

3.4.1. Cell Attachment

Initial cell adhesion of a tissue scaffold is crucial because it affects the overall cell-material interaction performance. The samples were cultured for 3 h and the cell attachment assay was conducted for every 30 min. This assay in this study was performed with standard haemocytometric counting of the cells that did not attach on the scaffolds after a certain period of time. Since the TCPS Petri dishes used for cell culture were parafilm coated, the cells that did not attach to the scaffolds remain in medium. Therefore, the cell amount remaining were counted and subtracted from the initial cell amount seeded, to find the number of cells adhered to samples. The assay was replicated three times for every sample and culture duration. The values were given as average attachment percentage against time and standard deviations were included for every value.

3.4.2. Cell Viability and Cell Yield

Cell viability is an in vitro colorimetric assay conducted to evaluate the metabolic activity of cells seeded on a material developed. This assay provides cytotoxicity performance of the material, and is generally performed with 3-(4,5-dimethylthiazol-2-yl)-2,5-diphenyltetrazolium bromide (MTT), a yellow colored salt, that only enzymes in viable cells can metabolize into purple colored

formazan. Therefore, the viability can be assessed by the intensity (or optical density) of the color formed after a certain period of culture via a plate reader. As a result, higher optical density of the aliquot obtained from medium indicates presence of higher number of viable cells on the developed material.

In this study, the assays were performed with 24-well Petri dishes after the first 24 h and replicated at 48 h intervals. The procedure started with discarding the culture media from the well and washing the samples with PBS twice. Then, the samples were placed into the incubator again with 600 µl media containing 10% v/v MTT for three hours under the same standard culture conditions. At the end of this incubation, the medium/MTT solution was discarded, and the samples were placed into the incubator for the last time with 1 ml DMSO in order to dissolve formazan crystals. After one hour of incubation, aliquots were transferred from each sample to a new clean 96-well microtiter plate, and the optical densities (540 nm) of these aliquots were measured with a plate reader (Ledetect 96, Labexim Products, Austria). Three replicates of each sample were assessed and the viability of the cells was presented as an average absorbance value with standard deviation.

Additionally, since a certain optical density value can only be obtained from a certain number of viable cells, the cell yield for a certain period of time can be detected with a similar MTT assay. Therefore, in this study, at the end of 7 days, the final cell yield, which is the average total number of viable cells present on/within each sample, was also determined by using viability assay.

3.4.3. Visual Assessments

The morphology of the cells cultured with the developed material was assessed using CLSM (Zeiss LSM 510, USA). The cell seeded samples after incubation for 4 days and 7 days were dual stained with AF-488/DRAQ5 in order to observe both the nucleus and the cytoskeleton of the cells. Briefly, the medium on the cells were discarded and the wells were gently rinsed with PBS twice. The cells were fixated using 4% (v/v) paraformaldehyde for 45 min, permeabilized using 0.1% Triton X-100 for 5 min, blocked using BSA for 30 min, and finally stained using AF-488 and DRAQ5, consecutively, for 20 min and 10

min, respectively, in the dark, at room temperature. Imaging of the stained samples was carried out immediately. In addition to the confocal imaging, the cell morphologies at the final day of incubation were observed with SEM for a better 3D visualization. Briefly, the media in the wells were removed, and cells were gently rinsed and fixated with the same procedure as the confocal imaging. The fixated cells were then dehydrated using ethanol with increasing concentrations between 30-100% (v/v) (10% intervals, 2 min each) and using 100% hexamethyldisilazane for 5 min. Finally, the samples were held open under the laminar flow cabin to evaporate hexamethyldisilazane and to obtain complete drying. The samples were sputter-coated using gold-palladium (coating thickness: ~3 nm), and the imaging was carried out at various magnifications under vacuum.

4. RESULTS AND DISCUSSIONS

4.1. Fibrous WE43 Magnesium Alloy-Like Compounds

In this study, WE43 magnesium alloy, developed for FDA-approved stent application, were fabricated with a novel approach. Unlike the traditional metal alloy fabrication techniques such as casting which uses pure elements as raw material, the electrospinning technique was employed and nitrates of the elements were used as starting materials. The major goal was to obtain a fibrous network inside the material with a pore size at micron scale which was not possible with the traditional approaches. Additionally, a calcination step was applied after the electrospinning to ensure the final product to be an alloy-like compound with a similar composition of the commercial WE43 magnesium alloy. The following sections present the results of the studies conducted and discuss the results with the state-of-art knowledge.

4.1.1. Preparation of Electrospinning Solutions

The commercial WE43 magnesium alloy has a composition of 93.6% Mg, 4% Y, 2.25% Nd and 0.15% Zr. Given with the atomic mass of the elements, the alloy can be represented with a stoichiometric formula of $Mg_{3.85}Y_{0.045}Nd_{0.0156}Zr_{0.0016}$ (Table 4.1). According to this formula and the molecular mass of the nitrates used, the initial electrospinning solution was prepared in distilled water with the amounts given in Table 4.1.

Metallic nitrates have good solubility in the water, even in low temperatures [280]. On the other hand, given with the number of different metal nitrates used, the interaction between the components added was found to prevent the complete homogeneous dissolution of all the nitrates at room temperature, even with vigorous stirring over 72 h at more than 1500 rpm. However, when the solution temperature was raised to 30°C, the nitrates were dissolved easily at 400 rpm after 24 h. The preliminary electrospinning attempt showed that this solution has viscosity too low to form electrospinning jet.

Table 4.1. Compositions and amounts used for solution preparation.

	Magnesium (Mg)	Yttrium (Y)	Neodymium (Nd)	Zirconium (Zr)
Composition (%)	93.6	4	2.25	0.15
Atomic Mass (g/mol)	24.305	88.9058	144.242	91.224
Number of moles (based on 100 g of alloy)	3.85	0.04499	0.015598	0.001644
Nitrates used	$Mg(NO_3)_2 \cdot 6H_2O$	$Y(NO_3)_3 \cdot 6H_2O$	$Nd(NO_3)_3 \cdot 6H_2O$	$ZrO(NO_3)_2 \cdot xH_2O$
Molecular Mass of Nitrates (g/mol)	256.41	383.01	438.35	231.23
Amount of nitrates dissolved for 1 g alloy (g)	0.9871	0.0172	0.0068	0.0004

The similar studies in the literature utilized polymers such as PVP or PVA in order to adjust the viscosity of the electrospinning solutions to a manageable level [281–283]. Therefore, the new solutions were prepared with PVP (MW ≈ 1.3×10^6) or PVA (MW ≈ $8.5\text{-}12.4 \times 10^5$) addition. The reason to choose PVP and PVA was that they are highly soluble in water, and the viscosity and the conductivity of their solutions as well as the resulting electrospun fiber diameter can easily be adjusted with different solvent content and concentration [135, 284]. Since a certain level of pore size distribution is desired for the developed electrospun alloy-like compound and the pore size of fibrous networks depends on the fiber diameter, a series of different solutions was prepared and tried for electrospinning. The solutions were prepared with nitrates of alloy components corresponding to the alloy weighing from 0.25 g to 5 g. PVP was found to be dissolved in water, ethanol or different ethanol/water mixtures at room temperature in 30-60 min at 200 rpm, and PVA was found to be dissolved in water at temperature between 70-90°C in ~2 h at 500 rpm. However, since the duration of stirring increases the viscosity of the polymer solutions [285] and at

least 24 h of stirring was needed to completely and homogeneously dissolve the nitrates, the electrospinning solutions were prepared by dissolving first the nitrates for 24 h and then PVP or PVA for their respective durations. A total of 96 nitrates/PVP solutions with 2 different PVP concentrations (2.5 or 5 wt.%), 4 different stirring temperatures (room, 30°C, 50°C or 90°C) and 12 different solvent concentrations, and a total of 72 nitrates/PVA solutions with 4 different PVA concentrations (2.5, 5, 10 or 15 wt.%), 3 different stirring temperature (70°C, 80°C or 90°C) and 6 different total nitrate salt amounts (0.25 g, 0.5 g, 1 g, 1.5 g, 2 g or 5 g) were prepared and examined in terms of total and homogeneous solubility. It was found that high level of stirring temperature decreased the observable viscosity of the solutions drastically as expected which made the solutions stirred at temperatures higher than 30°C viable for PVP electrospinning and temperatures higher than 80°C viable for PVA electrospinning. Additionally, both PVP concentrations as well as different ethanol/water concentrations ranging from pure ethanol (100/0 v/v) to pure water (0/100 v/v) and PVA concentrations up to 10 wt.% with salt content between up to 2 g were resulted in fully dissolved homogeneous solutions.

4.1.2. Electrospinning of WE43 Magnesium Alloy-Like Compounds

The electrospinning performance of the prepared solutions was examined visibly in terms of both initiation and continuity of spinning (Table 4.2 and 4.3). Additionally, the electrospinning instrument parameters such as applied voltage, solution feeding rate and feeder-collector distance, were optimized between 15-30 kV (with 1 kV intervals), 5-15 µl/min (with 0.5 µl/min intervals) and 10-20 cm (with 1 cm intervals), respectively, along with the solution parameters for continuous stable jet forming.

All the electrospinning solutions, except the ones prepared with 0/100, 5/95 and 100/0 (v/v) ethanol/water, were found to be spinnable. It is concluded that ethanol addition less than 10% volume was not enough to increase the viscosity of the water-based solution for initiation of an electrospinning jet, even at voltages as high as 30 kV. On the other hand, pure ethanol caused the exact opposite behavior, increasing the viscosity too high for the electrostatic force to exert the solution out of the feeding tip and stretch the jet to the collector.

Table 4.2. Optimization of solution parameters for electrospinning with PVP.

Set #	Ethanol/Water (v/v)	Temperature (°C)	PVP Concentration (wt.%)	Initiation/Continuity
1	0/100	30	2.5	NO/NO
			5	NO/NO
		50	2.5	NO/NO
			5	NO/NO
		90	2.5	NO/NO
			5	NO/NO
2	5/95	30	2.5	NO/NO
			5	NO/NO
		50	2.5	NO/NO
			5	NO/NO
		90	2.5	NO/NO
			5	NO/NO
3	10/90	30	2.5	YES/NO
			5	YES/NO
		50	2.5	YES/NO
			5	YES/NO
		90	2.5	YES/NO
			5	YES/NO
4	15/85	30	2.5	YES/NO
			5	YES/NO
		50	2.5	YES/NO
			5	YES/NO
		90	2.5	YES/NO
			5	YES/NO

Set #	Ethanol/Water (v/v)	Temperature (°C)	PVP Concentration (wt.%)	Initiation/Continuity
5	20/80	30	2.5	YES/NO
			5	YES/NO
		50	2.5	YES/NO
			5	YES/NO
		90	2.5	YES/NO
			5	YES/NO
6	25/75	30	2.5	YES/NO
			5	**YES/YES**
		50	2.5	YES/NO
			5	YES/NO
		90	2.5	YES/NO
			5	YES/NO
7	30/70	30	2.5	YES/NO
			5	YES/NO
		50	2.5	YES/NO
			5	YES/NO
		90	2.5	YES/NO
			5	YES/NO
8	35/65	30	2.5	YES/NO
			5	YES/NO
		50	2.5	YES/NO
			5	YES/NO
		90	2.5	YES/NO
			5	YES/NO

Set #	Ethanol/Water (v/v)	Temperature (°C)	PVP Concentration (wt.%)	Initiation/Continuity
9	40/60	30	2.5	YES/NO
			5	YES/NO
		50	2.5	YES/NO
			5	YES/NO
		90	2.5	YES/NO
			5	YES/NO
10	45/55	30	2.5	YES/NO
			5	YES/NO
		50	2.5	YES/NO
			5	YES/NO
		90	2.5	YES/NO
			5	YES/NO
11	50/50	30	2.5	YES/NO
			5	YES/NO
		50	2.5	YES/NO
			5	YES/NO
		90	2.5	YES/NO
			5	YES/NO
12	100/0	30	2.5	NO/NO
			5	NO/NO
		50	2.5	NO/NO
			5	NO/NO
		90	2.5	NO/NO
			5	NO/NO

Vongsetskul et. al. showed that as the ethanol percentage increases, the conductivity of the PVP solution decreases to a minimum whereas the water percentage near 100% caused the lowest viscosity possible in ethanol/water

based PVP solution [135]. Ethanol concentration higher than 50% increases the viscosity significantly, reaching maximum viscosity at 75% ethanol in the ethanol-water solvent system for PVP while reducing the conductivity of the solution exponentially. Therefore, solvents up to 50% ethanol concentration were tried for electrospinning. Between 10% and 50% ethanol addition to the solvent, provided spinnable solutions for all stirring temperatures and both PVP concentrations. However, all of these solutions, except the solution prepared with 25/75 (v/v) ethanol/water at 30°C with 5 wt.% PVP, failed to sustain a continuous electrospinning jet in order to collect a usable amount of scaffold thickness. Because the solvent at this level of concentration (25/75 v/v ethanol/water) has the most optimum moderate level of conductivity as well as viscosity in ethanol-water solvent system, which are neither too high to prevent jet formation or cause electrospraying instead nor too low to initiate the Taylor cone and/or sustain it in long term. Therefore, this solution was successfully and continuously electrospun by feeding 5 µl/min under 30 kV from a distance of 12-15 cm. By using this optimized solution and instrument parameters, all of the samples used for the following studies were prepared with 10 ml of the solution to achieve samples with same dimensions.

All the electrospinning solutions, except the ones prepared with 15 wt.% PVA, were found to be spinnable. In the literature high PVA concentrations were known to be spinnable [140]. However, it has been observed that the nitrate salt addition increase the conductivity and/or charge of the PVA solution for initiation of an electrospinning jet, even at voltages as high as 30 kV. On the other hand, 10 wt.% PVA, when combined with the nitrate salts, become adequate enough for the electrostatic force to exert the solution out of the feeding tip and stretch the jet to the collector. However, it has been found that this solution is still highly charged to maintain continuous jet formation once it started.

Conductivity or charge of a solution affecting the spinnability is a widely known behavior for electrospinning technique, and both high and low amounts can either prevent the solution from continuity or hinder the process completely [64]. Therefore, it is concluded that the PVA concentrations of 10 wt.% or higher are not suitable for electrospinning when combined with nitrate salts.

PVA requires high temperatures to be dissolved in water-nitrate solution, and as the temperature increases the viscosity of the final solution increases accordingly. However, solutions prepared at 70°C out of 3 temperatures experimented was found to have adequate viscosity to initiate jet formation but not enough to maintain continuity in spinning process. Therefore, it is concluded that at least 80°C is required for a PVA-nitrate-water solution system.

Table 4.3. Optimization of solution parameters for electrospinning with PVA.

Set #	PVA Concentration	Temperature (°C)	Salt Content (g)	Initiation/Continuity
1	0,25 g (2,5 wt.%)	70	0.25	YES/NO
			0.5	YES/NO
			1	YES/NO
			1.5	YES/NO
			2	YES/NO
			5	YES/NO
		80	0.25	YES/YES
			0.5	YES/YES
			1	YES/YES
			1.5	YES/YES
			2	YES/YES
			5	YES/YES
		90	0.25	YES/YES
			0.5	YES/YES
			1	YES/YES
			1.5	YES/YES
			2	YES/YES
			5	YES/YES

Set #	PVA Concentration	Temperature (°C)	Salt Content (g)	Initiation/Continuity
2	0,5 g (5 wt.%)	70	0.25	YES/NO
			0.5	YES/NO
			1	YES/NO
			1.5	YES/NO
			2	YES/NO
			5	YES/NO
		80	0.25	YES/YES
			0.5	YES/YES
			1	YES/YES
			1.5	YES/YES
			2	YES/YES
			5	YES/YES
		90	0.25	YES/YES
			0.5	YES/YES
			1	YES/YES
			1.5	YES/YES
			2	YES/YES
			5	YES/YES
3	1 g (10 wt.%)	70	0.25	YES/NO
			0.5	YES/NO
			1	YES/NO
			1.5	YES/NO
			2	YES/NO
			5	YES/NO

Set #	PVA Concentration	Temperature (°C)	Salt Content (g)	Initiation/Continuity
		80	0.25	YES/NO
			0.5	YES/NO
			1	YES/NO
			1.5	YES/NO
			2	YES/NO
			5	YES/NO
		90	0.25	YES/NO
			0.5	YES/NO
			1	YES/NO
			1.5	YES/NO
			2	YES/NO
			5	YES/NO
		70	0.25	NO/NO
			0.5	NO/NO
			1	NO/NO
			1.5	NO/NO
			2	NO/NO
			5	NO/NO
		80	0.25	NO/NO
			0.5	NO/NO
4	1.5 g (15 wt.%)		1	NO/NO
			1.5	NO/NO
			2	NO/NO
			5	NO/NO
		90	0.25	NO/NO
			0.5	NO/NO
			1	NO/NO
			1.5	NO/NO
			2	NO/NO
			5	NO/NO

Finally, solutions with PVA concentration 2.5 or 5 wt.% prepared at 80°C or 90°C containing 0.25-5 g of nitrate salts were found to be optimum for both jet initiation and continuous spinning. Therefore, this solution was successfully and continuously electrospun by feeding 5 µl/min under 30 kV from a distance of 12-15 cm. By using this optimized solution and instrument parameters, all of the samples used for the following studies were prepared with 10 ml of the solution to achieve samples with same dimensions.

4.1.3. Calcination of Electrospun Alloy-Like Compound

The nitrates of metals have high affinity for water [280]. Therefore, heating decomposes the nitrates into oxides of the metal, which is the key route adopted in this study to obtain alloy-like compound of the metallic alloy from the nitrate salts. In order to achieve the decomposition of the electrospun polymer-metal nitrate structure, a calcination step was applied to the samples electrospun with optimized parameters in the previous section. The temperature and the duration of the calcination process were determined by means of thermal analysis. The candidate sample prepared with PVP-metal nitrates and electrospun with optimized parameters as well as single electrospun PVP without the metal nitrate salts and metal nitrate salts dissolved without PVP with the optimum solvent and dried under vacuum were subjected to DTA/TG analysis in order to obtain decomposition, crystallization and other possible significant thermal behaviors. The temperature of the calcination was determined according to the comparison between the thermal plots of these three analyses and the duration of the calcination was determined by theoretical calculation proposed by Zivkovic and Dobovisek [276].

4.1.3.1. Differential Thermal Analysis and Thermogravimetry

The DTA/TG plots of the PVP electrospun without metal nitrate salts, metal nitrate salts prepared without PVP and the PVP-metal nitrates electrospun together were given in Figure 4.1. A sharp exothermic peak at 326°C (P3) and a corresponding 35% drop in weight were observed in DTA and TG plots of PVP, respectively. This corresponded to the decomposition of PVP, which starts around 350°C according to the multiple studies in the literature [286, 287]. On

the other hand, alloy salts prepared independent from PVP, showed multiple peaks at 100°C (P1), 180°C (P2), 425°C (P4) and 455°C (P5). The P1 peak was where residual water vaporized from the nitrate salts. The P2 peak at 180°C was believed to be where the decomposition of nitrates started.
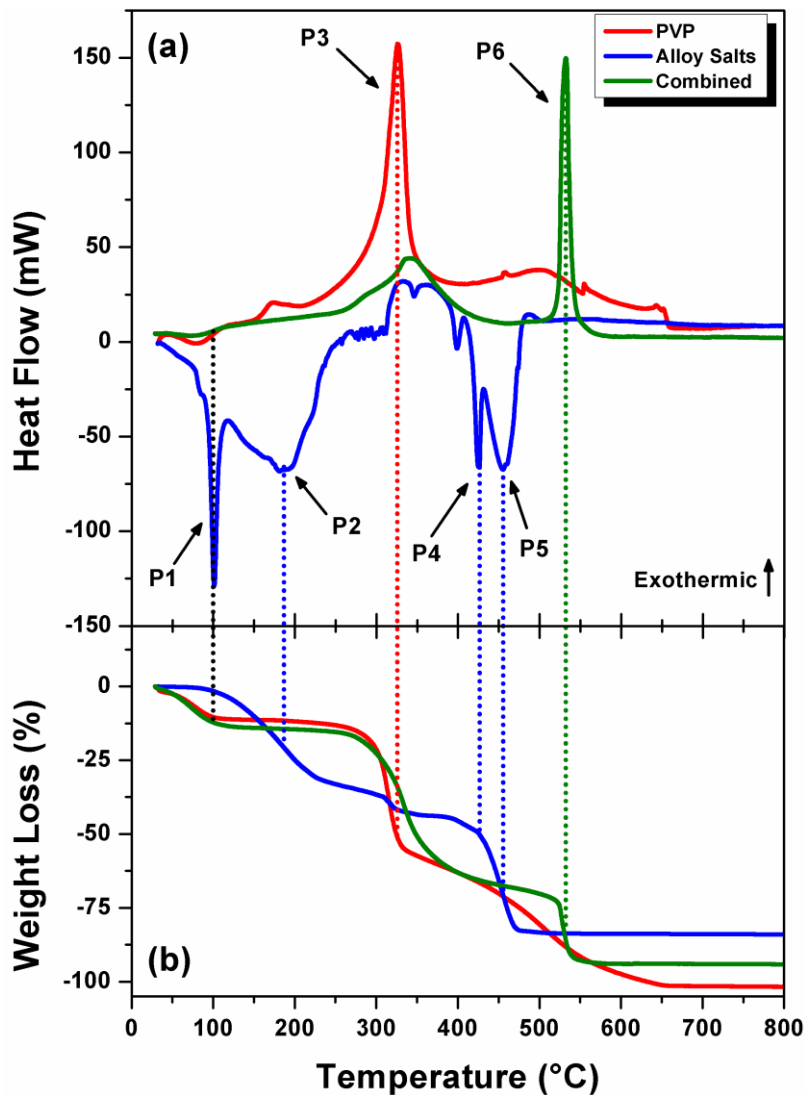

Figure 4.1.   (a) DTA and (b) TG plots of PVP electrospun without metal nitrate salts, metal nitrate salts prepared without PVP and the electrospun PVP-metal nitrates sample.

Paulik et. al. investigated the decomposition behavior of $Mg(NO_3)_2.6H_2O$ and found that the hexahydrate left the structure starting from the boiling point of water until the temperatures as high as 300-320°C reached. At that point, the nitrate became waterfree $Mg(NO_3)_2$ which started to decompose into the oxide form of magnesium, MgO. The decomposition was terminated between 420°C

and 480°C when the 85-90% of the initial weight decomposed and only MgO left [288]. Both DTA and TG plots of alloy salts followed similar pattern in this study (Figure 4.1), and given the fact that almost 94% of the composition contains magnesium nitrate, it can be concluded that metal nitrates in the sample became anhydrous between 100-300°C reaching a peak at 180°C (P2), and decomposed further into oxides between 320-480°C (P4 and P5). Additionally, the thermal plots of combined PVP and metal salts revealed a wide medium strength peak followed by a strong sharp peak (Figure 4.1). The wide peak was observed starting from 100°C, reaching its peak at around 330-340°C and continued until the temperature reached 430-450°C. Two primary weight losses were recorded during this period, which were responsible for 15% and an additional 50% weight loss of the sample at 100°C and 330-340°C, respectively. This clearly was in accordance with the findings for both single PVP and metal salts, and the single wide peak was the sum of PVP decomposition as well as hydrous and nitrate decompositions of metals into oxides. On the other hand, the strong sharp peak at 530°C (P6) was believed to represent the merging of the decomposed metal oxides, which thought to form a new crystallographic structure with an empirical formula, $Mg_aY_bNd_cZr_dO_x$, and therefore manifested itself as an exothermic peak. As a result of these findings, the key temperatures for calcination of the electrospun samples prepared with PVP were determined as 325°C, 425°C, 455°C and 530°C.

Additionally, DTA/TG plots of the PVA electrospun without metal nitrate salts and the PVA-metal nitrates electrospun together were given in Figure 4.2. A sharp endothermic peak at ~500°C, starting around 230°C and ending around 580°C (P1) and a corresponding ~85-90% drop in weight were observed in DTA and TG plots of PVA, respectively. This represented the pyrolysis of PVA according to the multiple studies in the literature [289, 290]. However, the pyrolysis process of PVA presented itself at ~230°C (P3) when combined with nitrate salts, according to the DTA/TG plot of electrospun PVA-metal nitrates sample, in which the precipitation of β'/β'' phases and β1 phase as well as β1 → β(stable) transformation occurred at 140-180°C (P2), 310°C (P4) and 350°C (P4), respectively. The decomposition of metal nitrates into oxides as well as merging of these oxides into empirical $Mg_aY_bNd_cZr_dO_x$, however, occurred

between 430-500°C (P5) and 500-510°C (P6), which is relatively consistent with the findings of metal nitrate salts and PVP combined salts (P4, P5 and P6 peaks of Figure 4.2). As a result of these findings, the key temperatures for calcination of electrospun samples prepared with PVA were determined as 230°C, 390°C, 465°C, 500°C and 505°C.
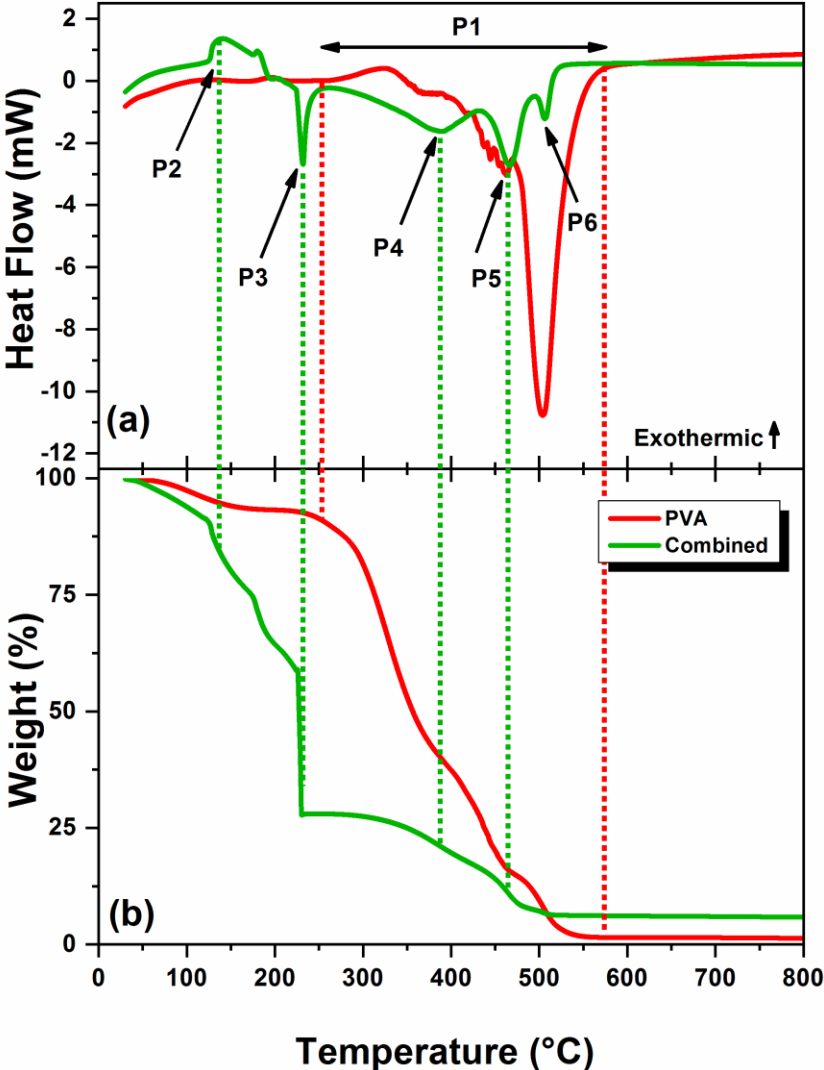

Figure 4.2.   (a) DTA and (b) TG plots of PVA electrospun without metal nitrate salts, and the electrospun PVA-metal nitrates sample.

As a result of the determined key temperatures from DTA plots of PVP, PVA, metal nitrate salts as well as electrospun samples prepared with PVP or PVA and the corresponding area values obtained from the determined DTA peaks, log [ln (S / S-S_t) / t] vs 1/T graphs for PVP peak at 325°C, for peaks of metal salts at 425°C and 455°C, for peak of combined PVP-salts at 530°C, for PVA

peak at 500°C and for peaks of combined PVA-salts at 230°C, 390°C, 465°C, and 505°C were plotted (Figure 4.3 and 4.4). The slopes and the y-axis intersections of the straight lines on each graph gave the activation energy and the pre-exponential factor of the reactions occurred on each peak, and the time required to complete those reactions at 99.99% were calculated with Eq. (4) (Table 4.4 and 4.5).
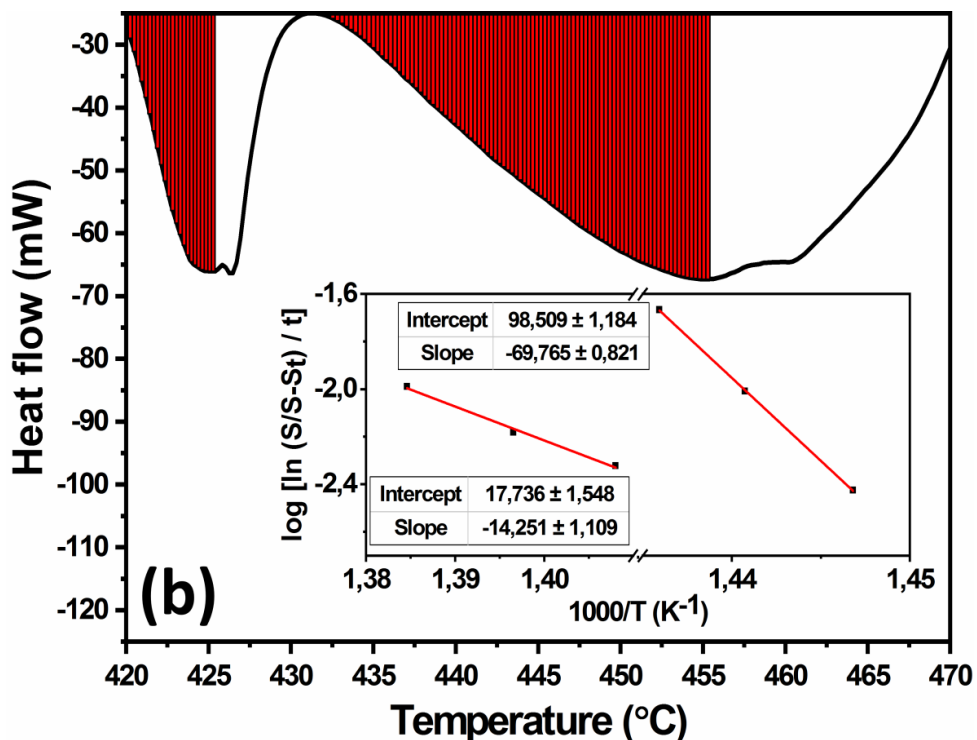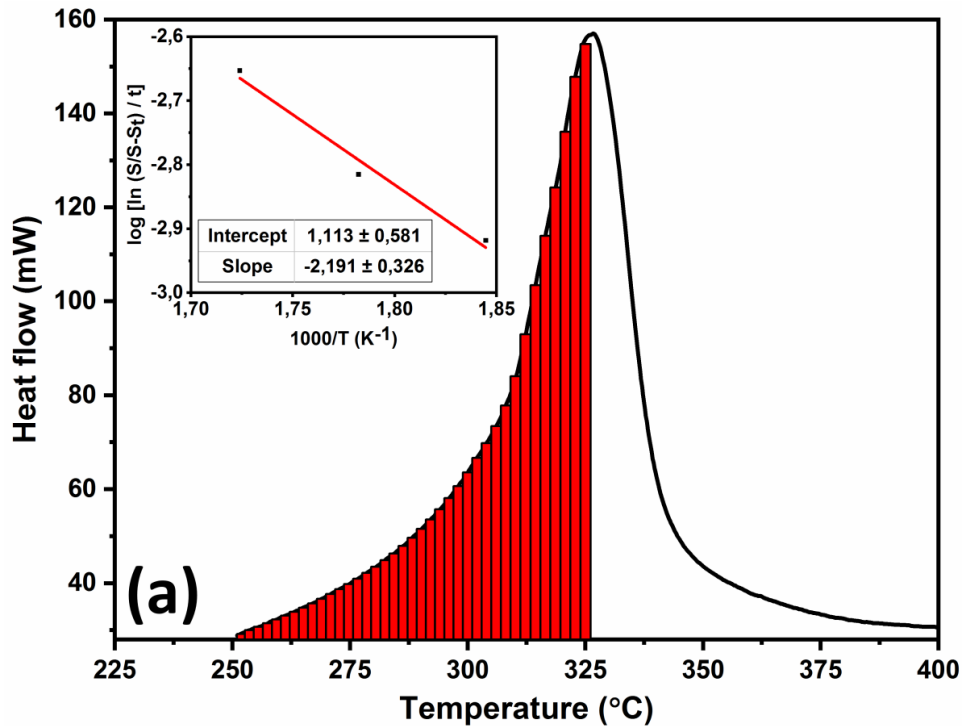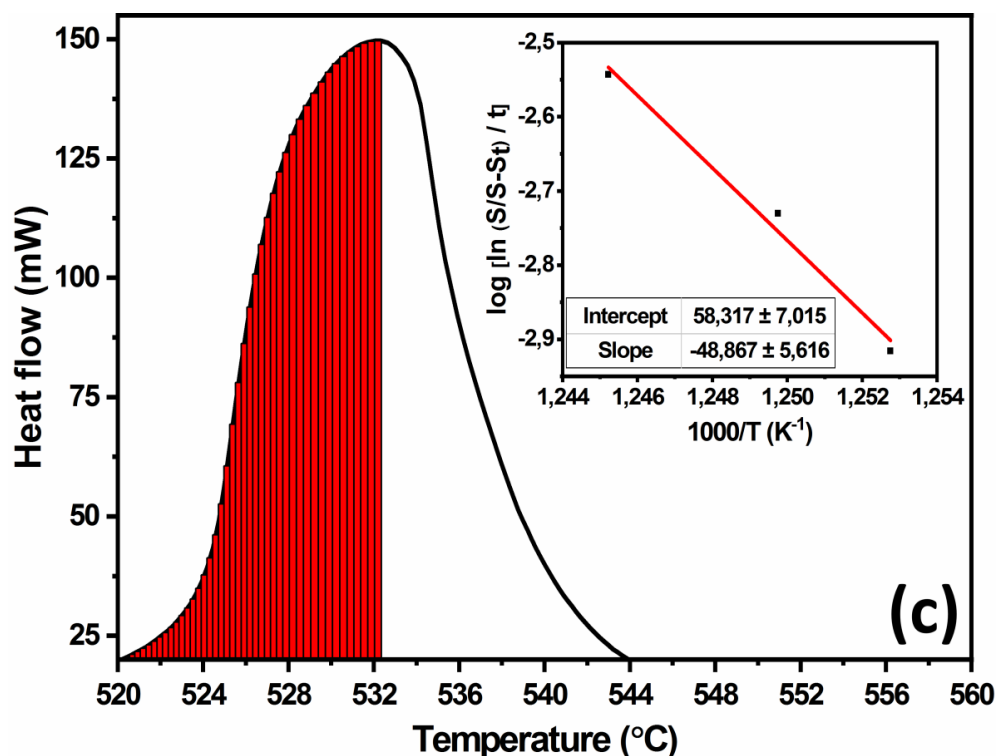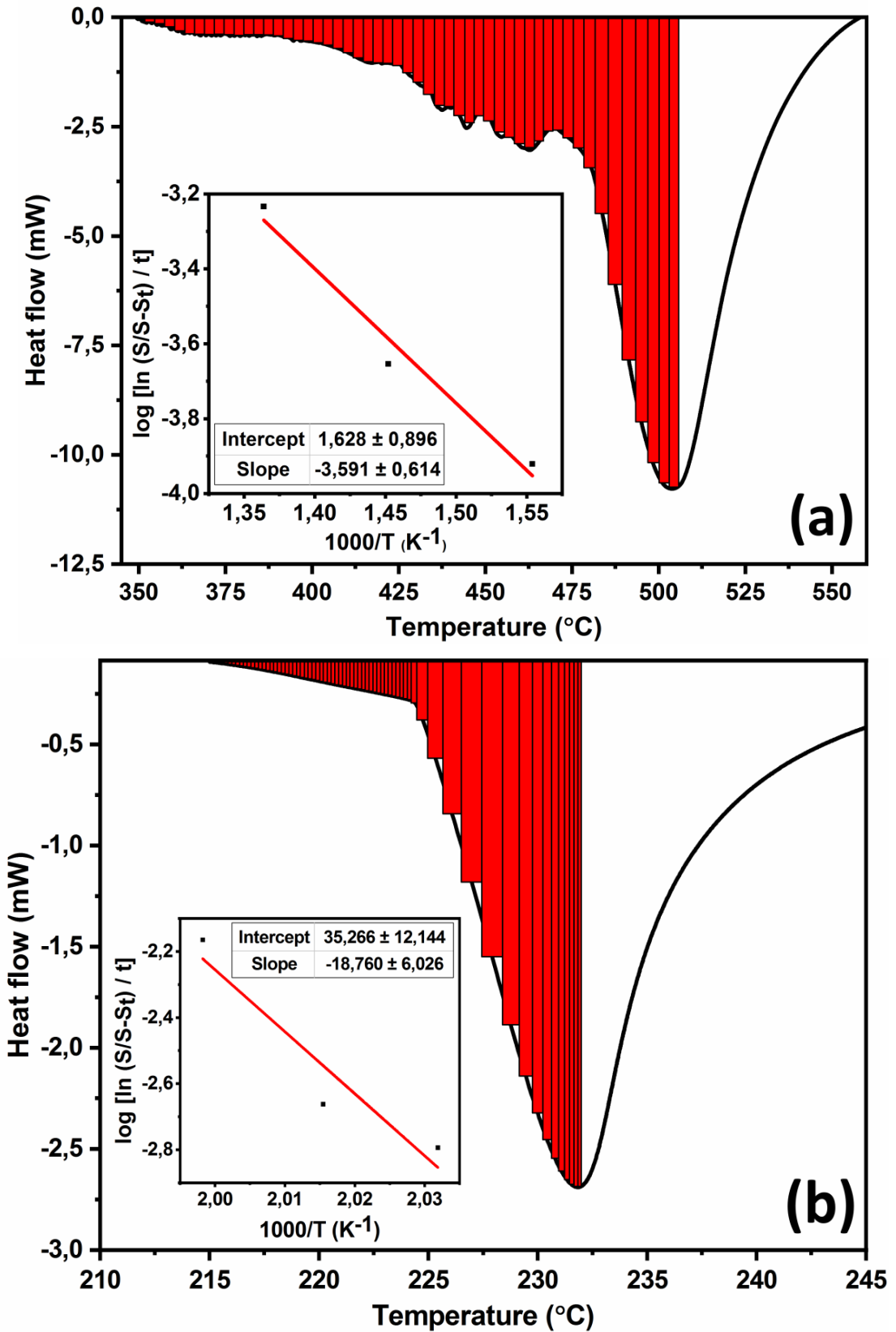
Figure 4.3.   Riemann fitting and the corresponding log [ln (S / S-S$_t$) / t] vs 1/T plots of DTA peaks used for calculations of (a) PVP peak at 325°C, (b) peaks of metal nitrate salts at 425°C and 455°C and (c) peak of combined PVP+salts at 530°C.
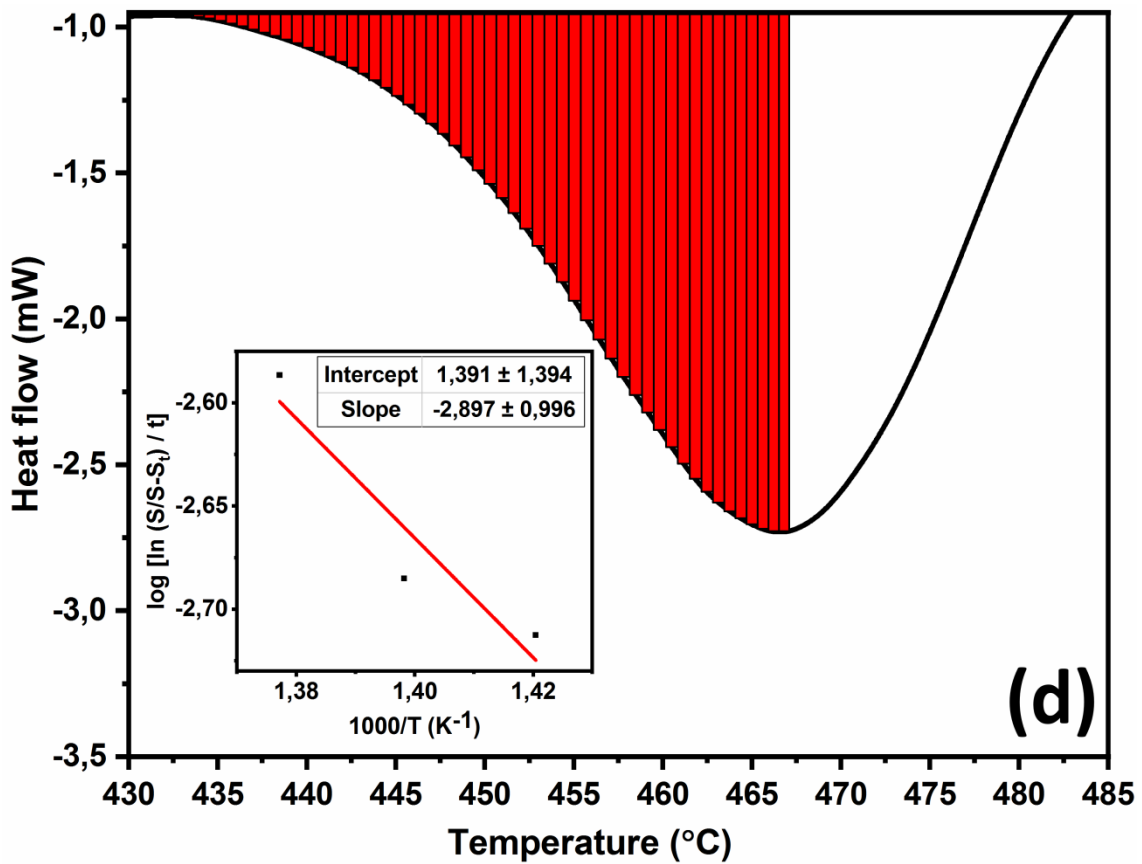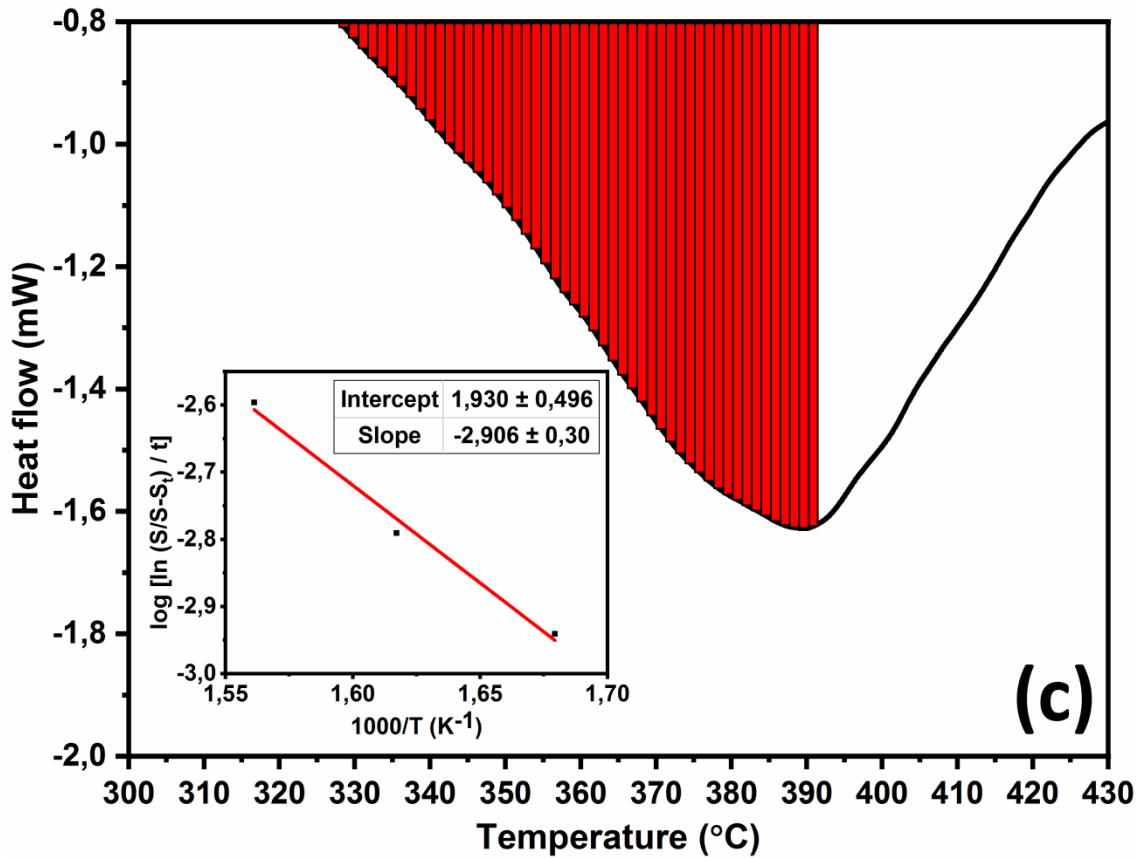
Table 4.4. Estimated activation energies, pre-exponential factors and reaction durations of different peaks obtained from samples prepared with PVP.

Plot	Temperature (°C)	Activation Energy (J/mol)	Pre-exponential Factor (s^{-1})	Duration (s)	Duration (h)
PVP	325	41.95	0.00121	28601.79	7.94
Metal salts	425	1335.70	0.00474	9165.12	2.55
	455	272.85	0.00499	7242.55	2.01
Combined	530	935.66	0.00139	24932.18	6.93

According to the significant temperatures obtained from DTA/TG plots (Figure 4.1) and the estimated corresponding reaction durations given in the Table 4.4, the designated heat treatment for the samples prepared with PVP was generated as 8 h at 325°C, 2.5 h at 425°C, 2 h at 455°C and 7 h at 530°C,

consecutively. Since the durations are based on mathematical estimations, all of the durations were also tried as ±1 h considering the possibility of a certain error margin.
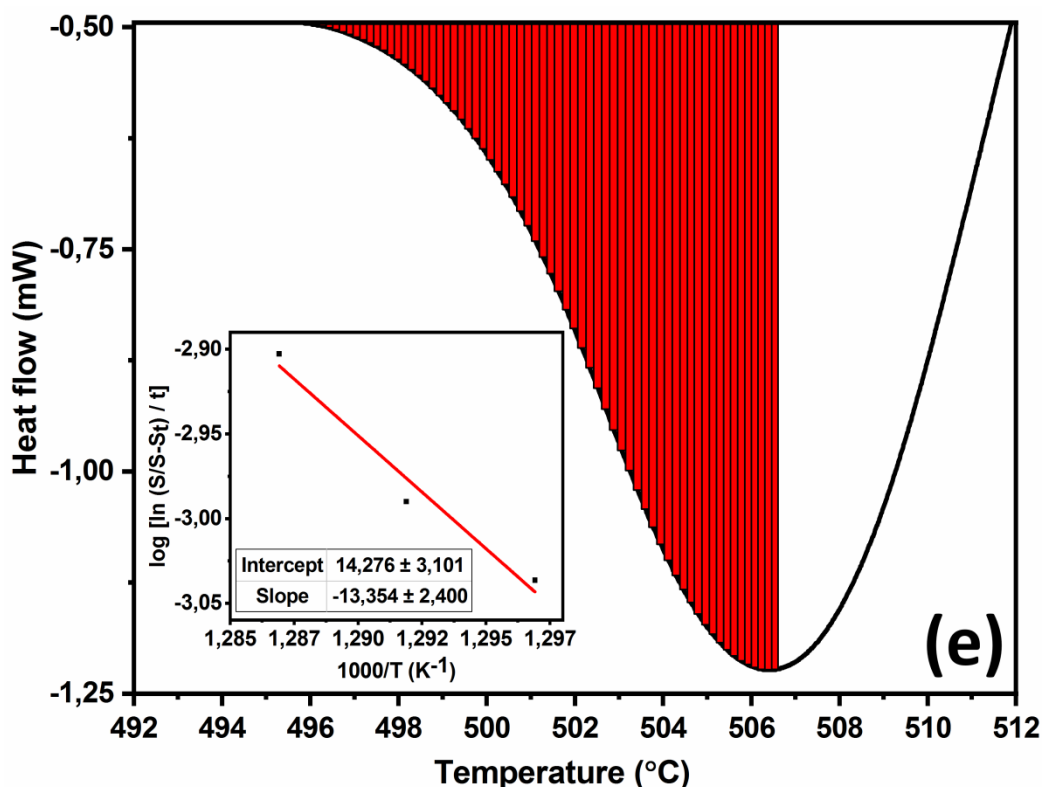

(a)

(b)

Figure 4.4. Riemann fitting and the corresponding log [ln (S / S-S$_t$) / t] vs 1/T plots of DTA peaks for single PVA at (a) 500°C and for PVA+salts combined at (b) 230°C, (c) 390°C, (d) 465°C and (e) 505°C.

Table 4.5. Estimated activation energies, pre-exponential factors and reaction durations of different peaks obtained from the samples prepared with PVA.

Peak	Temperature (°C)	Activation Energy (J/mol)	Pre-exponential Factor (s^{-1})	Duration (s)	Duration (h)
PVA	500	68.74	0.00012	287533.38	79.87
Combined	230	359.20	0.00175	21408.18	5.95
	390	55.62	0.00116	30085.41	8.36
	465	55.47	0.00195	17830.39	4.95
	505	255.69	0.00096	36456.48	10.13

Similar to the samples prepared with PVP, the designated heat treatment for the samples prepared with PVA was generated as 6 h at 230°C, 8.5 h at 390°C, 5 h at 465°C, 80 h at 500°C and 10 h at 505°C, consecutively, according to the temperatures obtained from DTA/TG plots (Figure 4.2) and the estimated

corresponding reaction durations given in the Table 4.5. All of these durations were also tried as ±1 h considering the possibility of a certain error margin.

4.2. Characterizations

4.2.1. Scanning Electron Microscopy and Energy-Dispersive X-Ray Spectroscopy

The SEM images of the samples prepared with PVP (not given here) and PVA (Figure 4.5.a) obtained showed successful electrospinning of the solutions prepared. The structures of both consisted of a fibrous network with interconnected porosity. However, after the designated heat treatment for PVP, it was found that PVP was only pyrolysed partially at the end and the most of the fibers lost their structural integrity before the nitrate salts were decomposed to oxides and merged together to form the alloy-like compound with fibrous structure. On the other hand, the designated heat treatment generated for the samples prepared with PVA was proved to be successful in maintaining the fibrous network during the calcination process (Figure 4.5.b). It was assumed that, these results were the consequence of the difference in the temperature and the durations of polymer peaks (325°C for PVP and 500°C for PVA). According to the thermal analysis, the temperature of PVP peak was found to be before the decomposition and the merging of the nitrate salts where the similar peak for PVA was started early and ended at almost at the same temperature where the merging was assumed to occur. As a result, PVP was decomposed before salts were decomposed into oxides and merged together which was failed because of the loss of structural integrity of the fibers. On the contrary, since PVA started decomposing early in the temperature scale and assumed to continue for nearly 200°C up until the decomposition and the merging of nitrate salts ended, polymer was still continued to be present in the fibers, providing structural support during the nitrate salt reactions and merging, therefore maintaining the fibrous structure until it finally completely decomposed after more than 80 h. The EDX analysis showed that the composition of the obtained fibrous structure consisted of primarily oxygen and magnesium where the rest was yttrium, neodymium and zirconium as expected (Figure 4.5.c). Since it was expected for nitrates to decompose into oxides after the calcination process, it was plausible to have almost ~68% (at.%) oxygen present in the

68

structure which was believed to be because of the oxides of the four components of the alloy. Also because the majority of the mimicked alloy is magnesium, the obtained compound was primarily MgO since the magnesium content was measured around ~28.5% (at.%). The EDX results showed that samples electrospun with PVA and calcinated with the designated heat treatment regime proved that it is possible to obtain a fibrous alloy-like compound with an empirical formula of $Mg_aY_bNd_cZr_dO_x$ which consists of merged oxides of the four components and therefore mimics the WE43 magnesium alloy.
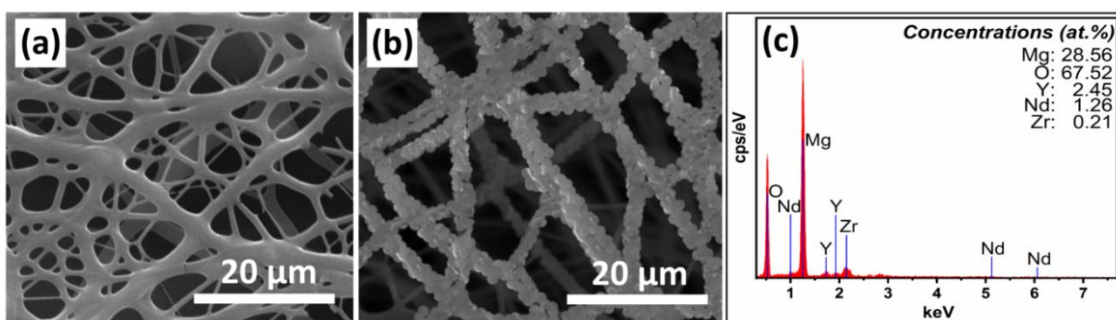

Figure 4.5.   SEM images of the samples prepared with PVA (a) after electrospinning, (b) after the designed heat treatment (Magnifications: x5000), and (c) EDX analysis of the heat treated sample.

4.2.2. X-Ray Photoelectron Spectroscopy

In this study, the chemical composition and the structure of the fabricated mats are crucial. The novel approach used to fabricate an alloy-like compound consists of different stages for the material content, in which polymer, metallic salts, alloy-like compound or a combination of these can be present at certain points of the entire process. However, the success of the process and the resulting desired structure depend on these contents to be in a certain order to continue with the determined course of experiments. One of the characterization methods utilized to keep track of the structural changes throughout the study is XPS. This method provides binding energy data of the bonds present in a structure which helps to interpret the contents of a material. Even though it is generally preferred for polymers, it can be applied to different

kinds of materials such as metals, as well. Therefore, XPS analyses were conducted for three different structures of this study; (i) electrospun PVA mats (without metallic nitrate salts), (ii) electrospun PVA containing metallic nitrate salts (mats pre-treatment) and (iii) electrospun WE43 alloy-like compound mats (post-heat treatment). The reason for choosing these three structures was to determine whether the initial electrospun structure as well as the structure after the heat treatment contains the necessary contents (PVA, metallic nitrate salts and/or metallic compound). The resulting plots were given in Figure 4.6.
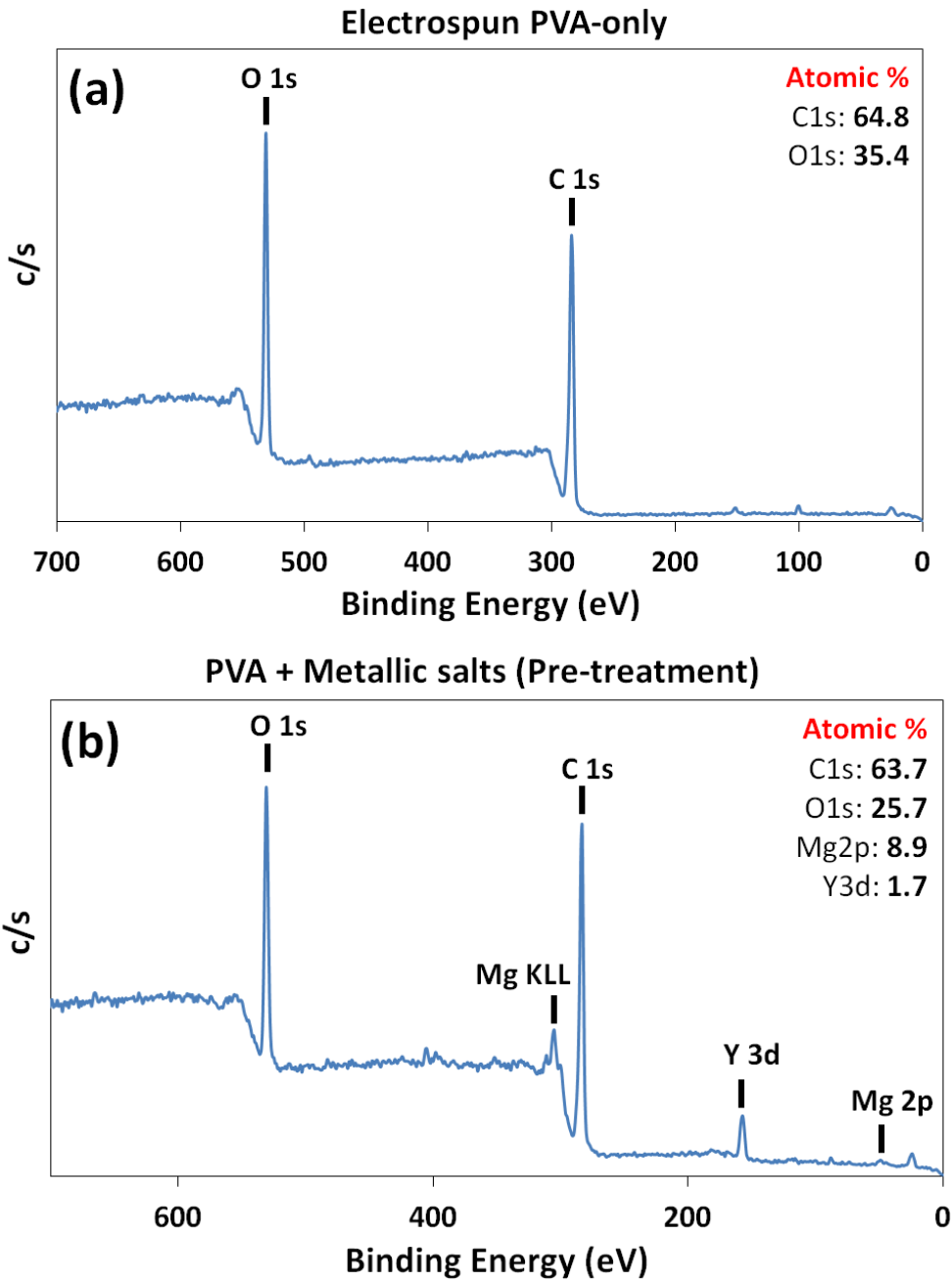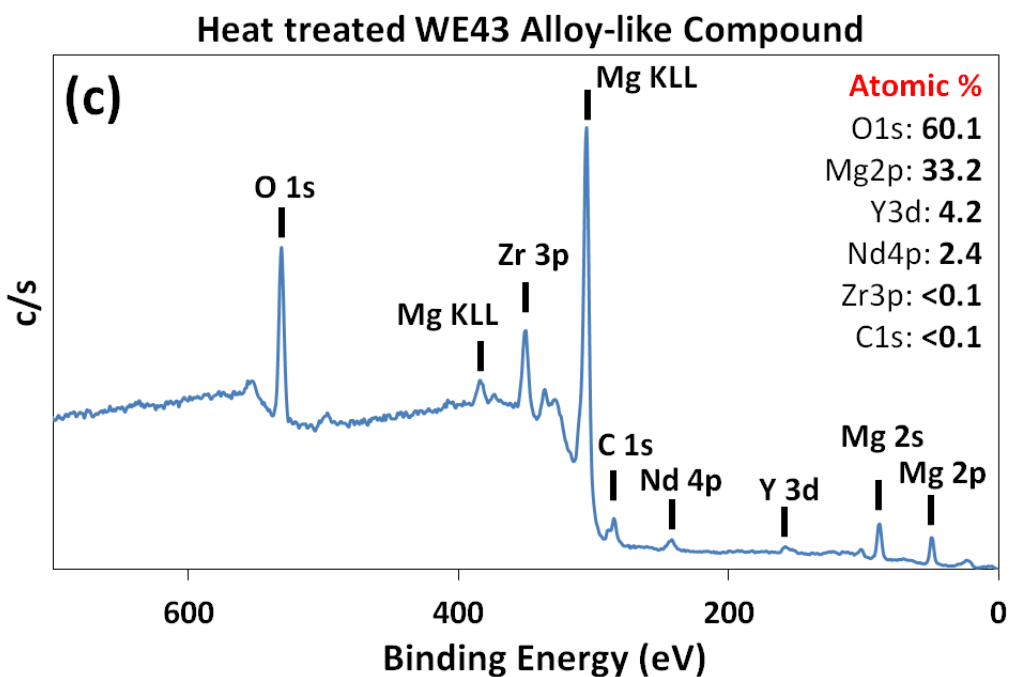
Figure 4.6.   XPS plots of (a) electrospun single PVA mat, (b) electrospun mat containing PVA and metallic nitrate salts (pre-treatment mat), (c) electrospun WE43 alloy-like compound (post-treatment mat)

Figure 4.6.a shows that the single-PVA was successfully electrospun with the given parameters. The peaks at 285 eV and 530 eV correspond to the C1s and O1s, respectively, which was expected from a polymeric structure. The shifts and the composition of these peaks are similar to those reported in the literature for PVA [291]. Figure 4.6.b, on the other hand, represents the metallic nitrate salts electrospun with PVA to obtain fibrous structure. However, since this structure is in pre-treatment stage, majority of the structure still contains PVA. Therefore C1s and O1s peaks are still present with high composition. However, because the structure now contains metallic nitrates, the plot shows peaks around 53 eV and 158 eV which respectively correspond to magnesium (Mg2p), the majority of the nitrate salts, and yttrium (Y3d), the nitrate salt with the second high amount present. The Mg2p and Y3d peaks, among other few peaks that represent WE43, can be found in the XPS data of other studies conducted by Ascencio et. al. [292], Ardelean et. al. [293] and Jin et. al. [294], confirming the findings of this study. The final plot in Figure 4.6.c shows the binding energies found in WE43 alloy-like compound obtained after heat treatment of the metallic nitrate salts electrospun with PVA. As it can be seen

from the figure, C1s peak almost disappeared to an undetectable composition (less than 0.1%) which means the polymer content was successfully removed during the heat treatment process. The other peaks around 50 eV, 89 eV, 305 eV and 386 eV that correspond to Mg2p, Mg2s, Mg KLL and Mg KLL of the magnesium content as well as peaks around 163 eV, 246 eV and 351 eV that represent Y3d of yttrium, Nd4p of neodymium and Zr3p of zirconium content, respectively, were found in the structure confirming the successful fabrication of the WE43 alloy-like compound by using the designated novel approach [292–294]. Finally, the peak with the highest composition were found to be O1s which represents the oxides in the structure such as MgO, YO, NdO and ZrO since the structure fabricated was planned to be an alloy-like compound containing oxides of the alloy targeted.

4.2.3. X-Ray Diffraction

Similar to XPS which analyzes the material structure based on the binding energies of the components, XRD can be also utilized to investigate material structures. The main difference is that XRD determine the crystallographic structures based on the diffraction of the x-rays. This method is generally used for metallic materials (compound or alloy) which are most of the time in crystalline form, rather than amorphous like the majority of the polymers. However, it can be used for polymers in such way that it can differentiate the crystalline structure from amorphous or semi-crystalline structures, like in this study. As mentioned in the previous section, it is crucial to determine the structural stages of the material developed during the fabrication process. Since the initial electrospun structure consists of polymer as well as metallic nitrate salts, the mats are expected to have mostly amorphous and/or semi-crystalline structure present. However, as the heat treatment concludes, the structure of the electrospun mats is expected to shift to a crystalline state because of the alloy-like compound formed and the polymer is pyrolysed. Therefore, XRD analyses were also conducted to the same three structures obtained along the fabrication process; (i) electrospun PVA mats (without metallic nitrate salts), (ii) electrospun PVA containing metallic nitrate salts (mats pre-treatment) and (iii) electrospun WE43 alloy-like compound mats (post-heat treatment). The resulting plots were given in Figure 4.7.
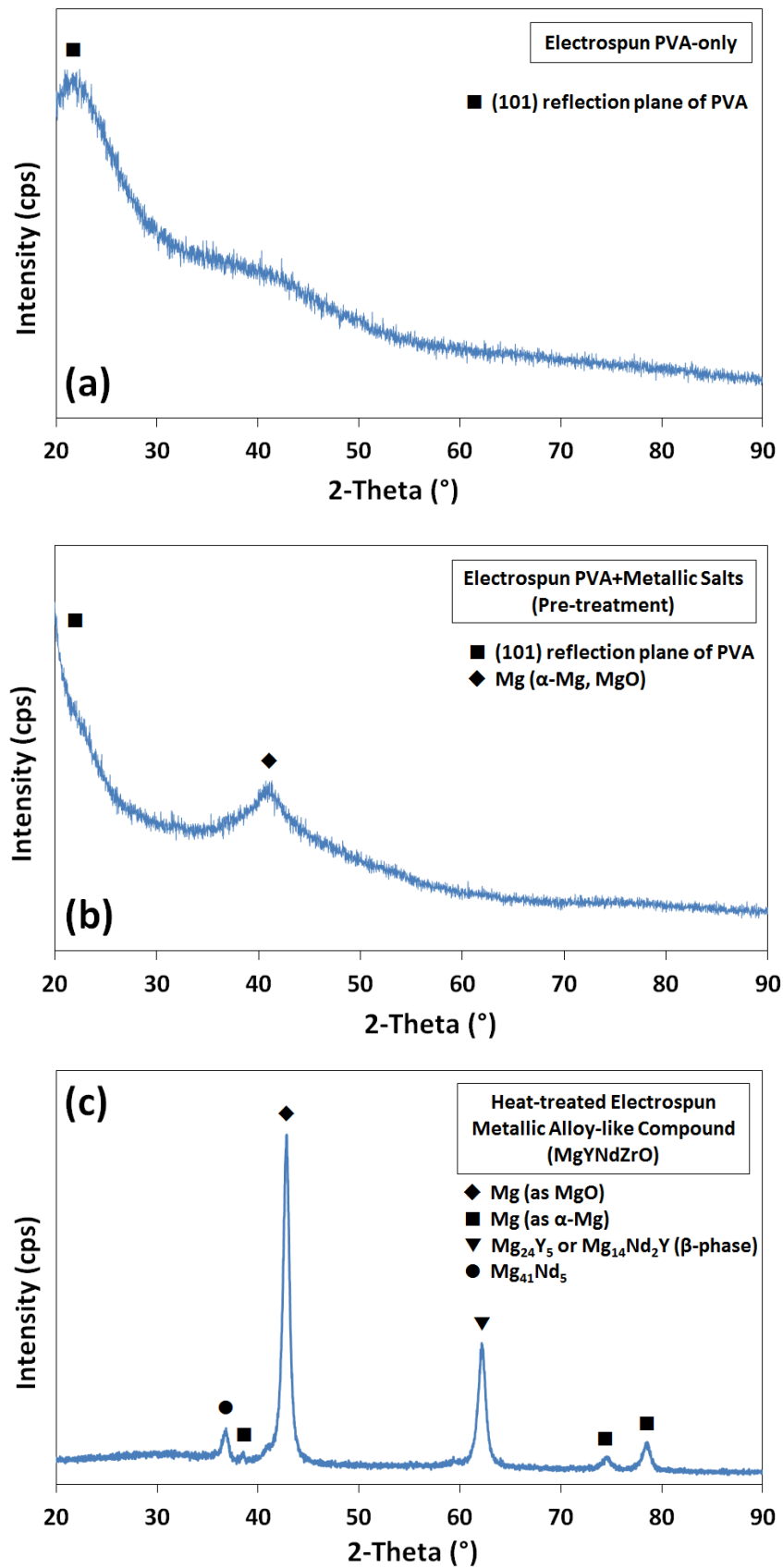
Figure 4.7.   XRD plots of (a) electrospun single PVA mat, (b) electrospun mat
containing PVA and metallic nitrate salts (pre-treatment mat), (c)
electrospun WE43 alloy-like compound (post-treatment mat)

In Figure 4.7.a, an XRD curve of semi-crystalline solid can be seen. The wide peak starting from around 20° (2θ) represents (101) plane of PVA which confirms the presence of the partial crystallinity of semi-crystalline PVA in the structure which is a result of intermolecular as well as intramolecular hydrogen bonding between polymer chains [295]. On the other hand, when the metallic alloy salts added to the electrospinning solution, the resulting electrospun mats showed an additional peak around 40° (2θ) (Figure 4.7.b) which is normally found in magnesium alloys or compounds as a representation of magnesium element, α-Mg or magnesium oxide (MgO) [267, 270]. Therefore, in addition to XPS analysis, the XRD analysis of this sample proved that the metallic nitrate salts were successfully incorporated into the electrospun fibers of the PVA. Finally, after the heat treatment process, the wide peak around 20° (2θ) disappeared as expected when the polymer content is removed, and sharp peaks at 36°, 38°, 42°, 62°, 74° and 78° (2θ) became present (Figure 4.7.c). The diffraction peaks at 38°, 74° and 78° (2θ) corresponds to Mg as α-Mg where the peak at 42° (2θ) represents Mg as magnesium oxide (MgO) [267, 270]. Additionally, according to Ascencio et. al [292], Kubasek et. al. [264] and Kang et. al. [296], the diffraction peak at 36° (2θ) is a result of Mg-Nd as $Mg_{12}Nd$ and/or $Mg_{41}Nd_5$ where the diffraction peak at 62° (2θ) is related to Mg-Y as $Mg_{24}Y_5$ and/or $Mg_{14}Nd_2Y$ (β-phase) as reported by the same studies as well as Asqardoust et. al. [273]. It can be seen from the results that after the heat treatment, the metallic nitrate salts transformed into different intermetallic compounds of Mg-Y or Mg-Nd in addition to the majority of phases such as α-Mg and MgO. These compounds and phases are distinctive confirmation of a successful WE43 alloy-like compound fabrication, according to the literature. Therefore, it is concluded that, with the designated heat treatment regime in this study, it is possible to develop a metallic alloy-like compound in WE43 alloy family by using metallic nitrate salts as precursor and electrospinning as the main fabrication method.

4.2.4. Wettability

The wettability of any tissue scaffold developed is important since the cells favor hydrophilic surfaces with approximately 50° contact angle value which is the contact angle value of commercial TCPS Petri dishes [297]. Therefore, it is

crucial to identify the wettability of a scaffold in terms of contact angle, so that it gives preliminary idea of how well the scaffold will perform in cell culture studies.

The contact angle values measured from three calcinated samples (Figure 4.8) were found to be 60.49°, 58.85° and 57.97°. Therefore, the average contact angle of a calcinated sample was 59.10° ± 1.28. In our previous studies, an average contact angle between 45° and 80° for a scaffold were found to be highly favorable for cell attachment and proliferation [53, 99, 298–300]. The fibrous and/or rough nature of a scaffold also widely known to increase the biocompatibility performance against the anchorage dependent animal cells due to providing high number of attachment points similar in natural extracellular matrix [301, 302]. The contact angle values obtained in this study met the requirement of being both similar to the commercial TCPS containers used widely in tissue culture experiments and in the suggested range of proposed contact angle values. Therefore, it is concluded that the combination of the fibrous structure as well as the wettability and the rough surface nature of the fibers in the developed samples were expected to provide good performance in terms of biocompatibility.
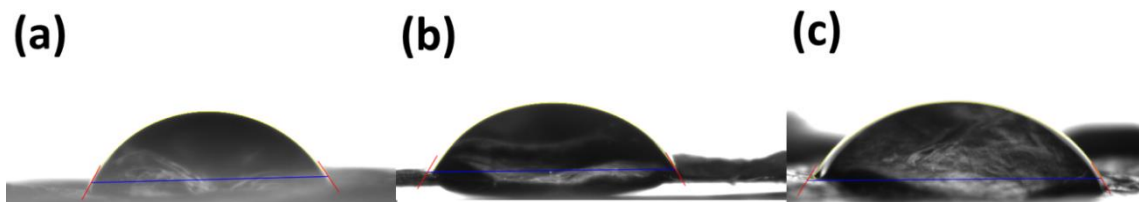
Figure 4.8.   Contact angle measurements obtained from three samples; (a) 60.49°, (b) 58.85°, and (c) 57.97°.

4.2.5. In Vitro Degradation

The in vitro degradation of a tissue scaffold is preferred to be at a certain rate that matches the new tissue forming during the healing process since the scaffold must provide sufficient structural support throughout the entire healing course but should also be replaced as the new tissue formed [303]. In case of peripheral nerve injuries, the degradation rate should at least be in conjunction with the healing rate of 2 mm per month so that the scaffold can keep the

protection, permeability and support necessary for nerve regeneration. In this thesis study, the developed alloy-like compound mats were tested against PBS and lysozyme containing degradation test solution for 6 months. The magnesium alloys studied and/or used for stent applications showed problematic degradation rates, not suitable for viable usage [304]. However, the environment for stent applications is highly different from most of the other locations in the body, since there is a significant amount of flow (blood). This creates a dynamic and more eroding degradation behavior that resulted in poor performance for magnesium alloys in terms of long term support, even though the excellent biocompatibility [305]. On the other hand, in this thesis study, the environment is significantly different since there is no major flow of any kind around the peripheral nerves. Therefore, the degradation behavior was more static than stent applications, which is found to be in favor of the magnesium alloy mimicked in this thesis. The 30 day interval results showed that the prepared samples were resilient against fast degradation (Figure 4.9). The first two months of degradation process resulted in only ~5% weight loss for each month (~5.21% for 30 days, ~5.34% for 60 days) in which the sample still had a significant portion (89.45%) of its starting structure. The subsequent months showed slight increases in degradation (~6.83%, ~6.95%, ~7.47% and ~7.26% for 90, 120, 150 and 180 days, respectively) resulting in remaining total weight of ~60.94% of its starting structure. As expected from an artificially developed alloy-like compound used in a static environment, the samples showed significantly lower degradation rate over six months unlike a similar alloy used for stent applications. These results were particularly promising for the developed samples since the low rate of degradation means longer support can be provided during the nerve regeneration process. However, it should also be noted that this low degradation rate should be adjusted in terms of sample size for shorter nerve injuries or injuries that can heal less than 6 months. Because, a few studies in the literature showed that alloys containing high amount of magnesium such as WE43 can affect the genetic expression of the nerve cells and/or nerve reconfiguration [215, 306]. Therefore a support material remaining still more than 50% intact even after the regeneration may require additional surgical intervention to remove the support material from the wound site to prevent any possible negative effect. It was concluded that the samples

prepared in this thesis can be a good candidate for nerve regeneration applications in terms of biodegradability, and it is also possible (and highly suggested) to adjust the degradation rate in terms of sample size for a more suitable and accurate support rate.
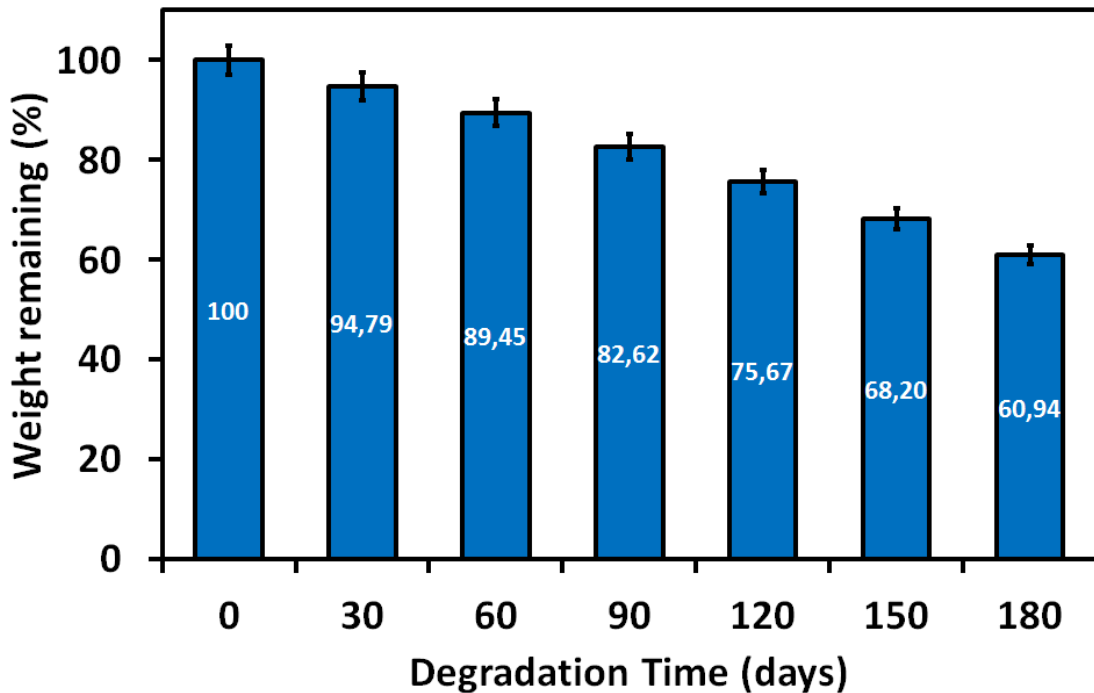
Figure 4.9.   In vitro degradation of calcinated fibrous samples for 6 months period.

4.2.6. Permeability Assays

The humidity of a wound site is an important part of a healing process. There are few guidelines of how much humidity should maintained for different types of wounds, however there is almost no information on how a nerve injury site should maintain its inner humidity for a better regeneration performance. In this thesis study, the developed samples were tested for water vapor transmission rate in order to obtain a possible relationship between the level of inter fiber porosity of the samples and the humidity permeability which later will be linked to the biocompatibility performance conducted at the end of the study. In the literature, at least a humidity permeation rate of 2500-5000 g/m^2.day is suggested for an open wound by different studies in order to prevent risk of wound site dehydration [208, 307, 308]. In this study, the average WVTR of the

prepared samples was found to be 5316 ± 49 g/m^2.day from at least 6 samples tested. This amount of dehydration rate was slightly higher than those suggested for an open wound; however, since a nerve injury site is a more enclosed space than an open wound, the internal pressure on the wound site border is a lot less than an open space which lowers the chance of vapor evaporation from the injury site. Therefore, it is concluded that the WVTR of the prepared samples was well within the acceptable range.

On the contrary of humidity permeation, nutrients, trophic factors and waste transmissions are required to be as high as possible in order to improve the nerve regeneration success over the course of the healing process. Lysozyme and BSA are both used widely in the literature for testing of permeability, as an acceptable representation of nutrient, trophic factor and waste transfer. Lysozyme and BSA, having MW around 14 and 65 kDa, respectively, are usually utilized in these studies in which at least 20% lysozyme (around 0.3-0.5 OD) and 10% BSA (around 1-1.2 OD) permeation is acceptable in the first 24 h [309, 310]. The optical densities obtained from the prepared samples at the end of 24 h and 48 h were found to be 0.47±0.01 and 1.09±0.02 for lysozyme and 0.61±0.02 and 1.13±0.01 for BSA. These results showed that the permeability of the prepared samples were well within the acceptable range and the permeation of lysozyme was found to be easier compared to BSA since the increase in permeation was higher at the end of 48 h. Chang et. al. [311] and Wang et. al. [312] were found similar results for PLGA and chitosan based nerve guidance conduits developed in their respective studies. Therefore, it is concluded that the developed samples were suitable for nerve regeneration applications in terms of solid molecule permeation required for the nerve healing process.

4.2.7. Absorption and Swelling
The fluid absorption capacity of a tissue scaffold is a representation of how the supporting material keeps the humid environment during the regeneration process. The scaffolds are also responsible for the transport of several constituents of the bodily fluids in the injury site, depending on the injury type. In nerve regeneration process, several nutrients and neurotrophic factors are

present at the injury site which require scaffold to allow transport easily and maintain at a certain concentration throughout the process. Therefore a certain level of fluid absorption capacity is crucial for a scaffold to be viable for a nerve regeneration application. However, a scaffold that is considered for a possible candidate should also be resilient to significant volume changes along with the fluid absorption. In nerve regeneration process, the volume changes can be highly undesired since it is crucial to keep both nerve endings in communication with each other in order to prevent Walleran degeneration. It is possible for a swelling scaffold to change its volume towards the injured nerve gap which can significantly hinder the axon endings to grow to each other. Therefore, an ideal nerve tissue scaffold should have a certain level of absorption capacity without showing any significant swelling in the injured site.

In this thesis study, the absorption capacity of the developed sample was found to be 71.23%±2.67. Due to the interconnected network of fibrous structure obtained at the end of the fabrication as well as mild hydrophilicity of this structure provided a fairly good water uptake ability for the developed nerve scaffold. The absorption capacity over at least 60% is usually an acceptable limit for a scaffold to be viable to retain the humid environment required for tissue regeneration, therefore the developed sample in this study was accepted as suitable.

Additionally, the developed samples showed 1.05%±0.19 swelling after 24 h of incubation and less than 1% shrinkage after being dried for 12 h. It was found that because of the alloy-like nature, the developed sample was highly resistant to any volume changes even if its relatively high water absorption capacity. In our previous studies as well as several literature studies, similar behavior can be found for fibrous networks [99, 298, 313, 314]. Because of their high surface area to volume ratio and high porosity, electrospun structures can absorb significant level of fluids depending on the material used. In this thesis, the developed structure had similar high surface area and porosity due to its large pores and fibrous network combined with an alloy-like base material which resulted in the obtained high absorption and low swelling/shrinkage values. Therefore it is concluded that the developed samples were safe to use in nerve

regeneration processes without facing any significant problems in terms of retaining humid environment and size changes throughout the healing.

4.3. In Vitro Cell Culture Studies

In this thesis study, the biocompatibility of fibrous WE43 alloy-like compound scaffolds fabricated with optimized electrospinning parameters and calcinated with controlled temperature-time parameters was determined with standard cell culture assays and imagings using commercial L929 ATCC CCL-1 mouse fibroblast cell line. L929 cells are one of the standard cell types recommended by ASTM for cytotoxicity analyses of scaffold materials [315] and are also widely utilized for evaluation of tissue scaffolds for nerve tissue engineering applications [316–320].

The primary aim of this thesis was to investigate the possibility of adapting electrospinning technique, a widely known fiber fabrication method, for a metallic alloy in order to fabricate a scaffold structure that meets the primary requirements of a nerve guidance conduit such as fibrous network, interconnected porosity, suitable degradation, water absorption and swelling capacity as well as fundamental biocompatibility. Therefore, in studies like this, the preliminary in vitro biocompatibility assessments were preferred to be conducted with low cost, easily cultured cell lines such as L929. Because, the fibroblast cells are the most common cell type of animal connective tissue found in almost every location of the body, and any type of potential scaffold candidate material should be tested for biocompatibility primarily with this type of cell before any further assessment. Any potential candidate that fails to be biocompatible with or shows toxicity to this type of cell, will unlikely show compatibility to a more specific and complex cell type such as nerve cells. As a result, the biocompatibility studies of the developed samples were conducted with L929 fibroblast cells in this thesis.

The scope of these studies was consisted of initial early stage cell attachment, cell viability and yield as well as visual imagings in which standard cell culture assays were utilized, and the results were presented with discussions in the following sections.

4.3.1. Cell Attachment

A good biocompatibility and a subsequent effective regeneration usually depend on the initial early stage cell attachment performance of the candidate material. It is the first stage of the cell-material interactions in which the cells needs structural support the most. Animal tissue cells are defined as anchorage dependent cells which mean the cells require a surface to attach before they can reproduce. The mechanism behind this lies in the surface proteins such as integrins and receptors such as growth factor receptors. They basically regulate mechanisms such as cell division, proliferation, growth or programmed death (apoptosis) through surface properties in which these mechanisms became favorable when the surface attachment unfold the folded surface proteins and expose receptors for growth factors [321]. Therefore, it is crucial for an animal tissue cell to attach to a surface as soon as possible in order to continue their normal life cycle. Several studies in the literature show that the initial cell attachment performance significantly affects the consequent short term and/or long term biocompatibility as well as the resulting regeneration performance [99, 322, 323]. Since these cell types are highly dependent to anchorage points, a high surface area is often favorable. The electrospinning technique provides significantly high surface areas through a fibrous interconnected network which is basically the same as the natural biological systems do through the ECM. This is the main reason for investigating the possibility of adopting this technique to a metallic alloy as the primary aim of this thesis study.

The early stage attachment performance of the developed samples was assessed for 3 h at 30 min intervals under standard culture environment. Since the developed samples are novel in terms of both base material as well as adoption of the technique used to fabricate that material, commercial tissue culture Petri dishes that are widely and effectively used for cell culture were selected for comparison and used as blank. The cells were attached to the sample surface at almost 50% of their initial seeding concentration within the first hour of the culture (Figure 4.10). In the following hour, more cells were found to attach to the sample surface at a steady rate up until the cell concentration attached reached to 80-85% of the initial concentration. The final hour of the attachment study showed a decline at the attachment rate where

only 10% more of the cells attached before the developed sample reached what was concluded to be as its performance limit. On the other hand, the blank TCPS used as comparison showed steady attachment rate through the 3 h period where it finally reached 80-85% attachment concentration of the initial seeding. The results were obtained as expected since it is a known fact that the wettability and the surface topography are two key factors that can improve the cell attachment and the developed samples were found to have wettability similar to TCPS as well as fibrous structure similar to natural ECM. On the other hand, the slightly better performance of the developed samples compared to TCPS was because of the difference in the surface/bulk topography. TCPS Petri dishes are commercially used high efficient culture dishes with a straight non-porous surface which can only allow the cells to grow as monolayer or in 2D. However, in contrast to TCPS dishes, the developed samples had both uneven/irregular surface topography as well as interconnected fibrous/porous 3D bulk structure which can allow the cells to attach also between fibers and/or into the pores at the same time interval. This resulted in the observed performance difference and showed that the developed scaffold can be a viable candidate of tissue biocompatibility.
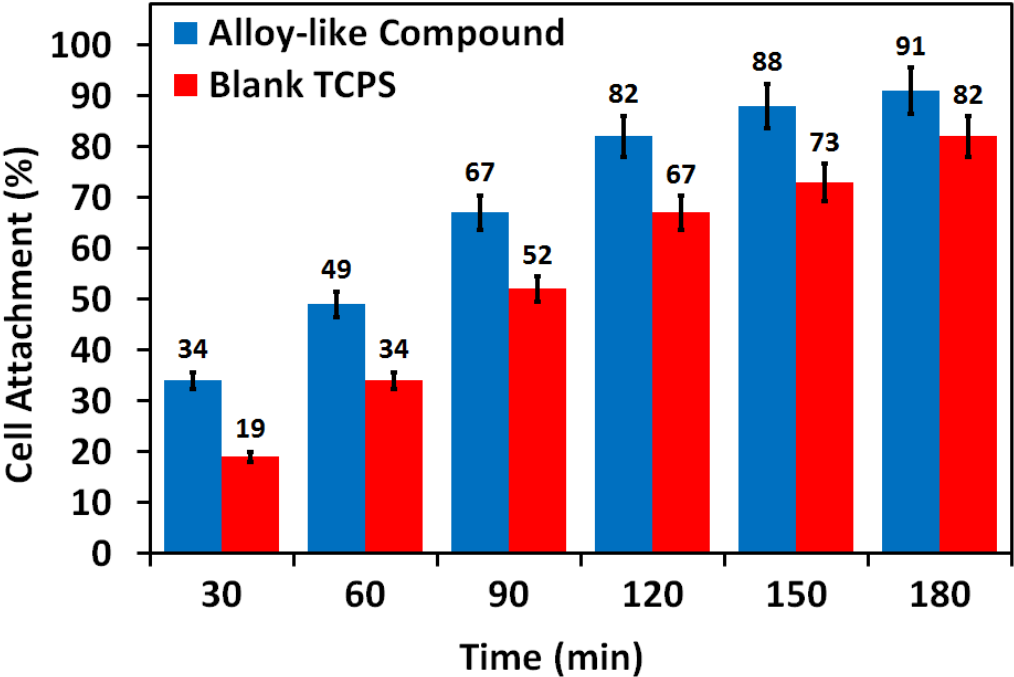

Figure 4.10. 3 h cell attachment performance of developed samples in compared to blank TCPS Petri dishes at 30 min intervals.

4.3.2. Cell Viability and Cell Yield

The next stage of a viable biocompatibility performance is the ability of the candidate material keeping the attached cells alive and functional over a certain amount of time depending on the cell type. In this time frame, the performance of the candidate material is measured in terms of toxicity or cell viability. One of the most common used methods for toxicity/viability assessment is MTT assay. MTT or 3-(4,5-dimethyl-2-thiazolyl)-2,5-diphenyl-2H-tetrazolium bromide is a yellow colored dye that is metabolized by the mitochondria of cells and the metabolites occurred after this process are formazan crystals that has purple color and insoluble in water. The main idea behind this assay is to observe the amount of tetrazolium dye converted into formazan crystals by optical means. Because this process can only be conducted by live cells and therefore the amount strongly depends on the number of live cells. By measuring the intensity of the resulting purple colored solution, it is possible to predict the viability of the cell at any time necessary [324].

In this thesis, an electrospun WE43 alloy-like compound has been developed and tested for biocompatibility performance. Similar to the initial early stage attachment performance assessment, the developed samples were also tested for viability in compared to the commercial tissue culture Petri dishes used widely for routine cell culture studies. The MTT viability results presented in Figure 4.11 showed that both the developed samples and the TCPS provided a steady inclining viability for L929 fibroblast cells on the course of 7 days. The developed samples also showed a slightly better performance compared to TCPS starting from the beginning of the culture period. This result was expected since, in the first stage of biocompatibility assessments, it was found that the developed samples performed better in providing early stage attachment for the fibroblast cells. It is proposed by several studies in the literature that the initial attachment can greatly influence the subsequent cell viability and proliferation, because of early initiation of metabolic activity [325, 326]. Therefore, the fibrous/porous structure, the 3D uneven surface and the suitable wettability of the developed samples in this thesis were not only effective for the initial stage but also increase the potential of the candidate material on the course of fibroblast cell life-cycle. The steady increase in

viability also confirmed that the developed candidate material have no toxicity to the cells. TCPS Petri dishes were performed as expected, providing good viability and showing no toxicity, however, as a result of their flat, non-porous surface, their potential of supporting cell culture is limited to commercial or laboratory scale cultivation. On the other hand, the developed sample performed better than TCPS Petri dishes, even though the difference was slightly but noticeable, therefore, it can be concluded that the developed samples can provide adequate biocompatibility and support which made them suitable for a proper candidate material for further and more advanced cell studies.
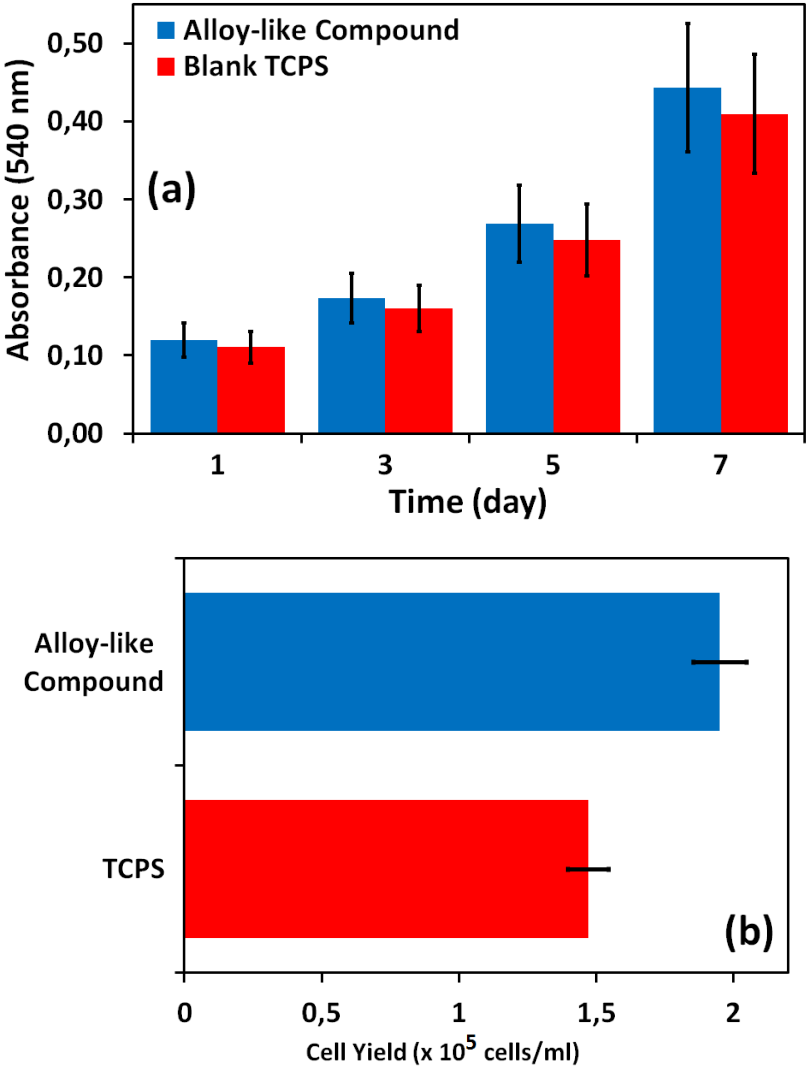

Figure 4.11. (a) 7-day viability performance and (b) final cell yield on the 7th day, for both developed samples and commercial TCPS Petri dishes.

4.3.3. Visual Assessments

The morphology of the cells cultured for biocompatibility studies is also as important as the metabolic activity of those cells. Every animal tissue cell has a certain characteristic structure, especially after a certain time passed in the culture. For instance, fibroblast cells used in this thesis has a spindle like shape obtained by the cell a couple of days after the initial attachment. When the fibroblast cells obtain this characteristic morphology, it represents that the cells are being cultured in a suitable, safe and supporting environment. Therefore, it is crucial to observe a culture visually, especially after a certain amount of days passed without any toxic effect encountered.

The visual inspection of the cells cultured in this thesis was conducted with two different imaging methods. The confocal laser scanning microscopy is an optical microscopy technique used along with biological marking, in which the certain portion of cells were marked with light sensitive biological agents, called stains, in order to observe the health and structure of those portions. The other method used in this study was scanning electron microscopy, in which it is possible to obtain visual depth of field from the cultured samples in order to inspect 3D morphologies. In CLSM, it is possible to inspect biological portions and their viability which are not possible with SEM whereas in SEM it is possible to observe the cell structure in 3D which is not possible with CLSM since it obtains visuals in 2D, section by section from the samples examined. Therefore, both microscopy techniques were utilized for visual assessment of samples cultured with cells in this thesis. Figure 4.12 and 4.13 shows CLSM and SEM images obtained from the samples, respectively, cultured with L929 fibroblast cells at the end of the 4th and the 7th day.

Confocal images showed that a significant number of cells has been attached and proliferated on the sample, even on day 4 of the culture. Since DRAQ5 stains nuclei of live cells, it can be seen from the images that cells proliferated on the sample had high viability on the 4th day and remain viable until the end of the culture on the 7th day. Also, the AF-488 stained actin filaments showed that the cells attached strongly on to the surface of the developed sample and even on the 4th day, they began to show the characteristic spindle-like morphology.

Finally, on the 7th day, most of the cells seemed to fully achieve their expected morphologies, with several actin filaments extended to different directions.
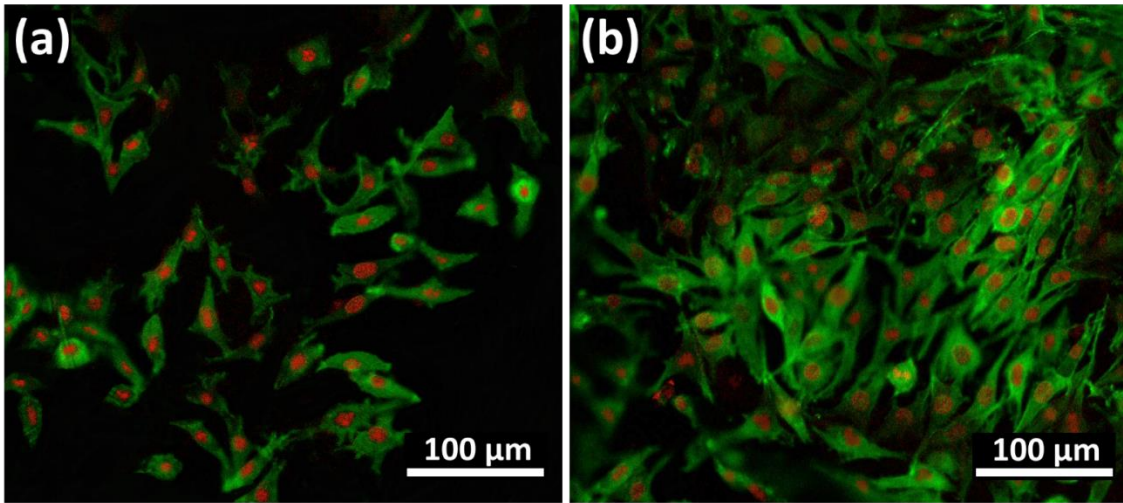
Figure 4.12. CLSM images of the developed samples on (a) day 4 (x20) and (b) day 7 (x20).

Similar results were also obtained from the visual inspection conducted with SEM. The images from day 7 showed several clustered cells proliferated on the surface. On the 7th day, almost the entire surface of the sample was covered leaving only small portions of fibers visible underneath. The characteristic spindle-like structure of the fibroblast cells was visible more distinctively with SEM images, and therefore consistent with the CLSM images obtained.
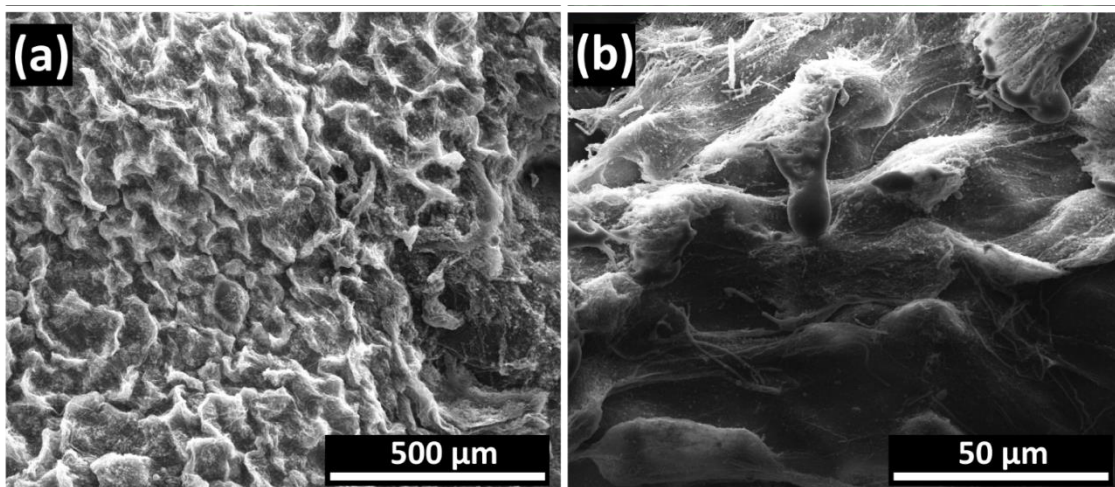
Figure 4.13. SEM images of the developed samples on day 7, at (a) x250 and (b) x2500 magnifications.

These results clearly indicated that the developed samples were not only biocompatible for showing no detectable toxicity, but also had a very good performance in supporting the cells to reach their healthy active phases. Therefore, it can be concluded that the developed samples has sufficient ability to support cultured fibroblast cells in terms of structure, which could made them suitable for further research on scaffolds for more complex cell/tissue types such as nerve conduits.

5. CONCLUSIONS

In this thesis study, electrospun, fibrous/porous alloy-like compound mimicking the commercial WE43 magnesium alloy was fabricated as a possible candidate for nerve tissue engineering applications. The candidate material was fabricated with an easy to use, versatile fiber fabrication technique called electrospinning, instead of traditional metal alloy fabrication methods. In the scope of this thesis, the possibility of adapting the electrospinning technique for alloy-like compound fabrication, the design of a proper calcination regime for the electrospun samples as well as the optimization of both these two major fabrication steps were investigated in detail. The characterization of the samples obtained at the end of fabrication, was also investigated in terms of physical and chemical properties as well as biocompatibility performance using SEM, EDX, XRD, XPS, contact angle, permeability, degradation and absorption/swelling measurements as well as cell attachment, cell viability and visual morphology assessments, and the results were presented and discussed extensively in the previous section.

Adapting the electrospinning technique to a metal alloy/alloy-like compound fabrication requires a solution or any soluble raw forms of alloy components in order to work. In order to obtain a precursor solution for the commercial WE43 magnesium alloy with a composition of 93.6% Mg, 4% Y, 2.25% Nd and 0.15% Zr, water soluble nitrates of alloy components $Mg(NO_3)_2.6H_2O$, $Y(NO_3)_3.6H_2O$, $Nd(NO_3)_3.6H_2O$ and $ZrO(NO_3)_2.xH_2O$ were used at the corresponding amounts. The nitrates were found to be easily soluble after 24 h with the given amounts at 30°C stirring temperature and 400 rpm stirring rate, up to 5 g of total nitrate amount.

The aqueous nitrate solutions were found to have viscosity not sufficient for stable and continuous electrospinning. Therefore, two different polymers, PVP (MW ≈ 1.3×10^6) and PVA (MW ≈ 8.5-12.4×10^5) were separately tried in order to increase the viscosity of the nitrate solution to a more suitable level for electrospinning. The optimization of the electrospinning solution parameters

was carried out in terms of nitrate and polymer concentration, solvent concentration, stirring temperature and stirring rate. The solutions prepared with PVP were tried with nitrate amount between 0.25 to 5 g, PVP concentration at 2.5 or 5 wt.%, ethanol/water solvent concentrations changing from 0/100 to 100/0 (v/v), stirring temperatures at room temperature, 30°C, 50°C or 90°C, and stirring rate between 200 and 700 rpm. On the other hand, the solutions prepared with PVA were tried with nitrate amounts at 0.25 g, 0.5 g, 1 g, 1.5 g, 2 g or 5 g, PVA concentration at 2.5, 5, 10 or 15 wt.%, stirring temperature at 70°C, 80°C or 90°C, and stirring rate between 200 rpm. It was found that stirring temperatures higher than 30°C and 80°C were viable for PVP and PVA, respectively where both PVP concentrations and all solvent concentrations ranging from pure ethanol (100/0 v/v) to pure water (0/100 v/v) as well as PVA concentrations up to 10 wt.% and nitrate amount up to 2 g were found as other viable parameters for both types of electrospinning solutions.

The optimization of the electrospinning process parameters was carried out in terms of applied voltage, solution feeding rate and syringe-collector distance. The voltage applied to the solutions was optimized between 15-30 kV with 1 kV intervals. The solution feeding rate, on the other hand, was optimized between 5-15 µl/min with 0.5 µl/min intervals. Finally the distance between the feeding syringe and the fiber collector was optimized between 10-20 cm with 1 cm intervals. The process parameter optimizations were carried out along with the preliminary electrospinning solution parameter optimizations in order to achieve electrospinning in terms of jet initiation and spinning continuity.

All solutions prepared with PVP, except the ones prepared with 0/100, 5/95 and 100/0 (v/v) ethanol/water, were found to be capable of initiating a spinning jet. However, only the solution prepared with 25/75 (v/v) ethanol/water at 30°C with 5 wt.% PVP was managed to keep spinning continuity until the fed solution depleted. This solution was successfully and continuously electrospun at 5 µl/min feeding rate under 30 kV from a distance of 12-15 cm. On the other hand, all solutions prepared with PVA, except the ones prepared with 15 wt.% PVA, were found to be capable of initiating a spinning jet. However, PVA solutions prepared at less than 80°C were found to fail at providing jet

continuity. Therefore, solutions with PVA concentration 2.5 or 5 wt.% prepared at 80°C or 90°C containing 0.25-5 g of nitrate salts were found to be optimum for both jet initiation and continuous spinning. These solutions were successfully and continuously electrospun at 5 µl/min feeding rate under 30 kV from a distance of 12-15 cm.

Following the successful fabrication of fibrous/porous structure of the polymer/nitrate raw components by using electrospinning, the obtained structures were subjected to heat treatment in order to remove polymer and calcinate the remaining nitrated into oxide compound that mimic the alloy. The heat treatment required for calcination was designed individually based on the type of solution prepared. The temperatures required were determined according to the thermal analyses conducted to the electrospun samples, polymer and nitrates separately. Based on the conducted thermal analyses, the key temperatures were determined as 325°C, 425°C, 455°C, 530°C and 230°C, 390°C, 465°C, 500°C, 505°C for calcination of the electrospun samples prepared with PVP and PVA, respectively.

The duration for which the determined temperatures were subjected to the electrospun samples were calculated theoretically based on the mathematical reaction kinetics assumptions proposed in the literature. According to key temperatures obtained, areas under each of these temperature peaks were estimated with Riemann sums approach from the corresponding thermal analyses plots. Based on these area data, log [ln (S / S-S_t) / t] vs 1/T graphs for PVP peak at 325°C, for peaks of metal salts at 425°C and 455°C, for peak of combined PVP-salts at 530°C, for PVA peak at 500°C and for peaks of combined PVA-salts at 230°C, 390°C, 465°C, and 505°C were plotted, and the slopes and the y-axis intersections of the straight lines on each graph gave the activation energy and the pre-exponential factor of the reactions occurred on each peak, and the time required to complete those reactions at 99.99% were calculated. Based on these calculations, the designated heat treatment for the samples prepared with PVP was found as 8 h at 325°C, 2.5 h at 425°C, 2 h at 455°C and 7 h at 530°C, and the designated heat treatment for the samples prepared with PVA was found as 6 h at 230°C, 8.5 h at 390°C, 5 h at 465°C, 80

h at 500°C and 10 h at 505°C.

After the fabrication with electrospinning and the calcination with the designed heat treatment regime, the prepared samples were subjected to a series of characterizations in which the physical and the chemical properties as well as the biocompatibility performance were assessed.

According to the SEM imaging, both of the samples prepared with PVP and PVA were successfully electrospun into a fibrous/porous mat. However, the SEM imaging conducted after the calcination showed that it is not possible to maintain the fibrous/porous structure for the samples prepared with PVP. The samples prepared with PVA, on the other hand, were still intact after the calcination. It was assumed that because the decomposition of PVP was occurred much earlier than the nitrate salts, compared to the decomposition of PVA which was found to be completed at higher temperatures, PVP failed to keep the fibers intact as their content calcinated to the alloy-like compound. Therefore, it is concluded that the alloy-like compound that mimicked WE43 alloy can only be successfully prepared with the polymer, PVA, with the composition and the optimized electrospinning and calcination parameters.

The EDX elemental analysis conducted to the sample successfully calcinated as a fibrous/porous structure showed the fiber composition mainly consisted of oxygen and magnesium where the rest was yttrium, neodymium and zirconium as expected. The high content of oxygen pointed out that the resulted structure was an alloy-like compound, containing the oxides of the four components of the alloy. These results confirmed the conclusion that it is possible to obtain a fibrous alloy-like compound with an empirical formula of $Mg_aY_bNd_cZr_dO_x$ which consists of merged oxides of the four components and therefore mimics the WE43 magnesium alloy.

In this thesis, the XPS and the XRD analyses were also conducted in order to monitor the different stages for the material content, in which polymer, metallic salts, alloy-like compound or a combination of these can be present at certain points of the entire process. Therefore, both analyses were conducted for three

different structures of this study; (i) electrospun PVA mats (without metallic nitrate salts), (ii) electrospun PVA containing metallic nitrate salts (mats pre-treatment) and (iii) electrospun WE43 alloy-like compound mats (post-heat treatment). The XPS results showed that PVA was successfully electrospun with the given parameters as peaks at 285 eV and 530 eV corresponding to the C1s and O1s of the polymer structure were present as two major peaks. On the other hand, pre-treatment samples showed additional peaks around 53 eV and 158 eV which respectively correspond to magnesium (Mg2p) and yttrium (Y3d), the two major nitrate salts used to prepare the samples, indicating the successful integration of nitrate salts into the fibers. The XPS data of the calcinated samples showed disappearance of the C1s peak since the polymer was thought to be completely decomposed, and other peaks around 50 eV, 89 eV, 305 eV and 386 eV that correspond to Mg2p, Mg2s, Mg KLL and Mg KLL of the magnesium content as well as peaks around 163 eV, 246 eV and 351 eV that represent Y3d of yttrium, Nd4p of neodymium and Zr3p of zirconium content, respectively, where highest peak was O1s, representing the oxides formed at the end of the calcination. The XRD analyses showed almost exact findings as XPS in terms of crystallographic diffraction data. The wide peak around 20° (2θ) representing the polymer on an XRD analysis, an additional wide peak around 40° (2θ) representing magnesium element, α-Mg or magnesium oxide (MgO), both of which disappeared after the calcination, and sharp peaks emerging after the calcination at 36°, 38°, 42°, 62°, 74° and 78° (2θ) representing Mg as α-Mg, Mg as magnesium oxide (MgO), $Mg_{12}Nd$ and/or $Mg_{41}Nd_5$, $Mg_{24}Y_5$ and/or $Mg_{14}Nd_2Y$ (β-phase) were the findings of XRD analyses. These results were also showed that PVA was successfully electrospun, the nitrate salts were successfully incorporated into the fibers and the calcination process was successfully created an alloy-like compound, containing the oxides of the four components of the mimicked WE43 alloy.

The further physical assessments showed that the developed samples had an average contact angle of 59.10° ± 1.28, average water vapor transmission rate of 5316 ± 49 g/m^2.day and average absorption capacity of 71.23%±2.67. The developed samples also showed 1.05%±0.19 swelling after 24 h of incubation and less than 1% shrinkage after being dried for 12 h; showed adequate

permeability for lysozyme and BSA; and was resilient against fast degradation, losing around ~5.21%, ~5.34%, ~6.83%, ~6.95%, ~7.47% and ~7.26% of its weight for 30, 60, 90, 120, 150 and 180 days, respectively and remaining at ~60.94% of its starting structure even after 6 months. All of these results showed that the developed samples were significantly suitable for a nerve tissue engineering application with these physical properties being within the required/acceptable range.

In the final stage of this thesis, the developed and assessed samples were investigated for a proper biocompatibility performance. The samples were cultured with L929 fibroblast cells under the standard culture conditions and assessed in terms of early stage cell attachment and the consequent cell viability as well as imagings conducted together with these assessments. The attachment assessment showed that the cells highly favored the surface of the developed electrospun fibrous/porous samples, reaching 50% attachment rate within the first hour and more than 90% attachment within 3 h. The viability assessment conducted by using standard MTT assay showed that the structure and the material of the developed samples were not only effective for the initial attachment of the cells but also potentially a good support on the course of fibroblast cell life-cycle without showing any kind of toxicity that hindered the cell activity. The visual inspection of the samples cultured for 4 and 7 days by using CLSM and SEM imagings was also confirmed the previous biocompatibility assessments and showed that the developed samples provided a healthy environment for the cells to proliferate, remain viable and reach their characteristic spindle-like morphology for 7 days.

The results obtained in this thesis, showed that it is possible to fabricate an alloy-like compound that mimics the commercial WE43 magnesium alloy by using electrospinning technique and a carefully designed heat treatment regime for calcination. The results also showed that nitrate salts of the alloy components can be used to prepare the electrospinning solution, PVA was a suitable polymer in increasing the viscosity, and most of the electrospinning solution parameters can be adjusted in order to obtain a continuously spinnable solution. It is also found that the theoretical reaction kinetics assumptions

adopted for calculating the calcination durations were viable for a material containing nitrate salts of WE43 alloy components and PVA. Based on the physical and chemical properties obtained and the subsequent biocompatibility performance assessments conducted, it can be concluded that a fibrous/porous morphology aimed in this thesis study for fabrication of an alloy-like compound material, and the developed compound which mimicked WE43 alloy were clearly a correct approach and a suitable choice in creating tissue engineering scaffolds, which was also confirmed with a wide variety of studies about similar structures found in the literature.

REFERENCES

[1]   V. Hasirci, D. Arslantunali, T. Dursun, D. Yucel and N. Hasirci, Medical Devices: Evidence and Research, 7 (**2014**) 405.

[2]   M. Wiberg and G. Terenghi, Surgical Technology International, 11 (**2003**) 303–10.

[3]   W.Z. Ray and S.E. Mackinnon, Experimental Neurology, 223 (**2010**) 77–85.

[4]   C.E. Schmidt and J.B. Leach, Annual Review of Biomedical Engineering, 5 (**2003**) 293–347.

[5]   V. Chiono and C. Tonda-Turo, Progress in Neurobiology, 131 (**2015**) 87–104.

[6]   W. Daly, L. Yao, D. Zeugolis, A. Windebank and A. Pandit, Journal of The Royal Society Interface, 9 (**2012**) 202–221.

[7]   X. Gu, F. Ding, Y. Yang and J. Liu, Progress in Neurobiology, 93 (**2011**) 204–230.

[8]   S. Agarwal, J. Curtin, B. Duffy and S. Jaiswal, Materials Science and Engineering: C, 68 (**2016**) 948–963.

[9]   C. Rapetto and M. Leoncini, Journal of Thoracic Disease, 9 (**2017**) S903–S913.

[10]   X. Gu, Z. Mao, S.-H. Ye, Y. Koo, Y. Yun, T.R. Tiasha, V. Shanov and W.R. Wagner, Colloids and Surfaces B: Biointerfaces, 144 (**2016**) 170–179.

[11]   X. Song, W. Liu, J. Wang, S. Xu, B. Liu, J. Liu and Y. Ma, Ceramics International, 43 (**2017**) 9831–9837.

[12]   B. Ding, C.K. Kim, H.Y. Kim, M.K. Seo and S.J. Park, Fibers and Polymers, 5 (**2004**) 105–109.

[13]   S. Sakai, Y. Yamada, T. Yamaguchi and K. Kawakami, Biotechnology Journal, 1 (**2006**) 958–962.

[14]   B. Vidyadharan, R.A. Aziz, I.I. Misnon, G.M. Anil Kumar, J. Ismail, M.M. Yusoff and R. Jose, Journal of Power Sources, 270 (**2014**) 526–535.

[15]   B. Vidhyadharan, N.K.M. Zain, I.I. Misnon, R.A. Aziz, J. Ismail, M.M. Yusoff and R. Jose, Journal of Alloys and Compounds, 610 (**2014**) 143–150.

[16]   W. Wang, L. Zhang, S. Tong, X. Li and W. Song, Biosensors and

Bioelectronics, 25 (**2009**) 708–714.

[17]   P. Viswanathamurthi, N. Bhattarai, H.Y. Kim, D.R. Lee, S.R. Kim and M.A. Morris, Chemical Physics Letters, 374 (**2003**) 79–84.

[18]   P. Viswanathamurthi, Scripta Materialia, 49 (**2003**) 577–581.

[19]   H. Wu and W. Pan, Journal of the American Ceramic Society, 89 (**2006**) 699–701.

[20]   K. Dalamagkas, M. Tsintou and A. Seifalian, Materials Science and Engineering: C, 65 (**2016**) 425–432.

[21]   P.H. Jensen, J.-Y. Li, A. Dahlström and C.G. Dotti, European Journal of Neuroscience, 11 (**1999**) 3369–3376.

[22]   S. Kehoe, X.F. Zhang and D. Boyd, Injury, 43 (**2012**) 553–572.

[23]   J.L.B. Senger, V.M.K. Verge, H.S.J. Macandili, J.L. Olson, K.M. Chan and C.A. Webber, Experimental Neurology, 302 (**2018**) 75–84.

[24]   M.F. Meek and J.H. Coert, Annals of Plastic Surgery, 60 (**2008**) 110–116.

[25]   S. Ichihara, Y. Inada and T. Nakamura, Injury, 39 (**2008**) 29–39.

[26]   R. Gupta, Experimental Neurology, 187 (**2004**) 500–508.

[27]   T. Matsuyama, M. Mackay and R. Midha, Neurologia Medico-Chirurgica, 40 (**2000**) 187–99.

[28]   H. Millesi, Annales de Chirurgie de La Main, 3 (**1984**) 18–34.

[29]   X. Jiang, S.H. Lim, H.-Q. Mao and S.Y. Chew, Experimental Neurology, 223 (**2010**) 86–101.

[30]   S.E. Mackinnon, V.B. Doolabh, C.B. Novak and E.P. Trulock, Plastic and Reconstructive Surgery, 107 (**2001**) 1419–1429.

[31]   H. Jia, Y. Wang, X.-J. Tong, G.-B. Liu, Q. Li, L.-X. Zhang and X.-H. Sun, Synapse, 66 (**2012**) 256–269.

[32]   M.E. Ortigiiela, M.B. Wood and D.R. Cahill, The Journal of Hand Surgery, 12 (**1987**) 1119–1123.

[33]   M.B. Chen, F. Zhang and W.C. Lineaweaver, Annals of Plastic Surgery, 57 (**2006**) 462–471.

[34]   S. Panseri, C. Cunha, J. Lowery, U. Del Carro, F. Taraballi, S. Amadio, A. Vescovi and F. Gelain, BMC Biotechnology, 8 (**2008**) 39.

[35]   S.A. Barbour and W. King, The American Journal of Sports Medicine, 31 (**2003**) 791–797.

[36]   M. Gabriel, F. Pukacki, Ł. Dzieciuchowicz, G. Oszkinis and P. Chęciński, European Journal of Vascular and Endovascular Surgery, 27 (**2004**) 590–596.

[37] G.C.W. de Ruiter and A. Kloet, Clinical Neurology and Neurosurgery, 134 (**2015**) 7–11.

[38] Y. Liu, J. Lao, K. Gao, Y. Gu and X. Zhao, Injury, 44 (**2013**) 655–660.

[39] T.H. Tung and S.E. Mackinnon, The Journal of Hand Surgery, 35 (**2010**) 332–341.

[40] G.M. Buncke, B. Rinker, W.P. Thayer, J. Ko, D. Tuder and B. Safa, The Journal of Hand Surgery, 40 (**2015**) e5.

[41] T.W. Hudson, G.R.D. Evans and C.E. Schmidt, Orthopedic Clinics of North America, 31 (**2000**) 485–497.

[42] J.S. Taras, N. Amin, N. Patel and L.A. McCabe, The Journal of Hand Surgery, 38 (**2013**) 1965–1971.

[43] J.S. Taras and S.M. Jacoby, Techniques in Hand & Upper Extremity Surgery, 12 (**2008**) 100–106.

[44] L.E. Kokai, Y.-C. Lin, N.M. Oyster and K.G. Marra, Acta Biomaterialia, 5 (**2009**) 2540–2550.

[45] S.E. Mackinnon, A.R. Hudson, R.E. Falk, D. Kline and D. Hunter, Neurosurgery, 15 (**1984**) 690–693.

[46] T. Schoeller, A. Otto, G. Wechselberger, B. Pommer and C. Papp, British Journal of Plastic Surgery, 51 (**1998**) 227–230.

[47] G.R.D. Evans, K. Brandt, M.S. Widmer, L. Lu, R.K. Meszlenyi, P.K. Gupta, A.G. Mikos, J. Hodges, J. Williams, A. Gürlek, A. Nabawi, R. Lohman and C.W. Patrick, Biomaterials, 20 (**1999**) 1109–1115.

[48] M. Lietz, L. Dreesmann, M. Hoss, S. Oberhoffner and B. Schlosshauer, Biomaterials, 27 (**2006**) 1425–1436.

[49] R. Bellamkonda, Biomaterials, 27 (**2006**) 3515.

[50] S.M. Willerth and S.E. Sakiyama-Elbert, Advanced Drug Delivery Reviews, 59 (**2007**) 325–338.

[51] G.C.W. de Ruiter, R.J. Spinner, M.J. Yaszemski, A.J. Windebank and M.J.A. Malessy, Neurosurgery Clinics of North America, 20 (**2009**) 91–105.

[52] D.F. Williams, Biomaterials, 29 (**2008**) 2941–2953.

[53] O. Ozkan and H. Turkoglu Sasmazel, Journal of Bioscience and Bioengineering, 122 (**2016**) 232–239.

[54] H.T. Şaşmazel, S. Manolache and M. Gümüderelioğlu, Plasma Processes and Polymers, 7 (**2010**) 588–600.

[55] H.T. Şaşmazel, M. Gumusderelioglu, A. Gürpinar and M.A. Onur, Bio-Medical Materials and Engineering, 18 (**2008**) 119–128.

[56]   S.C. Wittelsberger, K. Kleene and S. Penman, Cell, 24 (**1981**) 859–66.

[57]   D. Koch, W.J. Rosoff, J. Jiang, H.M. Geller and J.S. Urbach, Biophysical Journal, 102 (**2012**) 452–460.

[58]   L.R. Robinson, Muscle & Nerve, 23 (**2000**) 863–873.

[59]   A.M. Moore, R. Kasukurthi, C.K. Magill, H.F. Farhadi, G.H. Borschel and S.E. Mackinnon, Hand, 4 (**2009**) 180–186.

[60]   A. Hazari, M. Wiberg, G. Johansson-Rudén, C. Green and G. Terenghi, British Journal of Plastic Surgery, 52 (**1999**) 653–657.

[61]   F. Stang, G. Keilhoff and H. Fansa, Materials, 2 (**2009**) 1480–1507.

[62]   Y. Kim, V.K. Haftel, S. Kumar and R. V. Bellamkonda, Biomaterials, 29 (**2008**) 3117–3127.

[63]   G.H. Borschel, K.F. Kia, W.M. Kuzon and R.G. Dennis, Journal of Surgical Research, 114 (**2003**) 133–139.

[64]   H. Turkoglu Sasmazel and O. Ozkan, Current Tissue Engineering, 2 (**2013**) 91–108.

[65]   F. Stang, H. Fansa, G. Wolf and G. Keilhoff, Bio-Medical Materials and Engineering, 15 (**2005**) 3–12.

[66]   F. Stang, H. Fansa, G. Wolf, M. Reppin and G. Keilhoff, Biomaterials, 26 (**2005**) 3083–3091.

[67]   B.D. Bushnell, A.D. McWilliams, G.B. Whitener and T.M. Messer, The Journal of Hand Surgery, 33 (**2008**) 1081–1087.

[68]   T. Sedaghati, G. Jell and A. Seifalian, New Biotechnology, 31 (**2014**) 203–213.

[69]   J.W. Weisel, Journal of Thrombosis and Haemostasis, 5 (**2007**) 116–124.

[70]   S.T. Lord, Current Opinion in Hematology, 14 (**2007**) 236–241.

[71]   D. Kalbermatten, J. Pettersson, P. Kingham, G. Pierer, M. Wiberg and G. Terenghi, Journal of Reconstructive Microsurgery, 25 (**2009**) 027–033.

[72]   J. Pettersson, A. McGrath, D.F. Kalbermatten, L.N. Novikova, M. Wiberg, P.J. Kingham and L.N. Novikov, Neuroscience Letters, 500 (**2011**) 41–46.

[73]   J. Pettersson, D. Kalbermatten, A. McGrath and L.N. Novikova, Journal of Plastic, Reconstructive & Aesthetic Surgery, 63 (**2010**) 1893–1899.

[74]   Y. Yang, X. Gu, R. Tan, W. Hu, X. Wang, P. Zhang and T. Zhang, Biotechnology Letters, 26 (**2004**) 1793–1797.

[75]   E. Gámez, Y. Goto, K. Nagata, T. Iwaki, T. Sasaki and T. Matsuda, Cell Transplantation, 13 (**2004**) 549–564.

[76] I.H. Whitworth, R.A. Brown, C. Doré, C.J. Green and G. Terenghi, Journal of Hand Surgery, 20 (**1995**) 429–436.

[77] Y. Yang, F. Ding, J. Wu, W. Hu, W. Liu, J. Liu and X. Gu, Biomaterials, 28 (**2007**) 5526–5535.

[78] P.J. Apel, J.P. Garrett, P. Sierpinski, J. Ma, A. Atala, T.L. Smith, L.A. Koman and M.E. Van Dyke, The Journal of Hand Surgery, 33 (**2008**) 1541–1547.

[79] H. Zhang, Y. Wei, K. Tsang, C. Sun, J. Li, H. Huang, F. Cui and Y. An, Journal of Translational Medicine, 6 (**2008**) 67.

[80] T.W. Hudson, S. Zawko, C. Deister, S. Lundy, C.Y. Hu, K. Lee and C.E. Schmidt, Tissue Engineering, 10 (**2004**) 1641–1651.

[81] G.R.D. Evans, The Anatomical Record, 263 (**2001**) 396–404.

[82] X. Wang, J. He, Y. Wang and F.-Z. Cui, Interface Focus, 2 (**2012**) 278–291.

[83] H.S. Koh, T. Yong, C.K. Chan and S. Ramakrishna, Biomaterials, 29 (**2008**) 3574–3582.

[84] X. Wang, L. Chen, Q. Ao, A. Sharma and H.S. Sharma, Translational Neuroscience and Clinics, 1 (**2015**) 97–101.

[85] A.L. Dellon and B.W. Chang, Plastic and Reconstructive Surgery, 89 (**1992**) 576–8.

[86] M.F. Meek, Bio-Medical Materials and Engineering, 17 (**2007**) 329–34.

[87] A.S.P. Varejão, A.M. Cabrita, S. Geuna, P. Melo-Pinto, V.M. Filipe, A. Gramsbergen and M.F. Meek, Experimental Neurology, 183 (**2003**) 695–9.

[88] M.F. Meek and K. Jansen, Journal of Biomedical Materials Research Part A, 89A (**2009**) 734–738.

[89] M.F. Meek and W.F.A. Den Dunnen, Microsurgery, 29 (**2009**) 473–478.

[90] J.A. Stammen, S. Williams, D.N. Ku and R.E. Guldberg, Biomaterials, 22 (**2001**) 799–806.

[91] H. Ozer, H. Bozkurt, G. Bozkurt and M. Demirbilek, International Journal of Neuroscience, 128 (**2018**) 828–834.

[92] L. Nayyer, M. Birchall, A.M. Seifalian and G. Jell, Nanomedicine: Nanotechnology, Biology and Medicine, 10 (**2014**) 235–246.

[93] S.H. Oh, J.H. Kim, K.S. Song, B.H. Jeon, J.H. Yoon, T.B. Seo, U. Namgung, I.W. Lee and J.H. Lee, Biomaterials, 29 (**2008**) 1601–1609.

[94] S. Hsu, S.-H. Chan, C.-M. Chiang, C. Chi-Chang Chen and C.-F. Jiang, Biomaterials, 32 (**2011**) 3764–3775.

[95] Z.A. Gencer, S. Odabas, H.T. Sasmazel and E. Piskin, Journal of Bioactive and Compatible Polymers, 27 (**2012**) 419–428.

[96] M.S. Widmer, P.K. Gupta, L. Lu, R.K. Meszlenyi, G.R.D. Evans, K. Brandt, T. Savel, A. Gurlek, C.W. Patrick and A.G. Mikos, Biomaterials, 19 (**1998**) 1945–1955.

[97] D. Yucel, G.T. Kose and V. Hasirci, Biomaterials, 31 (**2010**) 1596–1603.

[98] C. Tonda-Turo, C. Audisio, S. Gnavi, V. Chiono, P. Gentile, S. Raimondo, S. Geuna, I. Perroteau and G. Ciardelli, Advanced Engineering Materials, 13 (**2011**) B151–B164.

[99] O. Ozkan and H. Turkoglu Sasmazel, International Journal of Polymeric Materials and Polymeric Biomaterials, 66 (**2017**) 853–860.

[100] S. Stokols and M.H. Tuszynski, Biomaterials, 25 (**2004**) 5839–5846.

[101] Y. Wang, W. Xu, X. Kou, Y. Luo, Y. Zhang, B. Ma, M. Wang and K. Huang, Protein Expression and Purification, 84 (**2012**) 173–180.

[102] A. Bozkurt, F. Lassner, D. O'Dey, R. Deumens, A. Böcker, T. Schwendt, C. Janzen, C. V. Suschek, R. Tolba, E. Kobayashi, B. Sellhaus, S. Tholl, L. Eummelen, F. Schügner, L. Olde Damink, J. Weis, G.A. Brook and N. Pallua, Biomaterials, 33 (**2012**) 1363–1375.

[103] Q. Ao, A. Wang, W. Cao, L. Zhang, L. Kong, Q. He, Y. Gong and X. Zhang, Journal of Biomedical Materials Research Part A, 77A (**2006**) 11–18.

[104] J.F. Kim, J.H. Kim, Y.M. Lee and E. Drioli, AIChE Journal, 62 (**2016**) 461–490.

[105] V. Chiono, G. Ciardelli, G. Vozzi, M.G. Sotgiu, B. Vinci, C. Domenici and P. Giusti, Journal of Biomedical Materials Research Part A, 85A (**2008**) 938–953.

[106] C. Sun, X. Jin, J.M. Holzwarth, X. Liu, J. Hu, M.J. Gupte, Y. Zhao and P.X. Ma, Macromolecular Bioscience, 12 (**2012**) 761–769.

[107] T. Rayna and L. Striukova, Technological Forecasting and Social Change, 102 (**2016**) 214–224.

[108] D. Banoriya, R. Purohit and R.K. Dwivedi, Materials Today: Proceedings, 2 (**2015**) 3409–3418.

[109] K.F. Leong, C.M. Cheah and C.K. Chua, Biomaterials, 24 (**2003**) 2363–2378.

[110] T. Cui, Y. Yan, R. Zhang, L. Liu, W. Xu and X. Wang, Tissue Engineering Part C: Methods, 15 (**2009**) 1–9.

[111] D. Radulescu, S. Dhar, C.M. Young, D.W. Taylor, H.-J. Trost, D.J. Hayes and G.R. Evans, Materials Science and Engineering: C, 27 (**2007**) 534–

539.

[112] A. Yamada, S.-I. Matsuyama, M. Todoriki, A. Kashiwagi, I. Urabe and T. Yomo, Biosystems, 92 (**2008**) 1–9.

[113] J. Xie, M.R. MacEwan, A.G. Schwartz and Y. Xia, Nanoscale, 2 (**2010**) 35–44.

[114] S.Y. Chew, R. Mi, A. Hoke and K.W. Leong, Advanced Functional Materials, 17 (**2007**) 1288–1296.

[115] W.E. Teo and S. Ramakrishna, Nanotechnology, 16 (**2005**) 1878–1884.

[116] Y. Zhu, A. Wang, S. Patel, K. Kurpinski, E. Diao, X. Bao, G. Kwong, W.L. Young and S. Li, Tissue Engineering Part C: Methods, 17 (**2011**) 705–715.

[117] L. Weng and J. Xie, Current Pharmaceutical Design, 21 (**2015**) 1944–59.

[118] M. Mirjalili and S. Zohoori, Journal of Nanostructure in Chemistry, 6 (**2016**) 207–213.

[119] G. Taylor, Proceedings of the Royal Society A: Mathematical, Physical and Engineering Sciences, 313 (**1969**) 453–475.

[120] N. Bhardwaj and S.C. Kundu, Biotechnology Advances, 28 (**2010**) 325–347.

[121] M.L.F. Nascimento, E.S. Araújo, E.R. Cordeiro, A.H.P. de Oliveira and H.P. de Oliveira, Recent Patents on Nanotechnology, 9 (**2015**) 76–85.

[122] S. Kidoaki, I.K. Kwon and T. Matsuda, Biomaterials, 26 (**2005**) 37–46.

[123] M. Mehrasa, M.A. Asadollahi, K. Ghaedi, H. Salehi and A. Arpanaei, International Journal of Biological Macromolecules, 79 (**2015**) 687–695.

[124] J.J. Stankus, J. Guan, K. Fujimoto and W.R. Wagner, Biomaterials, 27 (**2006**) 735–744.

[125] Z. Sun, E. Zussman, A.L. Yarin, J.H. Wendorff and A. Greiner, Advanced Materials, 15 (**2003**) 1929–1932.

[126] T.J. Sill and H.A. von Recum, Biomaterials, 29 (**2008**) 1989–2006.

[127] C.J. Thompson, G.G. Chase, A.L. Yarin and D.H. Reneker, Polymer, 48 (**2007**) 6913–6922.

[128] V. Beachley and X. Wen, Materials Science and Engineering: C, 29 (**2009**) 663–668.

[129] G. Eda, J. Liu and S. Shivkumar, Materials Letters, 61 (**2007**) 1451–1455.

[130] A.K. Haghi and M. Akbari, Physica Status Solidi (A), 204 (**2007**) 1830–1834.

[131] Y.P. Neo, S. Ray, A.J. Easteal, M.G. Nikolaidis and S.Y. Quek, Journal of Food Engineering, 109 (**2012**) 645–651.

[132] S.-H. Tan, R. Inai, M. Kotaki and S. Ramakrishna, Polymer, 46 (**2005**) 6128–6134.

[133] S.L. Shenoy, W.D. Bates, H.L. Frisch and G.E. Wnek, Polymer, 46 (**2005**) 3372–3384.

[134] A. Koski, K. Yim and S. Shivkumar, Materials Letters, 58 (**2004**) 493–497.

[135] T. Vongsetskul, T. Chantarodsakun, P. Wongsomboon, R. Rangkupan and P. Tangboriboonrat, Chiang Mai Journal of Science, 42 (**2015**) 436–442.

[136] H. Homayoni, S.A.H. Ravandi and M. Valizadeh, Carbohydrate Polymers, 77 (**2009**) 656–661.

[137] P.K. Baumgarten, Journal of Colloid and Interface Science, 36 (**1971**) 71–79.

[138] T. Uyar and F. Besenbacher, Polymer, 49 (**2008**) 5336–5343.

[139] I. Hayati, A.. Bailey and T.. Tadros, Journal of Colloid and Interface Science, 117 (**1987**) 205–221.

[140] C. Zhang, X. Yuan, L. Wu, Y. Han and J. Sheng, European Polymer Journal, 41 (**2005**) 423–432.

[141] A. Awal, M. Sain and M. Chowdhury, Composites Part B: Engineering, 42 (**2011**) 1220–1225.

[142] C. Meechaisue, R. Dubin, P. Supaphol, V.P. Hoven and J. Kohn, Journal of Biomaterials Science. Polymer Edition, 17 (**2006**) 1039–56.

[143] X. Zhang, M.M.R. Khan, T. Yamamoto, M. Tsukada and H. Morikawa, International Journal of Biological Macromolecules, 50 (**2012**) 337–347.

[144] Q.P. Pham, U. Sharma and A.G. Mikos, Biomacromolecules, 7 (**2006**) 2796–2805.

[145] J. Doshi and D.H. Reneker, Journal of Electrostatics, 35 (**1995**) 151–160.

[146] X. Yuan, Y. Zhang, C. Dong and J. Sheng, Polymer International, 53 (**2004**) 1704–1710.

[147] A.H. Touny and S.B. Bhaduri, Materials Science and Engineering: C, 30 (**2010**) 1304–1312.

[148] H. Jiang, D. Fang, B.S. Hsiao, B. Chu and W. Chen, Biomacromolecules, 5 (**2004**) 326–333.

[149] T.A. Telemeco, C. Ayres, G.L. Bowlin, G.E. Wnek, E.D. Boland, N. Cohen, C.M. Baumgarten, J. Mathews and D.G. Simpson, Acta

Biomaterialia, 1 (**2005**) 377–385.

[150] F. Zheng, S. Wang, S. Wen, M. Shen, M. Zhu and X. Shi, Biomaterials, 34 (**2013**) 1402–1412.

[151] E.-J. Lee, S.-H. Teng, T.-S. Jang, P. Wang, S.-W. Yook, H.-E. Kim and Y.-H. Koh, Acta Biomaterialia, 6 (**2010**) 3557–3565.

[152] K.N. Kontogiannopoulos, A.N. Assimopoulou, I. Tsivintzelis, C. Panayiotou and V.P. Papageorgiou, International Journal of Pharmaceutics, 409 (**2011**) 216–228.

[153] J.P. Theron, J.H. Knoetze, R.D. Sanderson, R. Hunter, K. Mequanint, T. Franz, P. Zilla and D. Bezuidenhout, Acta Biomaterialia, 6 (**2010**) 2434–2447.

[154] F. Mottaghitalab, M. Farokhi, V. Mottaghitalab, M. Ziabari, A. Divsalar and M.A. Shokrgozar, Carbohydrate Polymers, 86 (**2011**) 526–535.

[155] C.-Y. Wang, K.-H. Zhang, C.-Y. Fan, X.-M. Mo, H.-J. Ruan and F.-F. Li, Acta Biomaterialia, 7 (**2011**) 634–643.

[156] H. Zhang, Y. Zhao, F. Han, M. Wang and X. Yuan, Journal of Controlled Release, 152 (**2011**) e181–e182.

[157] W. Li, X. Li, W. Li, T. Wang, X. Li, S. Pan and H. Deng, European Polymer Journal, 48 (**2012**) 1846–1853.

[158] Y. Zhou, H. Yang, X. Liu, J. Mao, S. Gu and W. Xu, International Journal of Biological Macromolecules, 53 (**2013**) 88–92.

[159] K. An, H. Liu, S. Guo, D.N.T. Kumar and Q. Wang, International Journal of Biological Macromolecules, 47 (**2010**) 380–388.

[160] T.G. Kim, H.J. Chung and T.G. Park, Acta Biomaterialia, 4 (**2008**) 1611–1619.

[161] J. Rnjak-Kovacina, S.G. Wise, Z. Li, P.K.M. Maitz, C.J. Young, Y. Wang and A.S. Weiss, Acta Biomaterialia, 8 (**2012**) 3714–3722.

[162] Y.J. Lee, D.S. Shin, O.W. Kwon, W.H. Park, H.G. Choi, Y.R. Lee, S.S. Han, S.K. Noh and W.S. Lyoo, Journal of Applied Polymer Science, 106 (**2007**) 1337–1342.

[163] S. Safi, M. Morshed, S.A. Hosseini Ravandi and M. Ghiaci, Journal of Applied Polymer Science, 104 (**2007**) 3245–3255.

[164] Z. Ma and S. Ramakrishna, Journal of Membrane Science, 319 (**2008**) 23–28.

[165] L. Chen, L. Bromberg, T.A. Hatton and G.C. Rutledge, Polymer, 49 (**2008**) 1266–1275.

[166] J.J. Stankus, D.O. Freytes, S.F. Badylak and W.R. Wagner, Journal of

Biomaterials Science, Polymer Edition, 19 (**2008**) 635–652.

[167] P. Taepaiboon, U. Rungsardthong and P. Supaphol, European Journal of Pharmaceutics and Biopharmaceutics, 67 (**2007**) 387–397.

[168] Z.X. Meng, X.X. Xu, W. Zheng, H.M. Zhou, L. Li, Y.F. Zheng and X. Lou, Colloids and Surfaces B: Biointerfaces, 84 (**2011**) 97–102.

[169] D.-G. Yu, W. Chian, X. Wang, X.-Y. Li, Y. Li and Y.-Z. Liao, Journal of Membrane Science, 428 (**2013**) 150–156.

[170] T.T.T. Nguyen, C. Ghosh, S.-G. Hwang, N. Chanunpanich and J.S. Park, International Journal of Pharmaceutics, 439 (**2012**) 296–306.

[171] J.-M. Yang, L. Zha, D.-G. Yu and J. Liu, Colloids and Surfaces B: Biointerfaces, 102 (**2013**) 737–743.

[172] J. Quan, Y. Yu, C. Branford-White, G.R. Williams, D.-G. Yu, W. Nie and L.-M. Zhu, Colloids and Surfaces B: Biointerfaces, 88 (**2011**) 304–309.

[173] S. Huang, X. Kang, Z. Cheng, P. Ma, Y. Jia and J. Lin, Journal of Colloid and Interface Science, 387 (**2012**) 285–291.

[174] H.-M. Chen and D.-G. Yu, Journal of Materials Processing Technology, 210 (**2010**) 1551–1555.

[175] H. Zhang, S. Lou, G.R. Williams, C. Branford-White, H. Nie, J. Quan and L.-M. Zhu, International Journal of Pharmaceutics, 439 (**2012**) 100–108.

[176] M. V. Natu, H.C. de Sousa and M.H. Gil, International Journal of Pharmaceutics, 397 (**2010**) 50–58.

[177] J.S. Im, S.K. Lee, B.C. Bai and Y.-S. Lee, Journal of Industrial and Engineering Chemistry, 18 (**2012**) 325–330.

[178] F. Song, X.-L. Wang and Y.-Z. Wang, Colloids and Surfaces B: Biointerfaces, 88 (**2011**) 749–754.

[179] S.T. Yohe, V.L.M. Herrera, Y.L. Colson and M.W. Grinstaff, Journal of Controlled Release, 162 (**2012**) 92–101.

[180] J. Han, T.-X. Chen, C.J. Branford-White and L.-M. Zhu, International Journal of Pharmaceutics, 382 (**2009**) 215–221.

[181] M. Zamani, M. Morshed, J. Varshosaz and M. Jannesari, European Journal of Pharmaceutics and Biopharmaceutics, 75 (**2010**) 179–185.

[182] X. Xu, X. Chen, Z. Wang and X. Jing, European Journal of Pharmaceutics and Biopharmaceutics, 72 (**2009**) 18–25.

[183] R. Toshkova, N. Manolova, E. Gardeva, M. Ignatova, L. Yossifova, I. Rashkov and M. Alexandrov, International Journal of Pharmaceutics, 400 (**2010**) 221–233.

[184] C.G. Park, E. Kim, M. Park, J.-H. Park and Y. Bin Choy, Journal of

Controlled Release, 149 (**2011**) 250–257.

[185] S.S. Said, A.K. Aloufy, O.M. El-Halfawy, N.A. Boraei and L.K. El-Khordagui, European Journal of Pharmaceutics and Biopharmaceutics, 79 (**2011**) 108–118.

[186] L.K. Macri, L. Sheihet, A.J. Singer, J. Kohn and R.A.F. Clark, Journal of Controlled Release, 161 (**2012**) 813–820.

[187] M.S. Kim, J. Lee, S.J. Kim and H. Shin, Journal of Controlled Release, 152 (**2011**) e149–e151.

[188] X. Zhang, Z. Shi, W. Fu, Z. Liu, Z. Fang, W. Lu, Y. Wang and F. Chen, Applied Surface Science, 258 (**2012**) 2301–2306.

[189] H. Zhang, X. Jia, F. Han, J. Zhao, Y. Zhao, Y. Fan and X. Yuan, Biomaterials, 34 (**2013**) 2202–2212.

[190] I.-C. Liao, S. Chen, J.B. Liu and K.W. Leong, Journal of Controlled Release, 139 (**2009**) 48–55.

[191] H.S. Kim and H.S. Yoo, Journal of Controlled Release, 145 (**2010**) 264–271.

[192] H. Nie, M.-L. Ho, C.-K. Wang, C.-H. Wang and Y.-C. Fu, Biomaterials, 30 (**2009**) 892–901.

[193] I. Moreno, V. González-González and J. Romero-García, European Polymer Journal, 47 (**2011**) 1264–1272.

[194] T. Jiang, E.J. Carbone, K.W.H. Lo and C.T. Laurencin, Progress in Polymer Science, 46 (**2015**) 1–24.

[195] K.M. Yun, A.B. Suryamas, F. Iskandar, L. Bao, H. Niinuma and K. Okuyama, Separation and Purification Technology, 75 (**2010**) 340–345.

[196] S.J. Kim, Y.S. Nam, D.M. Rhee, H.-S. Park and W.H. Park, European Polymer Journal, 43 (**2007**) 3146–3152.

[197] N. Daels, S. De Vrieze, I. Sampers, B. Decostere, P. Westbroek, A. Dumoulin, P. Dejans, K. De Clerck and S.W.H. Van Hulle, Desalination, 275 (**2011**) 285–290.

[198] H.T. Sasmazel, International Journal of Biological Macromolecules, 49 (**2011**) 838–846.

[199] B. Veleirinho, D.S. Coelho, P.F. Dias, M. Maraschin, R.M. Ribeiro-do-Valle and J.A. Lopes-da-Silva, International Journal of Biological Macromolecules, 51 (**2012**) 343–350.

[200] S.-D. Wang, Y.-Z. Zhang, G.-B. Yin, H.-W. Wang and Z.-H. Dong, Materials Science and Engineering: C, 30 (**2010**) 670–676.

[201] S. Soliman, S. Pagliari, A. Rinaldi, G. Forte, R. Fiaccavento, F. Pagliari,

O. Franzese, M. Minieri, P. Di Nardo and S. Licoccia, Acta Biomaterialia, 6 (**2010**) 1227–1237.

[202] B.S. Jha, R.J. Colello, J.R. Bowman, S.A. Sell, K.D. Lee, J.W. Bigbee, G.L. Bowlin, W.N. Chow, B.E. Mathern and D.G. Simpson, Acta Biomaterialia, 7 (**2011**) 203–215.

[203] W. Ji, F. Yang, J.J.J.P. van den Beucken, Z. Bian, M. Fan, Z. Chen and J.A. Jansen, Acta Biomaterialia, 6 (**2010**) 4199–4207.

[204] X. Shen, D. Yu, L. Zhu, C. Branford-White, K. White and N.P. Chatterton, International Journal of Pharmaceutics, 408 (**2011**) 200–207.

[205] T. Okuda, K. Tominaga and S. Kidoaki, Journal of Controlled Release, 143 (**2010**) 258–264.

[206] C. Huang, S.J. Soenen, E. van Gulck, G. Vanham, J. Rejman, S. Van Calenbergh, C. Vervaet, T. Coenye, H. Verstraelen, M. Temmerman, J. Demeester and S.C. De Smedt, Biomaterials, 33 (**2012**) 962–969.

[207] G.D. Winter, Nature, 193 (**1962**) 293–4.

[208] S.-Y. Gu, Z.-M. Wang, J. Ren and C.-Y. Zhang, Materials Science and Engineering: C, 29 (**2009**) 1822–1828.

[209] F.L. Mi, S.S. Shyu, Y.B. Wu, S.T. Lee, J.Y. Shyong and R.N. Huang, Biomaterials, 22 (**2001**) 165–73.

[210] B. Pant, H.R. Pant, D.R. Pandeya, G. Panthi, K.T. Nam, S.T. Hong, C.S. Kim and H.Y. Kim, Colloids and Surfaces A: Physicochemical and Engineering Aspects, 395 (**2012**) 94–99.

[211] Y. Zhao, Y. Zhou, X. Wu, L. Wang, L. Xu and S. Wei, Applied Surface Science, 258 (**2012**) 8867–8873.

[212] J.H.F. de Baaij, J.G.J. Hoenderop and R.J.M. Bindels, Physiological Reviews, 95 (**2015**) 1–46.

[213] P. Trumbo, S. Schlicker, A.A. Yates and M. Poos, Journal of the American Dietetic Association, 102 (**2002**) 1621–1630.

[214] M.P. Staiger, A.M. Pietak, J. Huadmai and G. Dias, Biomaterials, 27 (**2006**) 1728–1734.

[215] X. Li, X. Liu, S. Wu, K.W.K. Yeung, Y. Zheng and P.K. Chu, Acta Biomaterialia, 45 (**2016**) 2–30.

[216] W.H. Ma, Y.J. Liu, W. Wang and Y.Z. Zhang, Brazilian Journal of Medical and Biological Research, 48 (**2014**) 214–225.

[217] L. Zhao, C. Cui, X. Wang, S. Liu, S. Bu, Q. Wang and Y. Qi, Applied Surface Science, 330 (**2015**) 431–438.

[218] K. Dong, Y. Song, D. Shan and E.-H. Han, Corrosion Science, 100

(**2015**) 275–283.

[219] L.R. Krishna, G. Poshal, A. Jyothirmayi and G. Sundararajan, Materials & Design, 77 (**2015**) 6–14.

[220] A.L. Yerokhin, X. Nie, A. Leyland, A. Matthews and S.J. Dowey, Surface and Coatings Technology, 122 (**1999**) 73–93.

[221] X. Lu, M. Mohedano, C. Blawert, E. Matykina, R. Arrabal, K.U. Kainer and M.L. Zheludkevich, Surface and Coatings Technology, 307 (**2016**) 1165–1182.

[222] I.J. Polmear, Materials Science and Technology, 10 (**1994**) 1–16.

[223] F. Pan, M. Yang and X. Chen, Journal of Materials Science & Technology, 32 (**2016**) 1211–1221.

[224] A.A. Luo, Materials Comparison and Potential Applications of Magnesium in Automobiles. Essential Readings in Magnesium Technology, S.N. Mathaudhu, A.A. Luo, N.R. Neelameggham, E.A. Nyberg, W.H. Sillekens (Eds), Springer International Publishing, Cham, 25–34, **2016**.

[225] A. Imandoust, C.D. Barrett, T. Al-Samman, K.A. Inal and H. El Kadiri, Journal of Materials Science, 52 (**2017**) 1–29.

[226] Y. Zhang, G. Wu, W. Liu, L. Zhang, S. Pang and W. Ding, Materials & Design, 67 (**2015**) 1–8.

[227] A.R. Moore, C.J. Torbet, A. Shyam, J.W. Jones, D.M. Walukas and R.F. Decker, Fatigue Behavior of Thixomolded® Magnesium AZ91D Using Ultrasonic Techniques. Essential Readings in Magnesium Technology, S.N. Mathaudhu, A.A. Luo, N.R. Neelameggham, E.A. Nyberg, W.H. Sillekens (Eds), Springer International Publishing, Cham, 227–232, **2016**.

[228] Z. Hu, X. Li, H. Yan, X. Wu, H. Qun and J. Lin, Journal of Alloys and Compounds, 685 (**2016**) 58–64.

[229] J. Bohlen, G. Cano, G. Kurz, K.U. Kainer, D. Letzig, D. Drozdenko, F. Chmelik and P. Dobron, Acta Physica Polonica A, 134 (**2018**) 714–719.

[230] F. Berge, L. Krüger, H. Ouaziz and C. Ullrich, Transactions of Nonferrous Metals Society of China, 25 (**2015**) 1–13.

[231] A. Dziubinska and A. Gontarz, Aircraft Engineering and Aerospace Technology, 87 (**2015**) 180–188.

[232] J.-Y. Lee, D. Steglich and M.-G. Lee, International Journal of Plasticity, 105 (**2018**) 1–23.

[233] M.Z. Naser, Acta Astronautica, 155 (**2019**) 264–273.

[234] L. Zhang, W. Chen, W. Zhang, W. Wang and E. Wang, Journal of Materials Processing Technology, 237 (**2016**) 65–74.

[235] M. Mitka, M. Gawlik, M. Bigaj, W. Szymanski and W.Z. Misiolek, Procedia Manufacturing, 15 (**2018**) 257–263.

[236] E. Mostaed, A. Fabrizi, D. Dellasega, F. Bonollo and M. Vedani, Journal of Alloys and Compounds, 638 (**2015**) 267–276.

[237] Z. Zeng, N. Stanford, C.H.J. Davies, J.-F. Nie and N. Birbilis, International Materials Reviews, 64 (**2019**) 27–62.

[238] K.B. Nie, K.K. Deng, X.J. Wang, F.J. Xu, K. Wu and M.Y. Zheng, Materials Science and Engineering: A, 624 (**2015**) 157–168.

[239] B.. Mordike and T. Ebert, Materials Science and Engineering: A, 302 (**2001**) 37–45.

[240] Z. Yang, J. Li, J. Zhang, G. Lorimer and J. Robson, Acta Metallurgica Sinica (English Letters), 21 (**2008**) 313–328.

[241] Y. Chen, Z. Xu, C. Smith and J. Sankar, Acta Biomaterialia, 10 (**2014**) 4561–4573.

[242] W.J. Joost and P.E. Krajewski, Scripta Materialia, 128 (**2017**) 107–112.

[243] K. Song, F.S. Pan, X.H. Chen, Z.H. Zhang, A.T. Tang, J. She, Z.W. Yu, H.C. Pan and X.Y. Xu, Materials Letters, 157 (**2015**) 73–76.

[244] S.N. Mathaudhu and E.A. Nyberg, Magnesium Alloys in U.S. Military Applications: Past, Current and Future Solutions. Essential Readings in Magnesium Technology, S.N. Mathaudhu, A.A. Luo, N.R. Neelameggham, E.A. Nyberg, W.H. Sillekens (Eds), Springer International Publishing, Cham, 71–76, **2016**.

[245] G.S. Frankel, Nature Materials, 14 (**2015**) 1189–1190.

[246] H. Furuya, N. Kogiso, S. Matunaga and K. Senda, Materials Science Forum, 350–351 (**2000**) 341–348.

[247] E. Aghion and B. Bronfin, Materials Science Forum, 350–351 (**2000**) 19–30.

[248] F. Czerwinski, Corrosion Science, 86 (**2014**) 1–16.

[249] G. Song, Advanced Engineering Materials, 7 (**2005**) 563–586.

[250] T. Schilling, M. Bauer, L. LaLonde, H.J. Maier, A. Haverich and T. Hassel, Cardiovascular Applications of Magnesium Alloys. Magnesium Alloys, InTech, **2017**.

[251] B. Heublein, R. Rohde, V. Kaese, M. Niemeyer, W. Hartung and A. Haverich, Heart (British Cardiac Society), 89 (**2003**) 651–6.

[252] C. Di Mario, H. Griffiths, O. Goktekin, N. Peeters, J. Verbist, M. Bosiers, K. Deloose, B. Heublein, R. Rohde, V. Kasese, C. Ilsley and R. Erbel, Journal of Interventional Cardiology, 17 (**2004**) 391–395.

[253] P. Zartner, R. Cesnjevar, H. Singer and M. Weyand, Catheterization and Cardiovascular Interventions, 66 (**2005**) 590–594.

[254] J. Li, Q. Zhang, M. Zhang and M. Egger, Cochrane Database of Systematic Reviews, (**2007**).

[255] M. Haude, R. Erbel, P. Erne, S. Verheye, H. Degen, D. Böse, P. Vermeersch, I. Wijnbergen, N. Weissman, F. Prati, R. Waksman and J. Koolen, The Lancet, 381 (**2013**) 836–844.

[256] I.V. Antoniac and D. Laptoiu, ASORIS - Revista de Ortopedie Si Traumatologie a Asociatiei de Ortopedie Romana-Italo-Spaniole, 4 (**2010**) 1–10.

[257] M. Pogorielov, E. Husak, A. Solodivnik and S. Zhdanov, Interventional Medicine and Applied Science, 9 (**2017**) 27–38.

[258] E.D. McBride, Journal of the American Medical Association, 111 (**1938**) 2464.

[259] H. Gao, M. Zhang, J. Zhao, L. Gao and M. Li, Materials Science and Engineering: C, 63 (**2016**) 450–461.

[260] B. Ullmann, J. Reifenrath, J.-M. Seitz, D. Bormann and A. Meyer-Lindenberg, Proceedings of the Institution of Mechanical Engineers, Part H: Journal of Engineering in Medicine, 227 (**2013**) 317–326.

[261] N. Erdmann, N. Angrisani, J. Reifenrath, A. Lucas, F. Thorey, D. Bormann and A. Meyer-Lindenberg, Acta Biomaterialia, 7 (**2011**) 1421–1428.

[262] H. Waizy, J. Diekmann, A. Weizbauer, J. Reifenrath, I. Bartsch, V. Neubert, R. Schavan and H. Windhagen, Journal of Biomaterials Applications, 28 (**2014**) 667–675.

[263] H. Windhagen, K. Radtke, A. Weizbauer, J. Diekmann, Y. Noll, U. Kreimeyer, R. Schavan, C. Stukenborg-Colsman and H. Waizy, BioMedical Engineering OnLine, 12 (**2013**) 62.

[264] J. Kubásek, D. Dvorský, M. Čavojský, D. Vojtěch, N. Beronská and M. Fousová, Journal of Materials Science & Technology, 33 (**2017**) 652–660.

[265] H.S. Jiang, M.Y. Zheng, X.G. Qiao, K. Wu, Q.Y. Peng, S.H. Yang, Y.H. Yuan and J.H. Luo, Materials Science and Engineering: A, 684 (**2017**) 158–164.

[266] D. Dvorský, J. Kubásek, D. Vojtěch and M. Čavojský, Acta Physica Polonica A, 134 (**2018**) 748–752.

[267] D. Dvorský, J. Kubásek and D. Vojtěch, Solid State Phenomena, 270 (**2017**) 205–211.

[268] C. Xiang, N. Gupta, P. Coelho and K. Cho, Materials Science and Engineering: A, 710 (**2018**) 74–85.

[269] H.S. Jiang, M.Y. Zheng, X.G. Qiao, K. Wu, Q.Y. Peng, S.H. Yang, Y.H. Yuan and J.H. Luo, Materials Science and Engineering A, 684 (**2017**) 158–164.

[270] L. Jiang, F. Xu, Z. Xu, Y. Chen, X. Zhou, G. Wei and H. Ge, International Journal of Electrochemical Science, 10 (**2015**) 10422–10432.

[271] G. Riontino, M. Massazza, D. Lussana, P. Mengucci, G. Barucca and R. Ferragut, Materials Science and Engineering A, 494 (**2008**) 445–448.

[272] P. Mengucci, G. Barucca, G. Riontino, D. Lussana, M. Massazza, R. Ferragut and E.H. Aly, Materials Science and Engineering A, 479 (**2008**) 37–44.

[273] S. Asqardoust, A. Zarei Hanzaki, H.R. Abedi, T. Krajnak and P. Minárik, Materials Science and Engineering: A, 698 (**2017**) 218–229.

[274] Y.H. Kang, X.X. Wang, N. Zhang, H. Yan and R.S. Chen, Materials Science and Engineering: A, 689 (**2017**) 435–445.

[275] J. Kubásek, D. Vojtěch, E. Jablonská, I. Pospíšilová, J. Lipov and T. Ruml, Materials Science and Engineering: C, 58 (**2016**) 24–35.

[276] Ž.D. Živković and B. Dobovišek, Thermochimica Acta, 32 (**1979**) 205–211.

[277] A.E. Santos, A.L. Braccialli, J. Vilela, C.R. Foschini and L.E.A. Sanchez, Polymer Composites, (**2018**).

[278] S. Hocker, N. Hudson-Smith, H.C. Schniepp and D.E. Kranbuehl, Polymer, 93 (**2016**) 23–29.

[279] L. Li, Q. Li, J. Yang, L. Sun, J. Guo, Y. Yao, L. Zhong and D. Lu, Materials Letters, 228 (**2018**) 435–438.

[280] B.O. Field and C.J. Hardy, Quarterly Reviews, Chemical Society, 18 (**1964**) 361.

[281] A. Baji and M. Abtahi, Advances in Nano Research, 1 (**2013**) 183–192.

[282] J. Xiang, X. Shen, F. Song, M. Liu, G. Zhou and Y. Chu, Materials Research Bulletin, 46 (**2011**) 258–261.

[283] Y. Ye, H. Fan and J. Li, Materials Letters, 64 (**2010**) 419–421.

[284] S.A. Theron, E. Zussman and A.L. Yarin, Polymer, 45 (**2004**) 2017–2030.

[285] H.-B. Cho, M.T.T. Huynh, T. Nakayama, S.T. Nguyen, H. Suematsu, T. Suzuki, W. Jiang, S. Tanaka, Y. Tokoi, S.W. Lee, T. Sekino and K. Niihara, Journal of Nanomaterials, 2013 (**2013**) 1–10.

[286] K. Sivaiah, K.N. Kumar, V. Naresh and S. Buddhudu, Materials Sciences

and Applications, 02 (**2011**) 1688–1696.

[287] Y.K. Du, P. Yang, Z.G. Mou, N.P. Hua and L. Jiang, Journal of Applied Polymer Science, 99 (**2006**) 23–26.

[288] F. Paulik, J. Paulik, M. Arnold and R. Naumann, Journal of Thermal Analysis, 34 (**1988**) 627–635.

[289] M. Mohammad Ali Zadeh, M. Keyanpour-Rad and T. Ebadzadeh, Ceramics International, 40 (**2014**) 5461–5466.

[290] X. Yang, C. Shao, H. Guan, X. Li and J. Gong, Inorganic Chemistry Communications, 7 (**2004**) 176–178.

[291] P. Louette, F. Bodino and J.-J. Pireaux, Surface Science Spectra, 12 (**2005**) 106–110.

[292] M. Ascencio, M. Pekguleryuz and S. Omanovic, Corrosion Science, 87 (**2014**) 489–503.

[293] H. Ardelean, A. Seyeux, S. Zanna, F. Prima, I. Frateur and P. Marcus, Corrosion Science, 73 (**2013**) 196–207.

[294] W. Jin, G. Wu, H. Feng, W. Wang, X. Zhang and P.K. Chu, Corrosion Science, 94 (**2015**) 142–155.

[295] A.G. El-Shamy, Progress in Organic Coatings, 127 (**2019**) 252–259.

[296] Y.H. Kang, D. Wu, R.S. Chen and E.H. Han, Journal of Magnesium and Alloys, 2 (**2014**) 109–115.

[297] M. Gümüşderelioğlu and H. Türkoğlu, Biomaterials, 23 (**2002**) 3927–3935.

[298] O. Ozkan and H. Turkoglu Sasmazel, Journal of Biomaterials Applications, 32 (**2018**) 1300–1313.

[299] S. Surucu and H. Turkoglu Sasmazel, International Journal of Biological Macromolecules, 92 (**2016**) 321–328.

[300] S. Surucu, K. Masur, H. Turkoglu Sasmazel, T. Von Woedtke and K.D. Weltmann, Applied Surface Science, 385 (**2016**) 400–409.

[301] X.M. Mo, C.Y. Xu, M. Kotaki and S. Ramakrishna, Biomaterials, 25 (**2004**) 1883–1890.

[302] H.S. Yoo, T.G. Kim and T.G. Park, Advanced Drug Delivery Reviews, 61 (**2009**) 1033–1042.

[303] H.-J. Sung, C. Meredith, C. Johnson and Z.S. Galis, Biomaterials, 25 (**2004**) 5735–5742.

[304] H. Wang, Y. Estrin and Z. Zúberová, Materials Letters, 62 (**2008**) 2476–2479.

[305] F. Witte, N. Hort, C. Vogt, S. Cohen, K.U. Kainer, R. Willumeit and F.

Feyerabend, Current Opinion in Solid State and Materials Science, 12 (**2008**) 63–72.

[306] W. Yang, P. Zhang, J. Liu and Y. Xue, Journal of Rare Earths, 24 (**2006**) 369–373.

[307] S.M. Bishop, M. Walker, A.A. Rogers and W.Y.J. Chen, Journal of Wound Care, 12 (**2003**) 125–128.

[308] S.E. Wharram, X. Zhang, D.L. Kaplan and S.P. McCarthy, Macromolecular Bioscience, 10 (**2010**) 246–257.

[309] D. Kim, S. Connolly, S. Zhao, R. Beuerman, R. Voorhies and D. Kline, Journal of Reconstructive Microsurgery, 9 (**1993**) 415–420.

[310] F.J. Rodríguez, N. Gómez, G. Perego and X. Navarro, Biomaterials, 20 (**1999**) 1489–500.

[311] C.-J. Chang and S. Hsu, Biomaterials, 27 (**2006**) 1035–1042.

[312] A. Wang, Q. Ao, Y. Wei, K. Gong, X. Liu, N. Zhao, Y. Gong and X. Zhang, Biotechnology Letters, 29 (**2007**) 1697–1702.

[313] W. Cui, L. Cheng, H. Li, Y. Zhou, Y. Zhang and J. Chang, Polymer, 53 (**2012**) 2298–2305.

[314] O. Ozkan and H.T. Sasmazel, Journal of Nanoscience and Nanotechnology, 18 (**2018**) 2415–2421.

[315] S.A. Brown, J.E. Lemons and N.B. Mateo, New Products and Standards. Biomaterials Science, B. Ratner, A. Hoffman, F. Schoen, J. Lemons (Eds), Elsevier, Amsterdam, 457–464, **1996**.

[316] C.R. Carvalho, R. López-Cebral, J. Silva-Correia, J.M. Silva, J.F. Mano, T.H. Silva, T. Freier, R.L. Reis and J.M. Oliveira, Materials Science and Engineering: C, 71 (**2017**) 1122–1134.

[317] J. Griffin, R. Delgado-Rivera, S. Meiners and K.E. Uhrich, Journal of Biomedical Materials Research Part A, 97A (**2011**) 230–242.

[318] K. Nawrotek, M. Tylman, K. Rudnicka, J. Gatkowska and J. Balcerzak, Journal of the Mechanical Behavior of Biomedical Materials, 60 (**2016**) 256–266.

[319] O. Suwantong, S. Waleetorncheepsawat, N. Sanchavanakit, P. Pavasant, P. Cheepsunthorn, T. Bunaprasert and P. Supaphol, International Journal of Biological Macromolecules, 40 (**2007**) 217–223.

[320] K. Yingsukwattana, S. Agthong, R. Mongkonnavin, Y. Tabata and S. Kanokpanont, Advanced Materials Research, 55–57 (**2008**) 701–704.

[321] M.A. Schwartz, The Journal of Cell Biology, 139 (**1997**) 575–578.

[322] C.Y. Yang, L.Y. Huang, T.L. Shen and J. Andrew Yeh, European Cells

and Materials, 20 (**2010**) 415–430.

[323] A. Ranella, M. Barberoglou, S. Bakogianni, C. Fotakis and E. Stratakis, Acta Biomaterialia, 6 (**2010**) 2711–2720.

[324] D. Gerlier and N. Thomasset, Journal of Immunological Methods, 94 (**1986**) 57–63.

[325] N. Panda, A. Bissoyi, K. Pramanik and A. Biswas, Materials Science and Engineering: C, 48 (**2015**) 521–532.

[326] Y. Maghdouri-White, G.L. Bowlin, C.A. Lemmon and D. Dréau, Materials Science & Engineering. C, Materials for Biological Applications, 43 (**2014**) 37–44.

HACETTEPE UNIVERSITY
GRADUATE SCHOOL OF SCIENCE AND ENGINEERING
THESIS/DISSERTATION ORIGINALITY REPORT

HACETTEPE UNIVERSITY
GRADUATE SCHOOL OF SCIENCE AND ENGINEERING
TO THE DEPARTMENT OF BIOENGINEERING

Date: 01/02/2019

Thesis Title / Topic: NERVE GUIDANCE CONDUIT APPLICATION OF MAGNESIUM ALLOYS

According to the originality report obtained by my thesis advisor by using the Turnitin plagiarism detection software and by applying the filtering options stated below on 01/02/2019 for the total of 95 pages including the a) Title Page, b) Introduction, c) Main Chapters, d) Conclusion sections of my thesis entitled as above, the similarity index of my thesis is 8%.

Filtering options applied:
1. Bibliography/Works Cited excluded
2. Quotes excluded
3. Match size up to 5 words excluded

I declare that I have carefully read Hacettepe University Graduate School of Science and Engineering Guidelines for Obtaining and Using Thesis Originality Reports; that according to the maximum similarity index values specified in the Guidelines, my thesis does not include any form of plagiarism; that in any future detection of possible infringement of the regulations I accept all legal responsibility; and that all the information I have provided is correct to the best of my knowledge.

I respectfully submit this for approval.

01/02/2019

Name Surname:	Ozan ÖZKAN
Student No:	N10164540
Department:	BIOENGINEERING
Program:	BIOENGINEERING
Status:	☐ Masters ☐ Ph.D. ☒ Integrated Ph.D.

ADVISOR APPROVAL

APPROVED.

Prof. Dr. Erhan BİŞKİN

CURRICULUM VITAE

Credentials

Name, Last Name : Ozan ÖZKAN

Place of Birth : Ankara

Marital Status : Married

E-mail : ozan.ozkan@atilim.edu.tr

ozan.ozkan@hotmail.com

Address : Atılım University, Department of Metallurgical and Materials Engineering, İncek, Gölbaşı, ANKARA

Education

High School : Gazi Anatolian High School, 2002

BSc : Dokuz Eylül University, Department of Metallurgical and Materials Engineering, 2006

PhD : Hacettepe University, Department of Bioengineering, 2019

Languages

Turkish : Native

English : Advanced (YDS-2017: 92.5, YÖKDİL-2017: 97.5)

Work Experience

Research Assistant, Atılım University, Department of Metallurgical and Materials Engineering, Ankara, Turkey (2007-   )

Visiting Scholar, York Plasma Institute, Department of Physics, University of York, York, United Kingdom (2015)

Areas of Experience

Metallic Materials, Polymeric Materials, Electrospinning, Heat Treatment, In Vitro Cell Culture, Tissue Engineering, In Vitro Bacterium Culture, Anti-bacterial Testing, Plasma Surface Modification, Freeze Drying, UV-Spectrometry, Fluorescence Microscopy, Mechanical Testing

Funding Projects and Budgets

Thesis Related Publications

Ozan Ozkan, Hilal Turkoglu Sasmazel, Erhan Biskin, Development of Electrospun WE43 Magnesium Alloy-Like Compound, Advanced Engineering Materials, 2019, *submitted*.

Ozan Ozkan, Hilal Turkoglu Sasmazel, Erhan Biskin, Electrospun WE43 Magnesium Alloy-Like Compound for Nerve Guidance Applications, *in preparation*.